

CONDUCTANCE PEAKS AT THE CYCLOTRON HARMONICS  
IN A CYLINDRIC PLASMA CAPACITOR

Thesis by  
James G. Downward IV

In Partial Fulfillment of the  
Requirements for the Degree of  
Doctor of Philosophy

California Institute of Technology  
Pasadena, California

1971

(Submitted May 21, 1971)

Acknowledgment

The author wishes to express his thanks to Professor Robert Harp for his guidance and advice throughout the course of this research. He is also indebted to Professor Roy Gould for many discussions relating to the theoretical and experimental aspects of this work. Many additional members of the plasma research group contributed to this research in a wide variety of ways. In particular I would like to thank Dr. Ray Fisher, Professor Reiner Stenzel, Richard Smith, Keith Burrell and John Wilgen for many useful discussions, and on occasion, direct assistance with the experiment. The critical and thorough reading given this manuscript by Richard Smith is especially appreciated.

Mrs. Ruth Stratton also deserves particular thanks, not only for typing this thesis, but also for her cheerful and helpful attitude. Her friendship has often been the sunshine on otherwise cloudy days.

The author gratefully acknowledges the support of the Office of Naval Research in carrying out this work.

ABSTRACT

The conductance peaks at the cyclotron harmonics in a plasma-filled cylindrical capacitor are investigated theoretically and experimentally. A theoretical model is developed and is shown to predict peak height variation with density, harmonic number, and sheath thickness which is in agreement with experimental measurements of the capacitor's complex admittance (susceptance and conductance) and absorption coefficient. A harmonic conduction peak is found to rise initially as density increases, only to fall to a minimum height as the upper hybrid frequency passes through that harmonic. The noise output of the capacitor is studied and is compared to the theoretical noise output at the harmonics which would be expected for a thermal plasma. The theoretical output is shown to be related to the capacitor's conductance. The capacitor's internal noise oscillations are found to be too intense for a thermal plasma, but the noise peaks at the harmonics show structure and amplitude variation with density in substantial agreement with the theoretical model. To test the validity of the theoretical model which treats the capacitor's center wire sheath as a vacuum region several Debye lengths thick, the conductance change for small decreases in sheath size is investigated both experimentally and theoretically. It is found that the amplitude of the conductance peak within a harmonic passband is very sensitive to small changes in sheath size. This fact leads to a new plasma diagnostic, sheath modulated transmission. Sheath modulated transmission experiments are found to enhance cyclotron harmonic wave

effects relative to the amplitude of the transmission peaks at harmonics and to provide information as to the location of the second harmonic band pass edge. Applications of this work to plasma diagnostics and suggestions for further work are made.

TABLE OF CONTENTS

|                |   |     |
|----------------|---|-----|
| Acknowledgment |   | ii  |
| Abstract       |   | iii |
| Chapter 1      | INTRODUCTION  | 1   |
|                | 1.1 Historical Background   | 2   |
|                | 1.2 Scope of the Investigation  | 4   |
| Chapter 2      | COLD PLASMA THEORY OF THE ADMITTANCE OF A<br>COAXIAL MAGNETOPLASMA CAPACITOR            |     |
|                | 2.1 The Quasistatic Approximation   | 6   |
|                | 2.2 Cold, Uniform Plasma  | 8   |
|                | 2.3 Nonuniform Cold Plasma  | 11  |
|                | 2.4 Effect of the Probe Sheath on the Cold<br>Plasma Admittance                         | 12  |
|                | 2.5 Effect of Losses on the Measured<br>Admittance                                      | 15  |
| Chapter 3      | HOT PLASMA THEORY OF THE ADMITTANCE OF A<br>COAXIAL PLASMA CAPACITOR                    |     |
|                | 3.1 Introduction  | 17  |
|                | 3.2 The Perpendicular Dielectric Constant<br>$K_{\perp}(\omega, k)$                     | 17  |
|                | 3.3 The Transparent Cylinder Admittance Model   | 22  |
|                | 3.4 Low Density Expansion for the Normalized<br>Conductance                             | 25  |
|                | 3.5 The Admittance for Two-Probe Transmission   | 27  |
|                | 3.6 Limitations of the Admittance Model   | 28  |
|                | 3.7 Numerical Computations  | 29  |
| Chapter 4      | EXPERIMENTAL MEASUREMENT OF THE COMPLEX<br>ADMITTANCE OF A CYLINDRICAL PLASMA CAPACITOR |     |
|                | 4.1 The Plasma  | 31  |
|                | 4.2 Plasma Uniformity   | 33  |
|                | 4.3 The Magnetic Field  | 35  |
|                | 4.4 The Plasma Capacitor  | 36  |

|           |  |    |
|-----------|--|----|
| 4.5       | Two-Probe Transmission for Determining $\omega_p^2/\omega^2$ and $kT_e$                              | 38 |
| 4.6       | Experimental Methods of Measuring the Capacitor Admittance   |    |
|           | A. Direct Measurement of a Hot Plasma Admittance at the Cyclotron Harmonics                          | 38 |
|           | B. Absorption of a Hot Plasma at the Cyclotron Harmonics   | 40 |
| 4.7       | Experimental Results   |    |
|           | A. Susceptance   | 42 |
|           | B. Conductance   | 46 |
| 4.8       | Discussion and Summary   | 55 |
| Chapter 5 | NOISE OSCILLATION ON THE CENTER CONDUCTOR OF A CYLINDRIC PLASMA CAPACITOR AT THE CYCLOTRON HARMONICS |    |
| 5.1       | Introduction   | 57 |
| 5.2       | Longitudinal Noise Oscillations in a Thermal Plasma Capacitor  | 59 |
| 5.3       | Experimental Measurement of Noise Oscillations at the Cyclotron Harmonics                            |    |
|           | A. The Apparatus   | 62 |
|           | B. Experimental Results  |    |
|           | i) Plasma Collision Frequency  | 63 |
|           | ii) Harmonic Noise   | 64 |
|           | iii) Instability Stimulated Harmonic Noise   | 71 |
| 5.4       | Discussion and Summary   | 74 |
| Chapter 6 | SHEATH MODULATION OF CYCLOTRON HARMONIC WAVES  |    |
| 6.1       | Introduction   | 79 |
| 6.2       | The Effect of Sheath Size on Harmonic Conduction Peaks   | 80 |
| 6.3       | Sheath Modulated Transmission  | 91 |
| 6.4       | Summary  | 96 |

|             |   |     |
|-------------|---|-----|
| Chapter 7   | SUMMARY AND SUGGESTIONS FOR FURTHER WORK  |     |
|             | Summary   | 98  |
|             | Suggestions for Further Work  | 104 |
|             | Conclusion  | 106 |
| Appendix I  | THE ADMITTANCE OF A COLD, NONUNIFORM CYLINDRICAL<br>PLASMA CAPACITOR                | 107 |
| Appendix II | THE DISPERSION RELATION FOR PERPENDICULARLY<br>PROPAGATING CYCLOTRON HARMONIC WAVES | 113 |

Chapter 1

INTRODUCTION

In the past decade the warm magnetoplasma has been increasingly studied primarily because of eventual fusion applications. A wide variety of experimental hot plasma phenomena is now understood to depend on the propagation of longitudinal electron waves propagating nearly perpendicularly to the magnetic field. These waves are called cyclotron harmonic waves (CHW) because they propagate in passbands adjacent to harmonics of the cyclotron frequency. Noise emission from a plasma at the cyclotron harmonics, rf transmission through a plasma perpendicular to the magnetic field, absorption of energy by a plasma, plasma pulse response, resonance rectification effects at a probe immersed in a magnetoplasma, and ionospheric resonances are all thought to depend on CHW propagation [1,2,3]. Numerous experiments have verified the dispersion properties of CHW propagation [2,3]; however, comparatively little has been done toward understanding the complex admittance of an rf antenna at the cyclotron harmonics or the effect of the size of the antenna sheath on the propagation of cyclotron harmonic waves. The conductance peaks associated with the complex admittance at the cyclotron harmonics deserve particular study. The conductance at the harmonics is related to the loss component of the rf electric field. Hence, a study of the harmonic conductance peaks directly relates to the plasma absorption and emission at the cyclotron harmonics. The coaxial capacitor was chosen for these studies because the rf electric field exciting the cyclotron harmonic waves is primarily perpendicular to the external magnetic

field. This chapter reviews briefly, previous work on cyclotron harmonic waves and then outlines the topics to be covered in the following chapters.

### 1.1 Historical Background

Plasma phenomena at the cyclotron harmonics were first observed in experiments measuring noise radiation from hot plasmas. In 1959 Wharton reported observing noise radiation at the cyclotron frequency and at the second and third cyclotron harmonics from various fusion oriented plasma devices [4]. About a year later Landauer observed noise emission peaks up to the 45th cyclotron harmonic in a PIG discharge [5]. Early attempts to explain harmonic noise radiation attributed the radiation to single particle radiation from electrons moving in cyclotron motion. Classical EM theory predicts that a single energetic electron gyrating in a magnetic field will emit radiation at the cyclotron frequency  $\omega_c$  and its harmonics  $n\omega_c$  [6]. However, this radiation should only be significant at relativistic electron energies.

Early experiments seemed initially to agree with the assumption of single particle emission. However, later experiments by Bekefi et al in 1962 in the positive columns of cathode produced discharges also showed strong emission and absorption up to the 10th cyclotron harmonic [7]. While streams of high temperature electrons occur in PIG discharges, the electron temperature in the positive column of a cathode produced discharge is of the order of only several electron volts. Single particle radiation theories could not account

for these results with such low electron temperatures. This suggested that the observed harmonic effects might be the result of collective behavior of the plasma electrons. Tanaka et al [8] and Canobbio and Croci [9] first proposed that cyclotron harmonic waves propagating nearly perpendicularly to the magnetic field could account for observed results. These waves had been previously investigated theoretically by I. Bernstein in 1958 [10] and Stix in 1962 [11].

Comprehensive reviews of cyclotron harmonic wave phenomena through 1965 have been done by Crawford [1] and Bekefi [43]. Since 1965 considerable work has gone into understanding cyclotron harmonic wave propagation between two probes in a plasma. Harp [2] has shown that the rf transmission between two probes can be explained in terms of an interference between a fast direct coupled signal and a slow cyclotron harmonic wave and has verified the theoretical CHW dispersion characteristics for a high density Maxwellian plasma. Mantei [3] later showed that the transmission between two probes could be described in terms of the plasma admittance between the probes and verified the dispersion relation over a wider density range. In addition, his experimental results on pulse transmission through a warm plasma confirmed that the ionospheric ringing observed in 1962 with the Alouette I satellite was a manifestation of cyclotron harmonic wave propagation. A very complete theoretical treatment of cyclotron harmonic wave phenomena has been done by Tataronis [12] who considered CHW propagation and instabilities for various electron distribution functions, propagation angles to the magnetic field, and collision frequencies.

A theoretical treatment of the coaxial plasma in a magnetic field was given by Crawford, Mantei and Tataronis in 1966 [13]. Their theory predicted standing cyclotron harmonic wave resonances occurring within the capacitor. Experiments performed in such a capacitor, both by them and by this author, have failed to detect any standing cyclotron harmonic wave resonances. The reason for the discrepancy between experimental observations and theoretical predictions seems to lie in their assumption that specular reflection of cyclotron harmonic waves occurred at the capacitor's boundaries.

## 1.2 Scope of the Investigation

The following two chapters reformulate the coaxial plasma capacitor problem in a different manner from that of Crawford, Mantei and Tataronis. In Chapter 2, the complex admittance of a cold plasma coaxial capacitor is presented and the modifications to the admittance caused by a density profile in the capacitor are discussed. Chapter 3 extends the theory of the plasma capacitor to the case where a warm uniform plasma fills the capacitor. The primary difference in the theoretical formulation presented here and that of Crawford et al [13] is that we assume the plasma to be infinite in extent but contained within a transparent grid capacitor, whereas Crawford et al assumed specularly reflecting capacitor walls which set up an infinite periodic set of images of the initial rf current distribution. This formulation allowed them to use the infinite plasma dielectric constant  $K_{\perp}(\omega, k)$  but also required that standing wave resonances be set up within the capacitor.

In Chapter 4 we present both direct and indirect experimental measurements of the capacitor's complex admittance and compare the results with the predictions from Chapter 3. The agreement obtained between theory and experiment in Chapter 4 is sufficiently good to allow the results of the theory to be applied to a study of noise output of the plasma capacitor at the cyclotron harmonics. This is done in Chapter 5 where the shape and character of the noise output are found to be predictable in terms of the theory developed in Chapter 3.

In Chapter 6, the influence of the antenna sheath on the launching and transmission of cyclotron harmonic waves is investigated by modulating the antenna sheath between two diameters. The experimental results of this modulation on the shape of both conductance curves and two probe transmission measurements is compared with predictions made by the theory presented in Chapter 3. Sheath modulation is found in certain cases to be a useful supplementary diagnostic technique for transmission measurements.

Chapter 7 provides a summary of some of the important results and conclusions, as well as suggestions for further work.

In the experiments and theory explained in the following chapters, the receiver frequency  $\omega$  is held fixed while the cyclotron frequency  $\omega_c$  is varied by sweeping the magnetic field. The ratio  $\omega_c/\omega$  is a direct measure of the magnetic field strength. The electron plasma density is expressed in terms of the normalized plasma frequency  $\omega_p^2/\omega^2$ .

Chapter 2

COLD PLASMA THEORY OF THE ADMITTANCE OF A  
COAXIAL MAGNETOPLASMA CAPACITOR

2.1 The Quasi-Static Approximation

In this chapter we consider the coaxial magnetocapacitor in the quasi-static limit. Normally the quasi-static approximation corresponds to setting [14,15]

$$\bar{\nabla} \times \bar{E} = - \frac{d\bar{B}}{dt} = 0 \quad (2.1)$$

where  $\bar{E}$  and  $\bar{B}$  are the rf electric and magnetic fields respectively. This approximation reduces the full set of Maxwell's equations to Laplace's equation

$$\epsilon \bar{\nabla}^2 \phi = 0 = \epsilon \bar{\nabla} \cdot (\bar{\nabla} \phi) = -\epsilon \bar{\nabla} \cdot \bar{E} \quad (2.2)$$

where  $\epsilon$  is the dielectric constant of the plasma. The assumption is that the fields vary sufficiently slowly in time so that the problem can be treated as an electrostatics problem. The validity of this approximation is considered by Vandenplas [14], who shows that the proper criterion for validity is that the solutions for the wave equation obtained from using the full set of Maxwell's equations

$$(\bar{\nabla}^2 + k_p^2) \bar{E} = 0 \quad (2.3)$$

where  $k_p^2 = \epsilon \mu_0 \omega^2$  and the solutions obtained from taking the gradient of Laplace's equation (equation 2.2)

$$\bar{\nabla}^2 \bar{E} = 0 \quad (2.4)$$

should be asymptotically identical in the region of interest. This occurs when  $\epsilon_{\perp} \mu_0 \omega^2 L^2 \ll 1$  where  $L$  is the characteristic dimension of the system [14]. This is equivalent to saying that the rotational part of the electric field is much less than the lamellar part  $|\bar{\nabla} \times \bar{E}| / |\bar{\nabla} \cdot \bar{E}| \ll 1$  [15].

For the experiments to be discussed later  $\omega/2\pi = 800$  MHz,  $K_{\perp} = \epsilon_{\perp}/\epsilon_0 < 1$  and the capacitor's radius is a maximum of 3.8 cm. For these values  $\epsilon_{\perp} \mu_0 \omega^2 L^2 \leq .4$   $K_{\perp}$  is usually sufficiently less than 1 for the quasi-static approximation to be valid for the direct coupled signal. Near  $\omega_c/\omega = 1$  where  $K_{\perp} \rightarrow \infty$ , the quasi-static approximation is not valid. Because the wavelength of the direct coupled EM signal within the cold plasma is much greater than the capacitor's diameter the capacitor can be treated as a uniform dielectric without worrying about standing wave resonances being set up between the capacitor's electrodes.

The symmetry of the problem places a further restriction on the solutions that a quasi-static theory can yield. Since we assume the capacitor is infinitely long and axially symmetric

$$\frac{d}{dz} = \frac{d}{d\phi} = 0$$

Thus

$$\bar{\nabla} \times \bar{H} \equiv 0 = \bar{J}_{\text{particle}} + \frac{d\bar{D}}{dt} \quad (2.5)$$

since both  $\bar{J}_{\text{particle}}$  and  $\bar{D}$  must be radial by symmetry. This fact is used in obtaining equation I.2 in Appendix I.

Equation 2.2 possesses an additional set of solutions for  $\epsilon \equiv 0$ . When  $\epsilon \equiv 0$  longitudinal waves ( $\bar{k} // \bar{E}$ , electrostatic oscillations) can propagate within the capacitor. For the hot plasma theory discussed in Chapter 3, the azimuthal symmetry requires that  $\bar{k}$  be parallel to  $\bar{E}$  for the longitudinal waves launched by the center wire of the capacitor. Equation 2.2 thus contains valid solutions both in the quasistatic limit for the direct coupled electromagnetic signal and in the electrostatic case for slowly moving ( $v_{\text{group}} \ll c$ ) short wavelength longitudinal oscillations.

### 2.2 Cold, Uniform Plasma

Consider a long plasma filled coaxial capacitor with inside wire radius = A and outside cylinder radius = B (Figure 2-1), axial

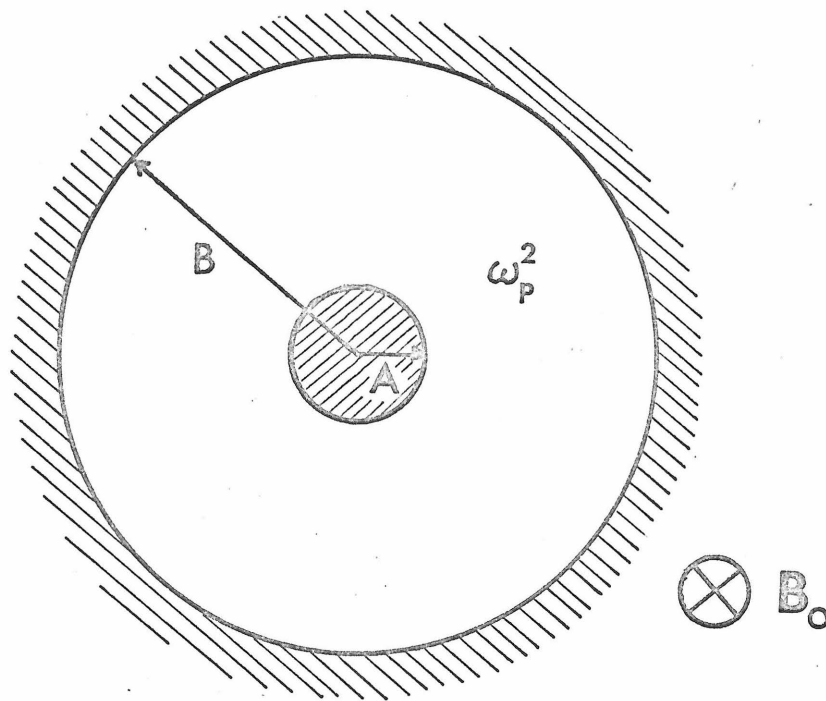


Figure 2.1 Plasma Capacitor with Uniform Plasma

to a magnetic field  $B_0$ . The capacitor is assumed to be sufficiently long so that fringing fields may be neglected.

For a cold plasma  $kT_e = 0$  the capacitor's admittance per unit length at frequency  $\omega$

$$Y = (2\pi i \omega \epsilon_0 / \ln(B/A)) K_{\perp} \quad (2.6)$$

is shown in Appendix I to be proportional to the perpendicular dielectric constant  $K_{\perp} = \epsilon_{\perp} / \epsilon_0$  of the plasma where

$$K_{\perp} = \left(1 - \frac{\omega_p^2}{\omega^2 - \omega_c^2}\right) \quad (2.7)$$

for a collisionless plasma [16].

Rewriting equation 2.6,  $Y = Y_0 K_{\perp}$  where  $Y_0$  is the capacitor's vacuum admittance. The normalized admittance becomes

$$\frac{Y}{Y_0} = K_{\perp} = (B - iG) / |Y_0| = K_R - iK_I \quad (2.8)$$

where  $B$  and  $G$  are the susceptance and conductance of the capacitor.

The normalized susceptance  $B / |Y_0| = K_R$  goes through zero at the upper hybrid frequency  $\omega_H^2 = \omega_p^2 + \omega_c^2$  where  $\omega_p$  is the plasma frequency,  $\omega_c$  is the cyclotron frequency, and  $\omega_H$  is the hybrid frequency. The normalized conductance  $G / |Y_0| = K_I$  is zero except at exactly  $\omega_c / \omega = 1$  where  $K_I$  must have a delta function to satisfy the Kramer-Kronig relation [17].

Loss mechanisms may be included in 2.6 by introducing an effective collision frequency  $\nu$  and by letting

$$\omega_p^2 \rightarrow \omega_p^2 (1 - i\nu/\omega)$$

$$\omega^2 \rightarrow (\omega - i\nu)^2$$

in 2.2. This gives

$$K_R = 1 - \frac{\omega_p^2 (\omega^2 + \nu^2 - \omega_c^2)}{(\omega^2 - \nu^2 - \omega_c^2)^2 + 4\nu^2 \omega^2} \quad (2.9)$$

$$K_I = \omega_p^2 (\nu/\omega) \frac{(\omega^2 + \nu^2 + \omega_c^2)}{(\omega^2 - \nu^2 - \omega_c^2)^2 + 4\nu^2 \omega^2}$$

The most significant change in  $K_I$  is that collisions create a Lorentzian peak in  $K_I$  of half width  $\Delta(\omega_c/\omega) = 2\nu/\omega$  located at  $\omega_c/\omega \approx 1$ .

In Figure 2.2  $K_I$  is given for  $\nu/\omega = 0$  for several

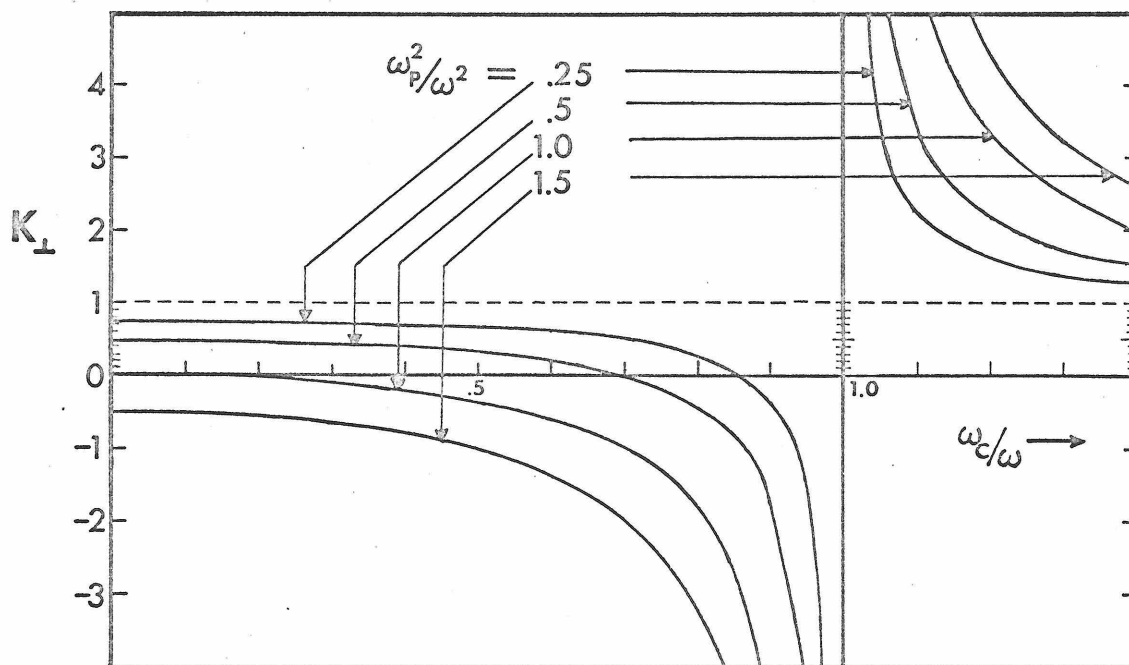


Figure 2.2  $K_I$  vs.  $\omega_c/\omega$  for a cold, collisionless plasma

densities.

### 2.3 Nonuniform Cold Plasma

A completely uniform plasma is not physically obtainable in the laboratory. Boundary conditions require that the plasma density go to zero at both the center wire and outside wall, leading to sheath regions. A shielded lead supporting the outer wire introduces further density gradients. An axial magnetic field reduces drift across the plasma column so that in the positive column of a cathode produced discharge the radial and azimuthal density profile depends primarily on the emission uniformity of the cathode's surface. As  $\omega_c$  is lowered, however, increased radial diffusion alters the large field density profile.

The primary effect of a radial density profile is to add a resistive component to the plasma admittance which is nonzero whenever a layer of plasma is resonant at the upper hybrid frequency. In Appendix I it is shown that the normalized admittance of a cylindrical capacitor is

$$\frac{Y}{Y_0} = \frac{\ln(B/A)}{B \int_A \frac{dr}{r K_{\perp}(r)}} \quad (2.10)$$

where  $K_{\perp}(r) = 1 - \omega_p^2(r)/(\omega^2 - \omega_c^2)$ .

In the limit that the plasma is uniform, equation 2.10 reduces to Equation 2.6. Depending on the choice of density profile, equation 2.10 can be either explicitly or numerically integrated if care is taken to include the pole in the denominator that occurs when  $\omega_c/\omega$  is

in the upper hybrid range and satisfies  $(\omega_c/\omega)^2 = 1 - \omega_p^2(r)/\omega^2$  [18].

Equation 2.10 was integrated for a parabolic density profile

$$\omega_p^2(r) = \omega_{po}^2 \left( 1 - \frac{(r^2 - A^2)}{(B^2 - A^2)} \right)$$

and the results presented in Figure 2.3. In Figure 2.3 the peak density  $\omega_{po}^2$  equals that of the uniform plasma. The zero of susceptance and the level of the susceptance curves is not altered greatly from the uniform plasma case, although the average density for the nonuniform plasma is only 50% that of the uniform plasma. These results show that the susceptance primarily depends on the peak density (near the center wire) rather than the average density. This is because the  $1/r$  electric field variation emphasizes contributions to the admittance from regions close to the center wire.

As seen in Figure 2.3, the parabolic density profile gives rise to a far greater normalized conductance than do collisions for reasonable values of  $\nu/\omega$ . In terms of an equivalent circuit model for the plasma capacitor, it is seen that the presence of a hybrid layer within the capacitor adds a series resistance to the plasma impedance (see Appendix I).

#### 2.4 Effect of the Probe Sheath on the Cold Plasma Admittance

As previously mentioned, boundary conditions requiring that the plasma density go to nearly zero at the walls and probes lead to sheath regions near the center wire and outside capacitor wall. It has been shown [19] that the rf properties of the sheath can be approximated by assuming that the sheath is a vacuum region  $\approx 5$  Debye

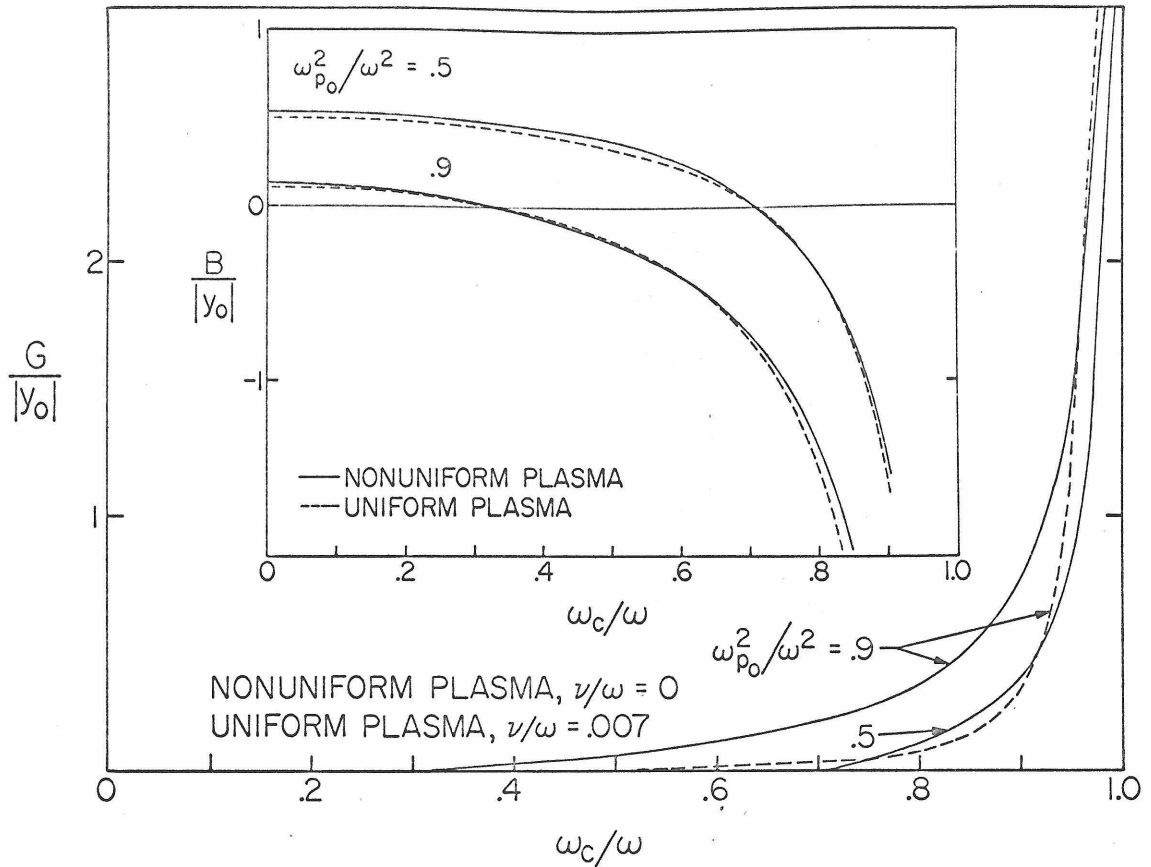


Figure 2.3 Normalized conductance and susceptance for a coaxial plasma capacitor with a parabolic density profile

lengths thick.

The capacitor's impedance is now modified by the presence of a series sheath capacitance whose primary effect on the susceptance will be to lower the average plasma density in the capacitor. Also, Harp, Kino, and Pavkovich [20] and Gould [21] have shown that electron transit time effects in the sheath contribute to the dissipative component of the plasma admittance.

In Figure 2.4 is shown the model of the plasma capacitor with a vacuum sheath around the center wire (radius =  $R_0$ ). A sheath at the

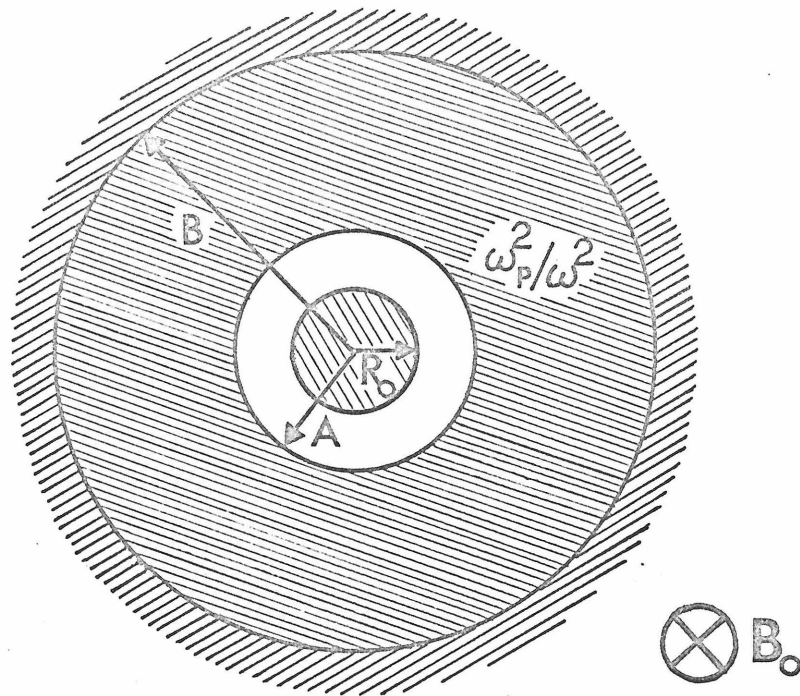


Figure 2.4 Uniform plasma capacitor with vacuum sheath around center wire

outside boundary is not included because  $B \gg A$  so that small changes in  $B$  would have only slight effect on the admittance.

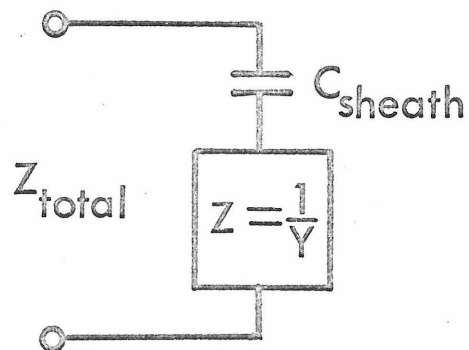


Figure 2.5 Equivalent circuit model for probe sheath

It is easily shown that (Figure 2.5)

$$(Y_{\text{tot}}/Y_o) = \frac{Z_o}{Z_{\text{tot}}} = \frac{Y/Y_o}{1 + \frac{\ln(A/R_o)}{\ln(B/R_o)} (Y/Y_o)} \quad (2.11)$$

Referring to equations 2.10 and 2.11 and Figure 2.3, the conductance of a plasma capacitor with a radial density profile and a vacuum sheath around the center wire will not maximize at  $\omega_c/\omega = 1$ . Instead it will maximize at the series resonance occurring between the sheath capacitance and the plasma inductance (the plasma admittance is negative in the hybrid range), and be small at  $\omega_c/\omega = 1$  where  $Y/Y_o \rightarrow \infty$ . For  $\omega_p^2/\omega_{\text{max}}^2 \approx 0$  the conductance maximum will occur just below  $\omega_c/\omega = 1$ . As the maximum plasma frequency increases in the capacitor, the location of the maximum of conductance shifts, towards lower values of  $\omega_c/\omega$ .

### 2.5 Effect of Losses on the Measured Admittance

In a very long coaxial capacitor filled with a spatially uniform cold plasma, the only loss mechanism in our model is collisions. In an experiment we would measure  $Y/Y_o = K_{\text{eff}}(\omega_{po}^2)$  where  $K_{\text{eff}}$  is the effective longitudinal dielectric constant.

Additional losses can come from a hybrid layer, from sheath transit time effects, and from electromagnetic dipole radiation out of the plasma. For the case in which density inhomogeneities are present, Appendix I shows a series resistance  $R$  is added to the plasma impedance. If the inhomogeneities are such that  $\langle \omega_p^2 \rangle \approx \omega_{po}^2$  then the admittance measured is

$$\frac{Y}{Y_0} \approx \frac{K_{\text{eff}}}{\left(1 + \frac{R}{Z_0} K_{\text{eff}}\right)} \quad (2.12)$$

From 2.12 we find that  $B/|Y_0|$  decreases for  $\omega_c/\omega$  in the hybrid range just as if the actual density were higher than it is.

### Chapter 3

#### HOT PLASMA THEORY OF THE ADMITTANCE OF A COAXIAL PLASMA CAPACITOR

##### 3.1 Introduction

Computing the admittance of a plasma capacitor becomes far more complex if the electron temperature is no longer assumed to be zero. For  $T_e > 0$  the dielectric tensor  $\underline{K}$  becomes a complex function of the wave vector  $\underline{k}$  and the frequency  $\omega$ . I. B. Bernstein was among the first to correctly use inversion techniques to find the dispersion relation  $K_{xx} = 0$  for longitudinal oscillations propagating perpendicularly to an external magnetic field in the x-direction [10]. These oscillations, cyclotron harmonic waves, have been the subject of intensive study during the past decade [1] and will be shown in this chapter to produce striking differences between the admittance of a cold plasma and the admittance of a hot plasma. Because the electric field in the capacitor is everywhere radial to the center wire, only the perpendicular component of the hot plasma dielectric constant is needed to describe the propagation of cyclotron harmonic waves. It has been shown [22,12] that the perpendicular dielectric constant for propagation in cylindrical geometry is identical with the  $K_{xx}$  element of the dielectric tensor for Cartesian geometry with the substitution of the perpendicular wave number  $k$  for  $k_x$ , the wave number for propagation in the x direction.

##### 3.2 The Perpendicular Dielectric Constant $K_{\perp}(\omega, k)$

For a Maxwellian electron velocity distribution, the perpendicular dielectric constant is

$$K_{\perp}(\omega, k) = 1 - \frac{(\omega - i\nu)}{\omega} \frac{\omega_p^2}{\omega_c^2} \frac{e^{-\lambda}}{(\lambda/2)} \sum_{n=1}^{\infty} \frac{I_n(\lambda)}{\left(\frac{\omega - i\nu}{n\omega_c}\right)^2 - 1} \quad (3.1)$$

where  $\lambda = (k v_{th}/\omega)^2$  and  $v_{th} = \sqrt{kT_e/m}$  = the mean square electron velocity for 1 degree of freedom and  $\nu$  is a phenomenological collision frequency [23]. The derivation of equation 3.1 is outlined in Appendix II.

If the admittance of an infinitely long cylindrical capacitor in a collisionless plasma could be measured at one value of  $k$ , the normalized susceptance  $B/|Y_0| = \text{Re}(K_{\perp})$  would behave as shown in Fig. 3.1 where  $\text{Re}[K_{\perp}(\omega, k)]$  is plotted up to the 5th harmonic for various values of  $k$  with  $kT_e = 5\text{ev}$ , and  $\omega_p^2/\omega_c^2 = .5$ . For  $k = 0$   $K_{\perp}(\omega, k)$  reduces to the cold plasma value. As  $k$  increases from zero, discontinuities appear at each harmonic. Between the higher harmonics for low  $k$ , the average level of the curves initially falls below the cold plasma level. As  $k$  increases yet further, the size of the discontinuities at first grows, reaches a maximum near  $k = 30\text{cm}^{-1}$  and then decreases until at  $k = \infty$ ,  $K_{\perp} = 1$ . If  $k$  were held fixed and the electron temperature varied, similar curves would result, since the relevant parameter is  $\lambda$ . Only for a cold plasma ( $\lambda = 0$ ), does  $\text{Re}[K_{\perp}] = 0$  mark the location of the upper hybrid frequency (UHF) where  $\omega^2 = \omega_p^2 + \omega_c^2$ .

In the quasi-static approximation, two types of signals can propagate perpendicular to the magnetic field for  $\omega_c/\omega \leq 1$ . The

first is a direct coupled signal in which the electric field obeys the relation  $\underline{D} = \epsilon_0 K \underline{E}$  where  $\nabla \cdot \underline{D} = \text{real charge density}$ . A second signal propagates as a slow longitudinal wave called a cyclotron harmonic wave (CHW). These waves satisfy the dispersion relation  $K_{\perp} = 0$  which is plotted in Fig. 3.2 for a Maxwellian velocity distribution with  $v/\omega = 0$ . These waves propagate without damping since the solutions to  $K_{\perp} = 0$  are purely real  $k$  for real  $\omega$ .

Connected with each harmonic is a passband in which longitudinal waves can propagate. Resonances ( $k \rightarrow \infty$ ) occur on the low  $\omega_c/\omega$  side of each harmonic while cutoffs ( $k \rightarrow 0$ ) approach each harmonic from both sides. As the density is increased from zero, the location of the UHF (at  $k = 0$ ) moves up the  $\omega/\omega_c$  axis. When its

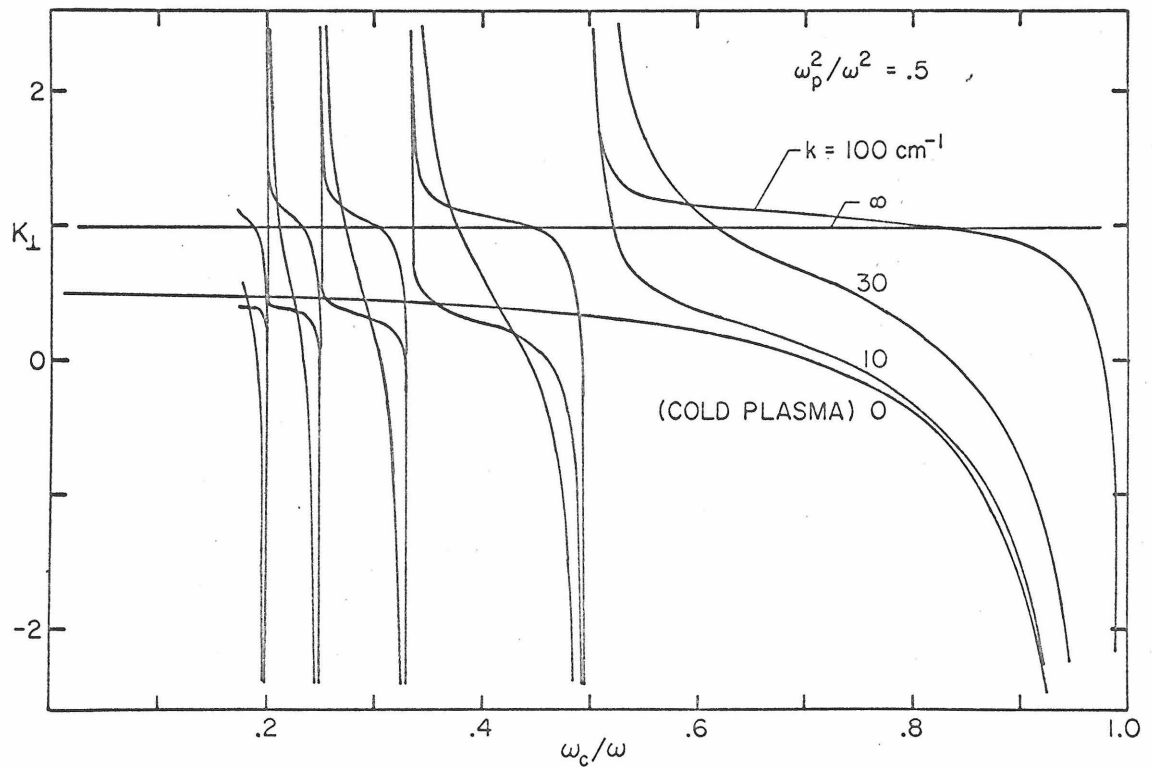


Figure 3.1. Hot plasma dielectric constant  $\text{Re}(K_{\perp})$  for various  $k$  with  $\omega_p^2/\omega^2 = .5$  and  $kT_e = 5 \text{ eV}$ .

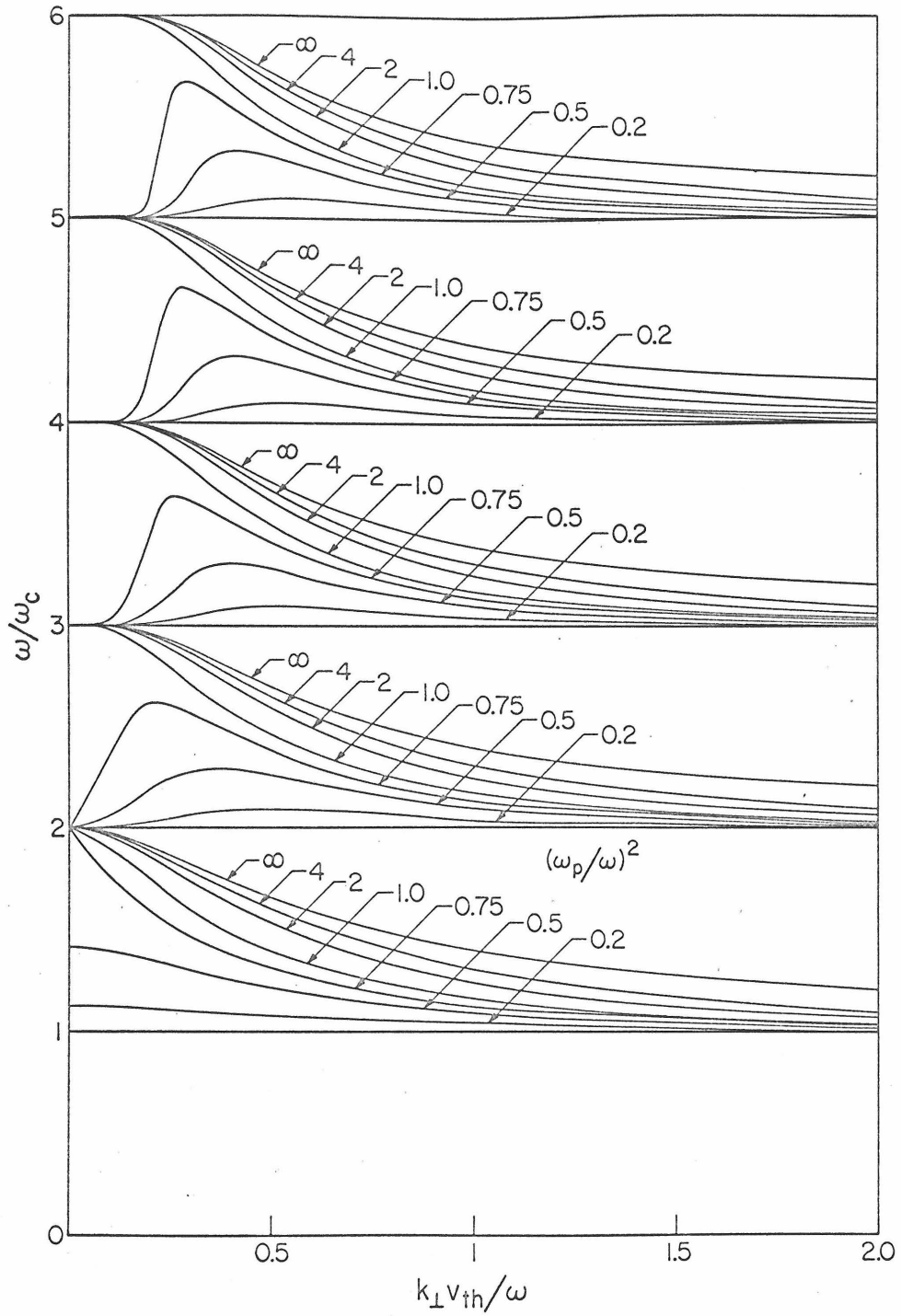


Figure 3.2 The dispersion relation  $K_{\perp} = 0$  for CHW propagating at right angles to the magnetic field in a plasma with a Maxwellian electron velocity distribution

location crosses each harmonic above the first, the dispersion relation changes from having two real solutions to having just one solution. The curves satisfying  $K_{\perp} = 0$  become a more rapidly changing function of  $k$  as  $\omega_p^2/\omega^2$  increases from zero.

Collisions round out the resonances in  $\text{Re}[K_{\perp}]$ , producing at each harmonic  $N$ , peaks in  $\text{Im}[K_{\perp}]$  of half width  $2\nu/N$  displaced slightly below the harmonic whose height scales as  $\omega_p^2/\nu$  for a given  $\lambda$ . At a harmonic  $\text{Im}[K_{\perp}]$  varies with  $k$  as shown in Figure 3.3. For  $kT_e = 5\text{eV}$ ,  $\nu/\omega = .02$  the maximum value occurs for  $k \sim 30 \text{ cm}^{-1}$ . This curve shows that the departures from cold plasma theory are greatest for a certain range of  $k$  largely independent of harmonic number.

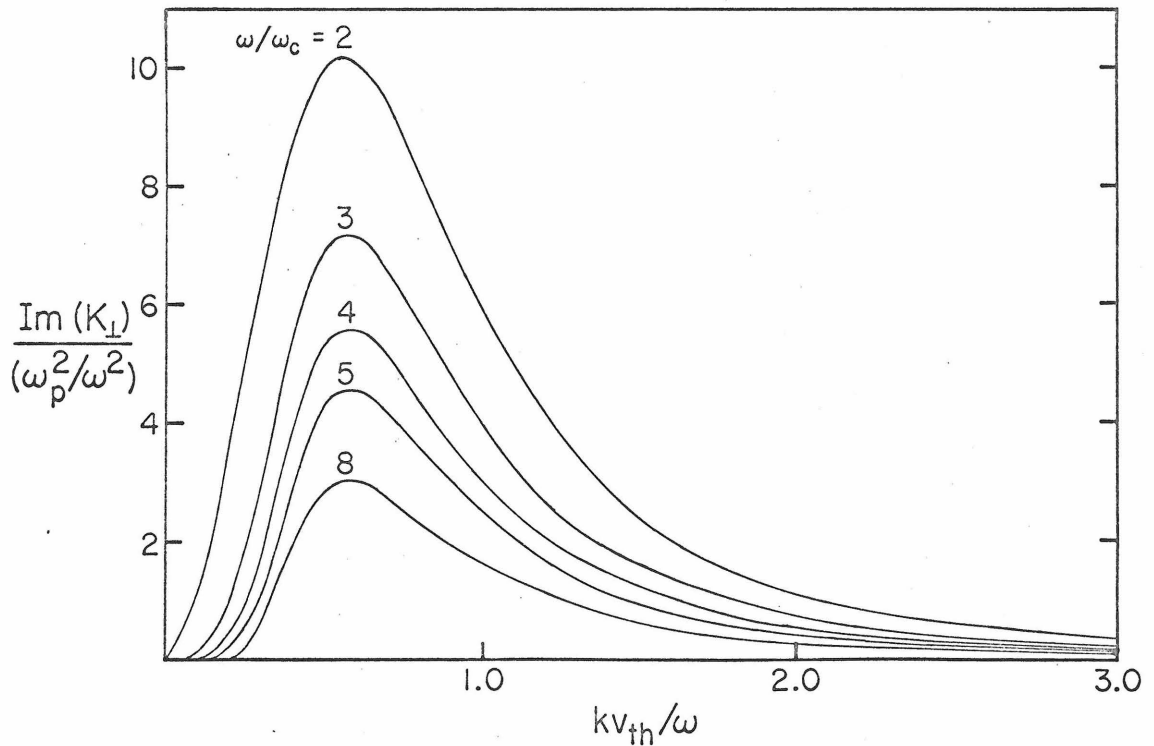


Figure 3.3  $\text{Im}(K_{\perp})$  at the harmonics vs.  $kv_{th}/\omega$  for  $\nu/\omega = .02$

### 3.3 The Transparent Cylinder Admittance Model

The admittance of a plasma capacitor will be some average over  $k$  of  $K_{\perp}(\omega, k)$ . The discussion of the previous section predicts discontinuities in the normalized susceptance and peaks in the normalized conductance, but cannot predict detailed behavior as either  $\omega_p^2$  or  $\omega_c$  is varied.

Crawford, Mantei and Tataronis [13] treated the plasma capacitor as a boundary value problem but their theoretical results for  $Y/|Y_0|$  predicted standing wave resonances which do not occur experimentally [24]. The primary difficulty with their formulation is the assumption of specular reflection of the electrons at the outer capacitor wall. If specular reflection of the electrons in the outward propagating cyclotron harmonic waves is assumed, then standing waves would naturally be set up within the volume of the capacitor. In real experiments, however, the physical properties of a plasma discharge and its behavior in a magnetic field such as collisions, transit time effects, instabilities, an unsymmetric density inhomogeneity, all would tend to decrease the coherent specular reflection of cyclotron harmonic waves.

In formulating our model, the following considerations were thought to be important. We consider an axial wire surrounded by a sheath. Harp [18] has shown that the rf sheath properties can be approximated by a vacuum region about 5 Debye lengths thick. Since longitudinal waves do not propagate through a vacuum sheath, the sheath itself is taken to be the launch site for the waves. Numerous experiments have demonstrated the presence of propagating waves in regions

near the center wire [25,26,2]. Since the electrostatic field falls off as  $1/r$ , the main contribution to the admittance comes from regions close to the center wire. Collisions, transit time effects, damping of the wave in the outside sheath, turbulence at the outer boundary, and conversion of the cyclotron harmonic waves in a hybrid layer into transverse electromagnetic waves all would tend to decrease the outside capacitor walls' influence on the standing wave contributions to the admittance [27,28].

A radial density profile can lead to standing longitudinal oscillations set up between the hybrid layers in the column [29]. However, this effect only seems prominent when transverse e.m. waves are scattered from the outside of a plasma column. Using rf probes several authors have investigated the interior of a plasma column excited by an outside dipole source [26,30]. Their studies indicate that the major component of the rf signal picked up by the probe represents the sum of a traveling wave and a direct coupled signal.

As a reasonable theoretical approximation, we assume the plasma to be infinite in size and measure the admittance between the cylindrical sheath at  $r = A$  and a transparent cylindrical grid located at the wall of the physical capacitor  $r = B$  (see Figure 2.4). This grid samples the outside potential, leaves the electrons free to move, and draws no current from the plasma. The sheath size affects the upper limit on  $k$  values averaged over in the admittance, while the outer radius affects the lower limit. The spacing of CHW interference oscillations in the admittance will depend linearly on the outside radius of the grid, but the amplitude of the admittance

is insensitive to the exact value of B . Because the potential varies as  $\ln(B/A)$ , the amplitude of the admittance changes slowly as B changes. A change in (B/A) by a factor of  $e = 2.72$  changes  $\ln(B/A)$  by less than 25% for the present experiment.

In the electrostatic approximation the rf potential in cylindrical coordinates set up by an oscillating cylindrical sheath of radius A is described by the Hankel transform of Poisson's equation\*

$$k^2 \phi(k) = \frac{\lambda(k)}{\epsilon_o K_{\perp}(\omega, k)} \quad (3.2)$$

where an  $e^{i\omega t}$  time dependence is assumed and the Hankel transform of the charge per unit length on the sheath is given by

$$\lambda(k) = (\lambda_o/2\pi) J_o(kA) . \quad (3.3)$$

Solving for  $\phi(k)$

$$\phi(k) = \frac{(\lambda_o/2\pi) J_o(kA)}{k^2 \epsilon_o K_{\perp}(\omega, k)} \quad (3.4)$$

Taking the inverse Hankel transform  $H^{-1}(\phi(k))$  of 3.4 to find the radial potential distribution

$$H^{-1}\{\phi(k)\} = \phi(r) = \int_0^{\infty} k \frac{\lambda_o J_o(kA)}{k^2 \epsilon_o K_{\perp}(\omega, k)} J_o(kr) \frac{dk}{2\pi} \quad (3.5)$$

Using equation 3.5  $\Delta V = \phi(A) - \phi(B)$ , and from charge conservation, the radial rf current per unit length is  $I = i\omega\lambda_o$  . Thus,

---

\* 
$$f(r) \equiv \int_0^{\infty} kF(k) J_o(kr) dk$$

$$\begin{aligned}
 Y/Y_0 &= \frac{I/\Delta V}{Y_0} = \ln(B/A) \left\{ \int_0^{\infty} dk \frac{J_0(kA) [J_0(kA) - J_0(kB)]}{k K_{\perp}(\omega, k)} \right\}^{-1} \\
 &= K_{\text{eff}} = K_R = iK_I
 \end{aligned}
 \tag{3.6}$$

At high densities equation 3.6 also predicts an oscillating series of maxima and minima below the harmonics. If  $k$  is such that an integral number of half wavelengths fit between the probe sheath and the grid at the same time that  $K_{\perp}(\omega, k)$  becomes small, then the admittance will show maxima and minima as  $\omega_c$  is varied. The spacing of these oscillations depends primarily on the outside radius  $B$  of the capacitor.

The integral in 3.6 must be evaluated numerically, but it is first possible to infer some of its properties by inspection. Since the term  $F(k) = J_0(kA) [J_0(kA) - J_0(kB)]$  weights low values of  $k$  heavily for the values of  $A$  and  $B$  employed in the experiment to be discussed in the next chapter, the normalized susceptance plots are expected to have their  $B/|Y_0| = 0$  point close to the location of the cold plasma upper hybrid frequency. Because  $F(k)$  oscillates with a fast and slow frequency component determined by  $A$  and  $B$  respectively, the integral's behavior is more sensitive to changes in  $A$  than in  $B$ .

### 3.4 Low Density Expansion for the Normalized Conductance

At low density ( $\omega_p^2/\omega^2 \ll 1$ ) a simple expression for  $K_{\perp} = G/|Y_0|$  may be found by assuming  $K_{\perp}(\omega, k) \approx 1 - \Delta(k)$  for all  $k$ . For  $v/\omega > 0$ , Fig. 3.3 shows this is valid for  $\omega_c/\omega < 1$  since  $\text{Im}(K_{\perp})$

maximizes for  $(kv_{th}/\omega) \sim .5$  at each harmonic. Since the maximum value of  $\text{Im}(K_{\perp})$  decreases with increasing harmonic number, this approximation improves with increasing harmonic number. Expanding equation 3.6

$$Y/Y_0 = \ln(B/A) \left\{ \int_0^{\infty} \frac{dk}{k} J_0(kA) [J_0(kA) - J_0(kB)] (1 + \Delta(k) + \Delta^2(k) + \dots) \right\}^{-1} \quad (3.7)$$

Using the integral  $\ln(B/A) = \int_0^{\infty} dk [J_0(kA) - J_0(kB)] J_0(kA)/k$ ,

$$Y/Y_0 \approx \ln(B/A) \left\{ \ln(B/A) + \int_0^{\infty} \frac{dk}{k} J_0(kA) [J_0(kA) - J_0(kB)] \Delta(k) \right\}^{-1}$$

If  $\Delta(k)$  is small, the integral is itself small since it must be less than  $\Delta(k)|_{\max} \ln(B/A)$ . Expanding once more and using 3.1 for  $\Delta(k) = 1 - K_{\perp}(\omega, k)$

$$Y/Y_0 = K_{\text{eff}} \approx 1 - \frac{(1 - i \frac{v}{\omega}) \frac{\omega_p^2}{\omega_c^2}}{\ln(B/A)} \sum_{n=1}^{\infty} \frac{F_n(\omega_c)}{(\frac{\omega - i v}{n \omega_c})^2 - 1} \quad (3.8)$$

where

$$F_n(\omega_c) = \int_0^{\infty} \frac{dk}{k} \frac{e^{-\lambda I_n(\lambda)}}{(\lambda/2)} J_0(kA) [J_0(kA) - J_0(kB)]$$

At the  $n^{\text{th}}$  harmonic only the  $n^{\text{th}}$  term contributes appreciably, so writing  $K_{\perp}$  in partial fractions we obtain

$$G/|Y_0| = K_{\perp} = \frac{n^2 v \omega_p^2}{2\omega} \frac{F_n(\omega_c)}{\ln(B/A)} \left[ \frac{1}{(\omega - n\omega_c)^2 + v^2} + \frac{1}{(\omega + n\omega_c)^2 + v^2} \right] \quad (3.9)$$

Since the second term is negligibly small, for low densities we expect Lorentzian shaped peaks whose height varies linearly with  $\omega_p^2/v$ .

### 3.5 The Admittance for Two-Probe Transmission

Mantei has shown that the transmitted signal between two probes can be expressed in terms of the plasma admittance between the probes [3]. In the limit that the rf voltage on the transmitting probe is held constant and the plasma impedance between the probes is much greater than the input impedance of the receiving probe and detector (Figure 3.4), the detected signal (using a square law detector) is proportional to  $|Y(t \rightarrow r) / Y_0(t \rightarrow r)|^2$  where  $Y(t \rightarrow r)$  is the admittance between transmitting and receiving probes and  $Y_0(t \rightarrow r)$  is the vacuum admittance between the probes.

Although based on a slightly different set of assumptions, the expression for this admittance is identical to equation 3.6 if  $B$  is considered to be the separation of the probes immersed in an infinite plasma and if the launch site of the cyclotron harmonic waves is taken to be the sheath at  $r = A$ . If the probes are far apart, the receiving probe is a negligibly small perturbation on the rf field around the transmitting probe which should be purely radial if the plasma boundaries are far away. Under these conditions the receiving probe acts to sample the radial rf field as if it were part of a cylindrical concentric grid around the sending probe. The received signal will thus be proportional to the admittance between the center probe and the outer concentric shell of radius  $B$ . Equation 3.6 can thus be used to calculate the normalized admittance between two probes.

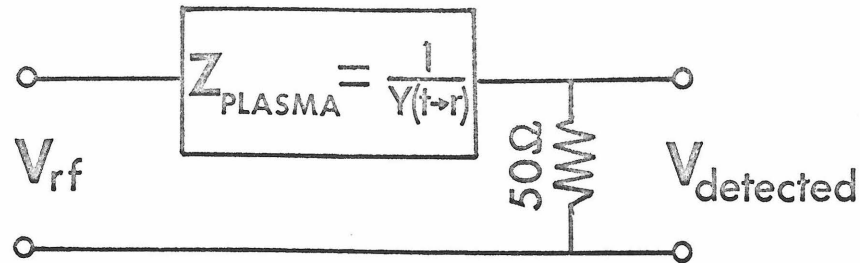


Figure 3.4. Admittance Model for Two-Probe Transmission

### 3.6 Limitations of the Admittance Model

In addition to neglecting the finite capacitor length, stray admittance to the insulated coax supporting the center wire, or radiation, this admittance model neglects the effects of a density profile.

In most cases, the effect of the experimental density profile will be sufficiently small that we may still expect reasonable agreement with theory. The plasma density remains essentially uniform over a distance  $R$  in which the potential difference  $\phi(A) - \phi(R)$  reaches greater than 80% of its value at the outside cylinder (see Section 4.2).

CHW interference effects will be modified by the nonuniformity. As a cyclotron harmonic wave propagates outward through a density profile, its  $k$  value changes and the wave can be reflected by a hybrid layer before reaching the outside wall. The primary hot plasma effect of a density profile on the admittance will be to average out some of the cyclotron harmonic interference effects that depend most strongly

on density uniformity. Only as the density becomes large and the dispersion relation insensitive to changing density will interference effects appear strongly.

At  $\omega = n\omega_c$  the integral weights values of  $k$  close to zero most heavily. Because the dispersion relation is roughly independent of density at  $\omega = n\omega_c$  near  $k = 0$ , the agreement between experiment and theory is expected to be good at the harmonic conduction peaks. Also, since waves generated just above the harmonics have low group velocity for low density, they are attenuated by collisions in regions close to the center wire before either the outer boundary or density gradient can influence propagation.

The effect of the sheath on the plasma admittance can be approximated by including a vacuum sheath explicitly in the formulation for the admittance in a manner identical to that done for the cold plasma model discussed in Section 2.3.

### 3.7 Numerical Computations

Equation 3.6 was integrated numerically for values of  $\omega_p^2/\omega^2$  from .05 to 1.1 and for  $\omega_c/\omega$  from .1 to 1. The perpendicular electron temperature was taken to be 5 eV to compare with experimental conditions.  $\nu/\omega$  was chosen to be .005 for the computer plots of the normalized admittance and conductance shown. Other values of  $\nu/\omega$  were investigated to study harmonic line shape and peak height variation. The value of  $B$  was taken to be the outside radius of the experimental capacitor and the effective sheath radius  $A = .06$  cm approximates the expected sheath thickness for  $\omega_p^2/\omega^2 \sim .3$ . The value of  $A$  was not adjusted to vary with density in the calculation

because the computation time would have increased substantially.

The integration routine for evaluating equation 3.6 was optimized to minimize computation time (2-3 seconds per value of  $\omega_c/\omega$  on an IBM 360/75). When the first value of  $\omega_c/\omega$  was called by the program, the value of  $J_0(kA)[J_0(kA) - J_0(kB)]/k$  was computed once for each value of  $k$  used in the Simpson's rule integration subroutine and stored for later use when other values of  $\omega_c/\omega$  were called.  $K_{\perp}(\omega, k)$  was evaluated by setting

$$K_{\perp}(\omega, k) = 1 - \frac{(\omega - i\nu)}{\omega} [\omega_p/\omega_c]^2 \arg(\omega, k)$$

and

$$\arg(\omega, k) = \frac{\exp[-\lambda]}{(\lambda/2)} \sum_{n=1}^{\infty} \frac{I_n(\lambda)}{(\frac{\omega - i\nu}{n\omega_c})^2 - 1}$$

where  $\lambda = (kv_{th}/\omega_c)^2$ .

The quantity  $\arg(\omega, k)$  was evaluated once for each value of  $\omega_c/\omega$  used for each value of  $k$  called for in the integration routine.

$\arg(\omega, k)$  was stored and used to calculate  $K_{\perp}(\omega, k)$  for each value of  $\omega_p^2/\omega^2$  wanted. This allowed the admittance for twelve densities to be calculated in only slightly more time than would have been required to calculate the admittance for one density.  $\arg(\omega, k)$  was evaluated by computing the two highest  $n$  values of  $I_n(\lambda)$  needed for accuracy and computing all other  $I_n(\lambda)$  using a backwards recursion relation.

Chapter 4

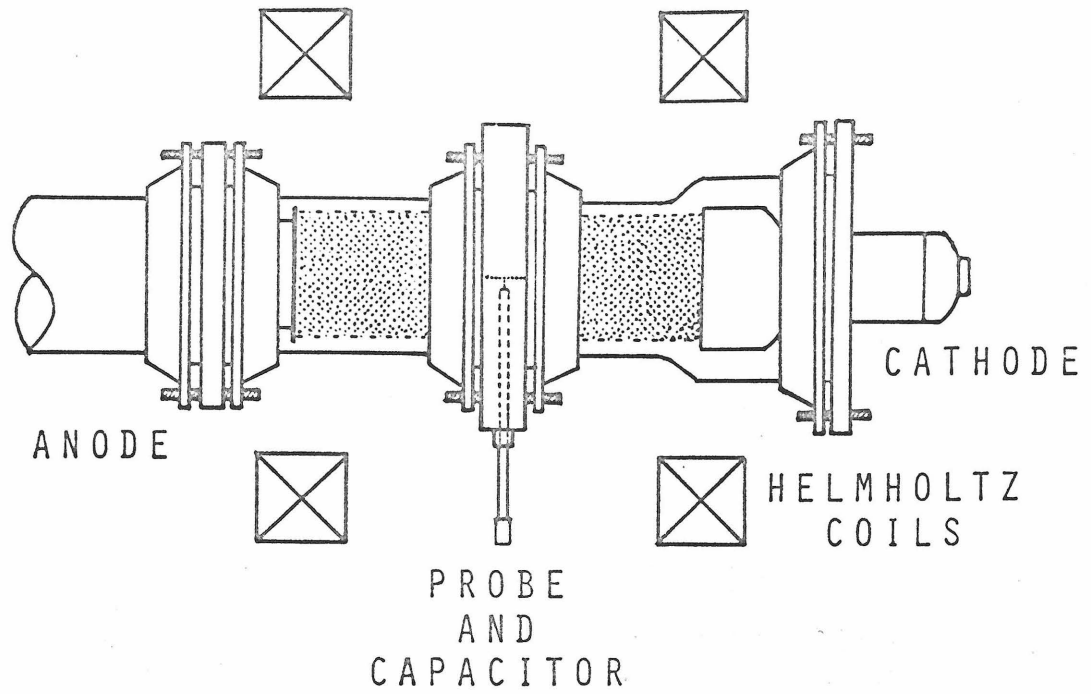
EXPERIMENTAL MEASUREMENT OF THE COMPLEX ADMITTANCE  
OF A CYLINDRIC PLASMA CAPACITOR

4.1 The Plasma

The experiments were carried out in the positive column of a hot cathode argon DC discharge (Fig. 4.1). The plasma column (26 cm in length) was produced in a 7.5 in. ID discharge tube constructed from Pyrex glass pipe. The cathode had a 6 cm diameter flat nickel surface which was oxide coated. It was uniformly heated from behind by helical bifilar filaments. The cathode was cleaned, rebuilt (when needed), coated with oxide and activated by procedures which are described by Rosebury [31].

The discharge tube was connected to a vacuum system which was capable of producing ultimate pressures of  $< 5 \times 10^{-7}$  torr. Initially activated cathodes poisoned (emission dropped) after only several days' use. This was found to be caused by the silicon diffusion pump oil (DC705). DC705 diffusing into the discharge volume left an insulating silicon monoxide coating on the cathode surface. This problem was remedied by changing to an organic diffusion pump oil and by placing an absorption baffle between the diffusion pump and the discharge volume.

The plasma discharge had a cathode-anode voltage drop of 14-18 volts when properly activated. Under ideal conditions the discharge voltage remained constant within several volts as the magnetic field was varied or as the discharge current changed. At low discharge



.2 MM TUNGSTEN WIRE PROBE  
← 5 CM →

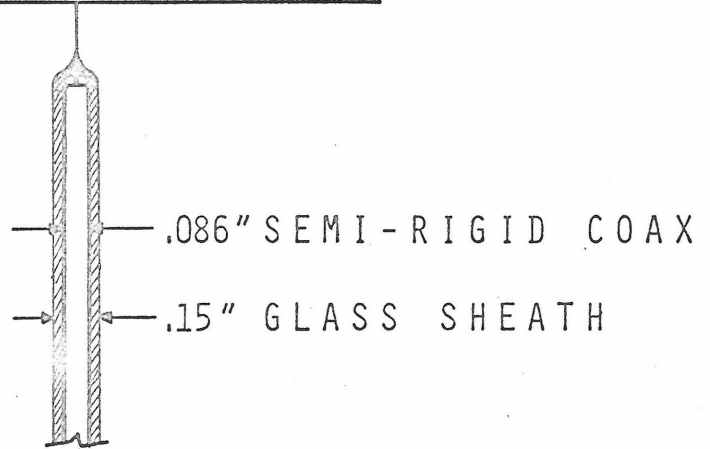


Figure 4.1 Experimental Apparatus and Probe Assembly

voltages the plasma was relatively quiet as measured by the level of the probe open circuit voltage. At higher voltage drops the plasma became noisy and generally unstable. Discharge currents from  $\sim 10$  milliamps to 2 amps were used to produce plasma electron densities from  $10^8 \rightarrow 10^{10}/\text{cm}^3$ . The plasma density is measured in terms of the normalized plasma frequency  $\omega_p^2/\omega^2$ . The neutral gas pressure as measured with a nude ionization gauge was  $\sim 10^{-3}$  torr and was chosen to minimize the discharge voltage and the plasma noise.

#### 4.2 Plasma Uniformity

The plasma radial density profile depended largely on the uniformity of emission of the oxide cathode. Under the best conditions radial density profiles existed in the column which varied with discharge current and magnetic field. The radial density profile was measured using a Langmuir probe, 3 mm long, oriented perpendicular to the magnetic field. The theory for a Langmuir probe in a magnetic field is exceedingly complicated [32], but it is possible to get a relative measure of density from the ion saturation current at a given bias voltage and a measure of the electron temperature from the slope of the V-I characteristics when the probe draws electron current.

Typical radial density plots are shown in Fig. 4.2. The ion saturation current is shown as a function of radius for various discharge currents ( $I_D$ ) and magnetic fields ( $I_B =$  magnet current). In most cases the discharge is essentially uniform (less than 10% density variation) out to 2 cm and then falls off toward the capacitor's wall. The radial density profiles obtained are typical of what can be expected for the positive column of an argon arc in a magnetic

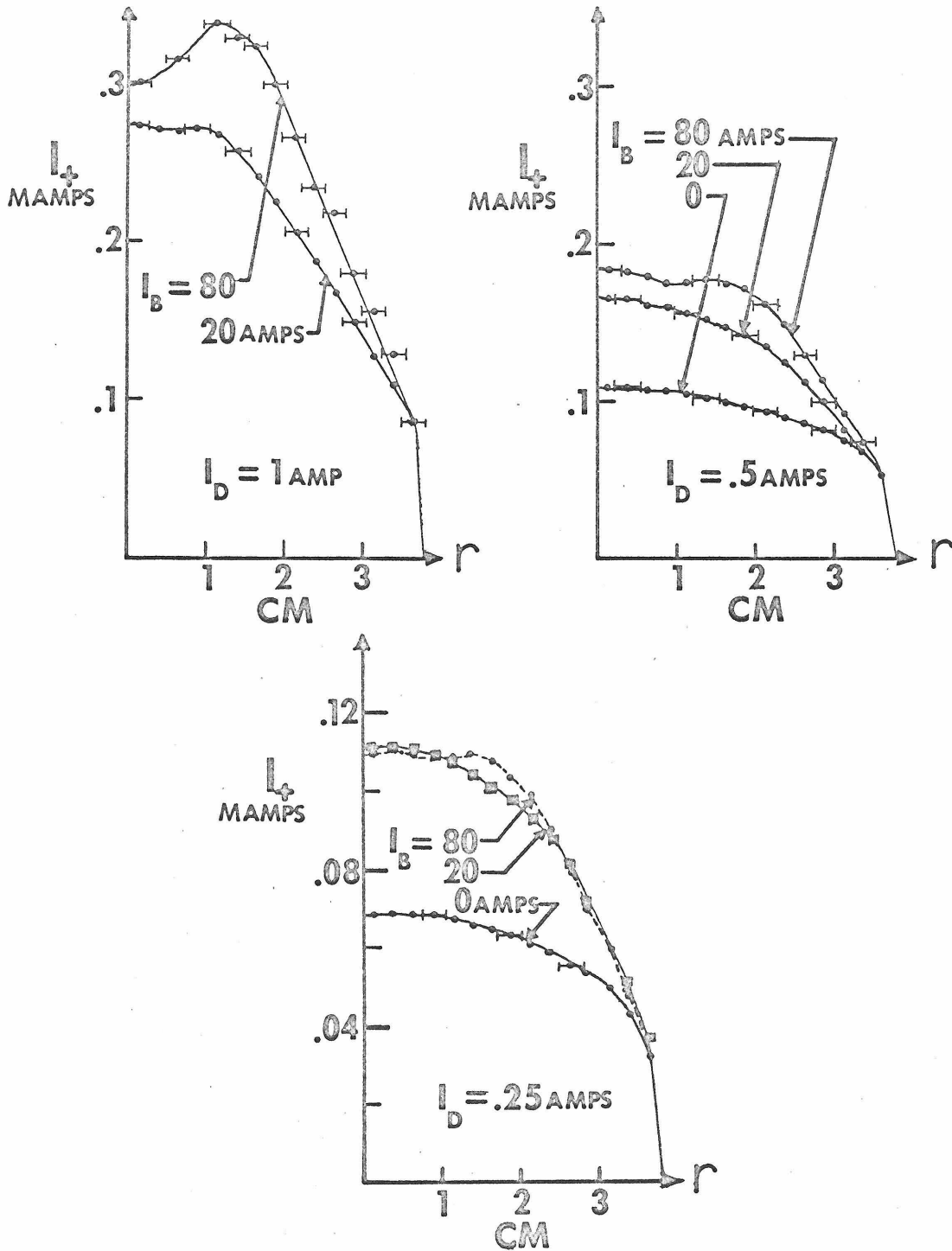


Figure 4.2 Langmuir probe ion saturation current  $I_+$  for various magnet currents  $I_B$  and discharge currents  $I_D$ . Neutral gas pressure =  $1.3 \times 10^{-3}$  torr argon.  $\omega_c = 812$  MHz for  $I_B = 100$  amps.

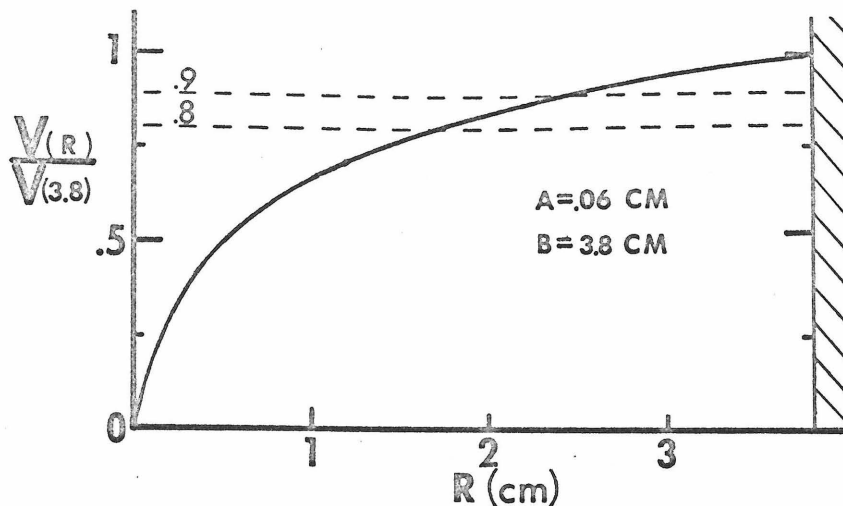


Figure 4.3 Fraction of full potential difference between the center wire ( $R = A$ ) and the capacitor's outer radius ( $R = B$ ) that is reached at radius  $R$

field [33]. In Fig. 4.3 is shown a plot vs. radius of the fraction of full potential reached in a cylindrical capacitor. For a capacitor with a 3.8 cm radius, about 85% of the full potential difference is reached at a radius of  $\approx 2$  cm from the column center.

Langmuir probe temperature measurements were also made and it was found that the electron temperature was constant out to about 2 cm. At larger radii the electron temperature slowly decreased toward the capacitor wall. Electron temperature data from the Langmuir probe indicated that  $kT_e \approx 4-5$  eV.

#### 4.3 The Magnetic Field

The plasma discharge was axial to a pair of Helmholtz coils. The plasma capacitor was situated between the two coils (Fig. 4.1) in

a region in which the field uniformity over the capacitor volume was  $\sim .1\%$  as measured with an NMR gaussmeter. The magnet current passed through a shunt to provide a voltage for an X-Y recorder proportional to the magnetic field. The magnet current could be slowly swept from its maximum to a preset minimum value. The magnetic field was calibrated in terms of the normalized cyclotron frequency  $\omega_c/\omega$ .

#### 4.4 The Plasma Capacitor

The plasma capacitor was an aluminum ring through which probes were inserted via rotating vacuum seals. The initial capacitor had an inside diameter of 7.6 cm and a length of 2.5 cm. A subsequent version of 6 cm diameter and 5 cm length was also used in an attempt to decrease fringing fields and increase density uniformity. No major changes resulted in changing the capacitor dimensions--a fact which gives credence to the assertion that the plasma close to the center probe has the predominant effect on the admittance.

Two rf probe assemblies and a Langmuir probe could be positioned radially to a precision of 1 mm in the capacitor. In transmission experiments both rf probes were used, while for admittance measurements the probe not in use was withdrawn into the outer plasma region. For general use, a carefully straightened tungsten wire probe  $\sim .2$  mm diameter, 5 cm long, was attached to a glass sheathed .086 cm semirigid coax (Figure 4.1) and aligned axial to the magnetic field. The semirigid coax, in turn, was vacuum sealed into a 1/4-inch piece of tubing which fed through the rotary vacuum seal in the aluminum ring. The probe wires were so built as to clip onto the

center conductor of the semirigid coax. A carefully matched rf connector was connected to the semirigid coax 1/4-inch tubing assembly outside of the plasma.

In an attempt to reduce the probe's influence to a minimum, probes made with .008-inch diameter semirigid coax were also used. This coax was sheathed in  $\sim$  .015-inch outside diameter capillary glass tubing for rigidity and connected to .002-inch diameter tungsten wire probes. The .002-inch diameter 5 cm long tungsten probes were held parallel and straight by tension supplied from  $\sim$  .01-inch glass fibers cemented to the capacitor wall. The small size of the wire probe also made it possible to excite cyclotron harmonic waves more strongly and to decrease the size of the probe sheath. It had the disadvantage that the probes could not be moved radially.

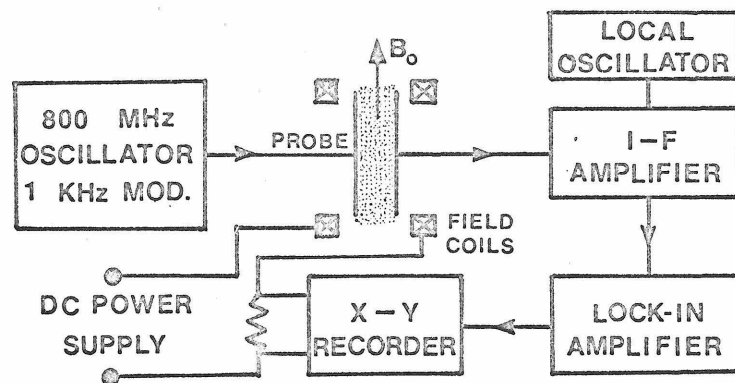


Figure 4.4 Experimental set-up for two-probe transmission measurements

#### 4.5 Two-Probe Transmission for Determining $\omega_p^2/\omega^2$ and $kT_e$

Transmission between two probes immersed in a plasma can be used to determine both the plasma density  $\omega_p^2/\omega^2$  and the electron temperature  $kT_e$  [2,30]. The experimental transmission set-up is shown in Figure 4.4. The minimum of transmission as the magnetic field ( $\omega_c/\omega$ ) is swept marks the location of the upper hybrid frequency  $\omega_H^2 = \omega_p^2 + \omega_c^2 = \omega^2$  where  $\omega_H$  is the upper hybrid frequency,  $\omega$  is the transmitted frequency,  $\omega_p$  = plasma frequency, and  $\omega_c$  = electron cyclotron frequency. The discharge can thus be calibrated in terms of  $\omega_p^2/\omega^2$  as found from transmission minima. The electron temperature is found from the spacing of the CHW oscillations in transmission which gives the wave number  $k$  at a given  $\omega/\omega_c$ . With the aid of a dispersion diagram (Figure 3.2),  $v_{th}$ , and thus  $kT_e$ , can be found.

#### 4.6 Experimental Methods of Measuring the Capacitor's Admittance

##### A. Direct Measurement of a Hot Plasma's Admittance at the Cyclotron Harmonics

In the first experiment the coax was connected to a phase sensitive admittance measuring system consisting of a GR 1602B admittance meter, a Relcom double balanced mixer, and a lock-in detector amplifier (Figure 4.5). The output junction voltage of the 1602B admittance meter is proportional to the total admittance, so by adjusting the reference phase either the conductance or susceptance could be measured and plotted directly on an X-Y recorder versus magnetic field ( $\omega_c/\omega$ ). The y axis was calibrated using the known normalized vacuum

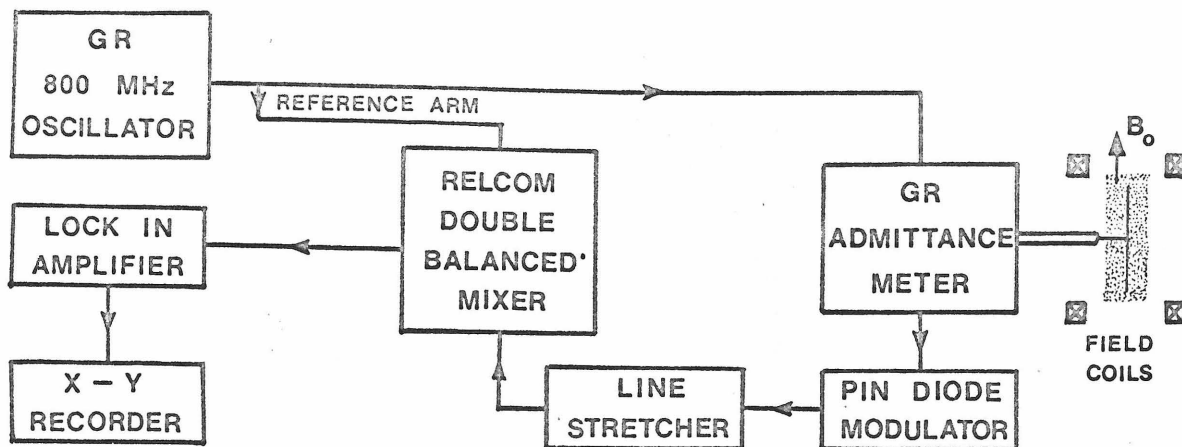


Figure 4.5 Phase sensitive admittance measuring system

susceptance  $B/|Y_0| = 1$ . The electrical length of the probe assembly was adjusted to be an integral number of half wavelengths from the junction of the admittance meter by slightly varying the frequency of the oscillator (freq.  $\sim 800$  MHz). The rf voltage at the bridge junction was held constant using a GR1263C amplitude regulating power supply. The plasma density was calibrated as a function of discharge current using the location of the upper hybrid frequency found in two-probe transmission measurements [2] and from the location of the zero susceptance point on susceptance records. The pressure was  $.9 \times 10^{-3}$  torr argon as measured with an ion gauge operating at reduced emission current. The perpendicular electron temperature was found using the spacing between oscillations in the two-probe transmission

records [2]. Depending on the discharge conditions and the magnetic field,  $kT_e$  was found to vary between 2 and 5 eV with the average value in the range 4-5 eV. Langmuir probe measurements produced similar results and showed that the electron temperature was essentially uniform out to the edge of the discharge. Using collision data from Brown's Basic Data of Plasma Physics, 1966 [34], the electron-neutral collision frequency was estimated to be  $\nu/\omega = .004$ .

B. Absorption of a Hot Plasma at the Cyclotron Harmonics

An indirect, but in certain limits valid, method of measuring the normalized conductance  $K_I = G/|Y_0|$  at the cyclotron harmonics is to measure the absorption coefficient of the plasma. This method was used to see if the conductance peaks could be used as a diagnostic tool when measured by a simpler method.

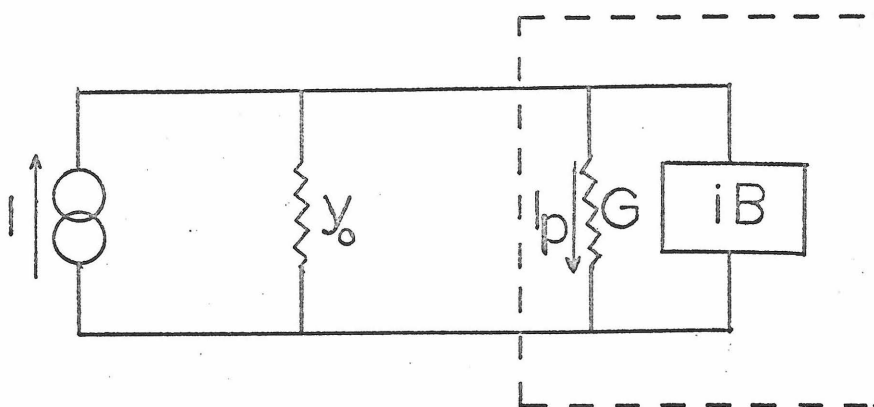


Figure 4.6 50 ohm rf generator connected through 50 ohm transmission line to the plasma capacitor's admittance (enclosed in dashed box).

Consider a transmission line (Figure 4.6) where  $Y = G + iB$  is the plasma admittance and  $y_o$  is the characteristic admittance of the transmission line (20 mmhos). The power absorbed by the plasma  $P_{abs}$  is given by

$$P_{abs} = i_p^2 / G = i^2 \left| \frac{G}{y_o + G + iB} \right|^2 \frac{1}{G} \quad (4.1)$$

The absorption coefficient is defined as the ratio of the absorbed power in the plasma to the power incident on a matched load.

$$\text{absorption coefficient} = A = \frac{P_{abs}}{P_{inc}} = \frac{4G/y_o}{\left| 1 + \frac{G}{y_o} + iB/y_o \right|^2} \quad (4.2)$$

From the direct measurement of the plasma admittance we know that  $G < B$  and  $B \ll y_o$ . In this limit 4.2 becomes

$$A \approx \frac{4G/y_o}{(1 + G/y_o)^2} \approx 4G/y_o \quad (4.3)$$

The last approximation in 4.3 is good to 14% for the largest conduction peak measured and to 5% in general.

Absorption experiments were performed using the same geometry as used in the direct measurement of the capacitor admittance. The experimental set-up is shown in Figure 4.7. The HP ratio meter used with square law crystal detectors measures the ratio of reflected to incident Rf voltage in the 50 ohm coaxial system. Using an external recorder bias,  $a = 1 - |r|$  was measured where  $|r|$  is the reflection coefficient ( $|r| = |V_{reflected}/V_{incident}|$ ). Now  $A = 1 - |r|^2$ , so

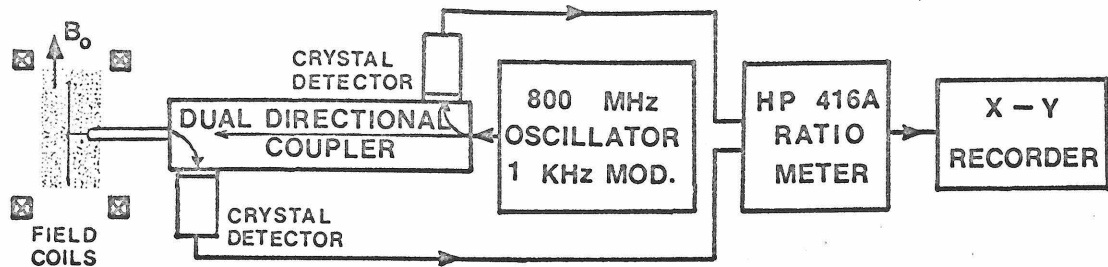


Figure 4.7 Experimental set-up for measuring the harmonic absorption peaks

$$A = 1 - |r|^2 = 2a - a^2 \approx 2a \quad (4.4)$$

if the reflected power is small. Hence,  $G/y_0 \approx A/4 = (2a - a^2)/4$ .

The absorption coefficient was measured and plotted on an X-Y recorder as a function of magnetic field. The plasma density was again inferred from the location of the upper hybrid frequency in transmission experiments. The pressure was  $1.3 \times 10^{-3}$  torr argon and the electron temperature the same as in the previously discussed experiment. The collision frequency was estimated to be  $\nu/\omega \approx .006$ .

#### 4.7 Experimental Results

##### A. Susceptance

Both experimental (Figure 4.8) and theoretical (Figure 4.9) results computed using equation 3.6 exhibit similar behavior as density and magnetic field are varied. On the theoretical plots the susceptance zero closely follows the location of the upper hybrid

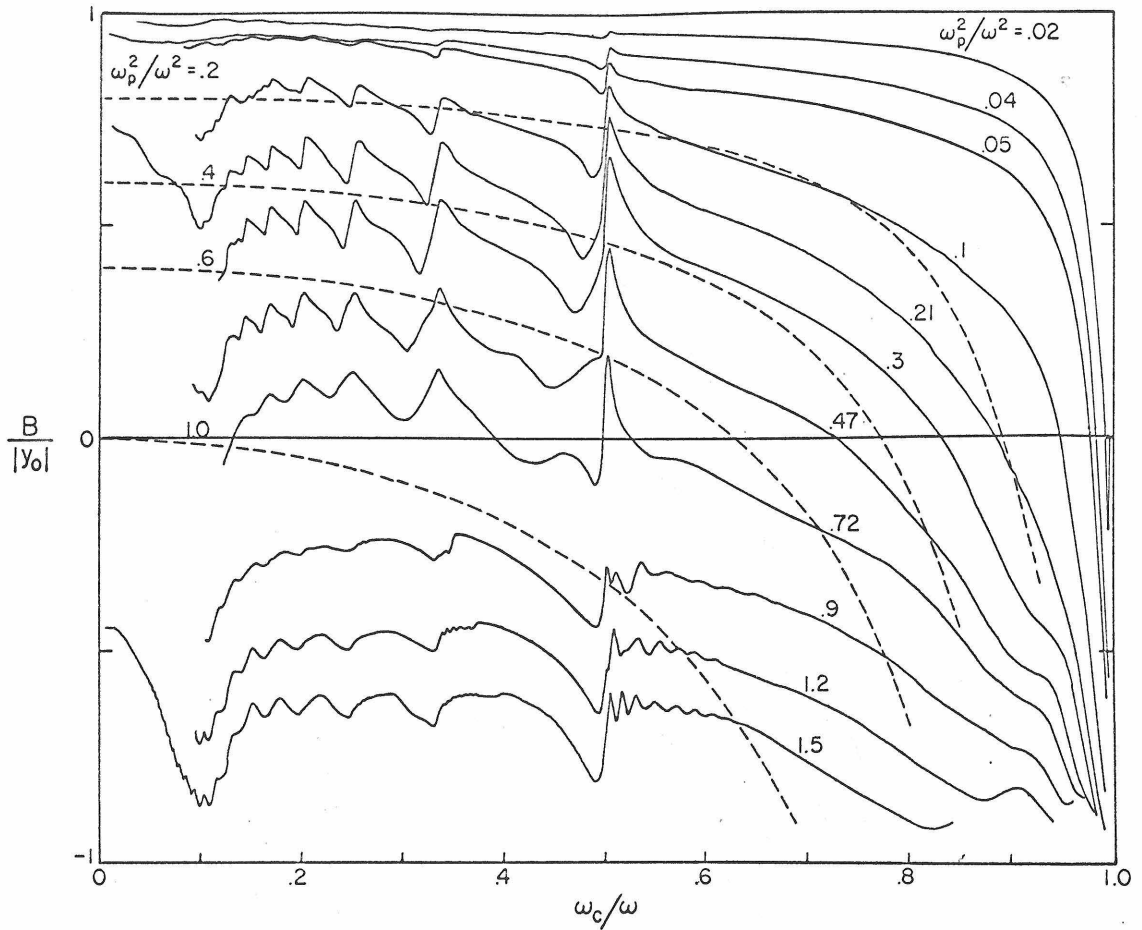


Figure 4.8. Experimental susceptance records for the plasma capacitor. The dashed line is the cold plasma normalized susceptance. The capacitor radius = 3.8 cm.

frequency. Experimentally it was found that the upper hybrid frequency obtained from the susceptance zero agreed with that found in transmission measurements only at low discharge currents. This indicates that the plasma density became more inhomogeneous as the discharge current increased.

For  $\omega_p^2/\omega^2 \leq .1$  the theoretical and experimental curves follow the general shape of  $K_1$  for a cold plasma. The actual sheath thickness at low density ( $\sim .3$  cm for  $\omega_p^2/\omega^2 = .05$ ) is considerably

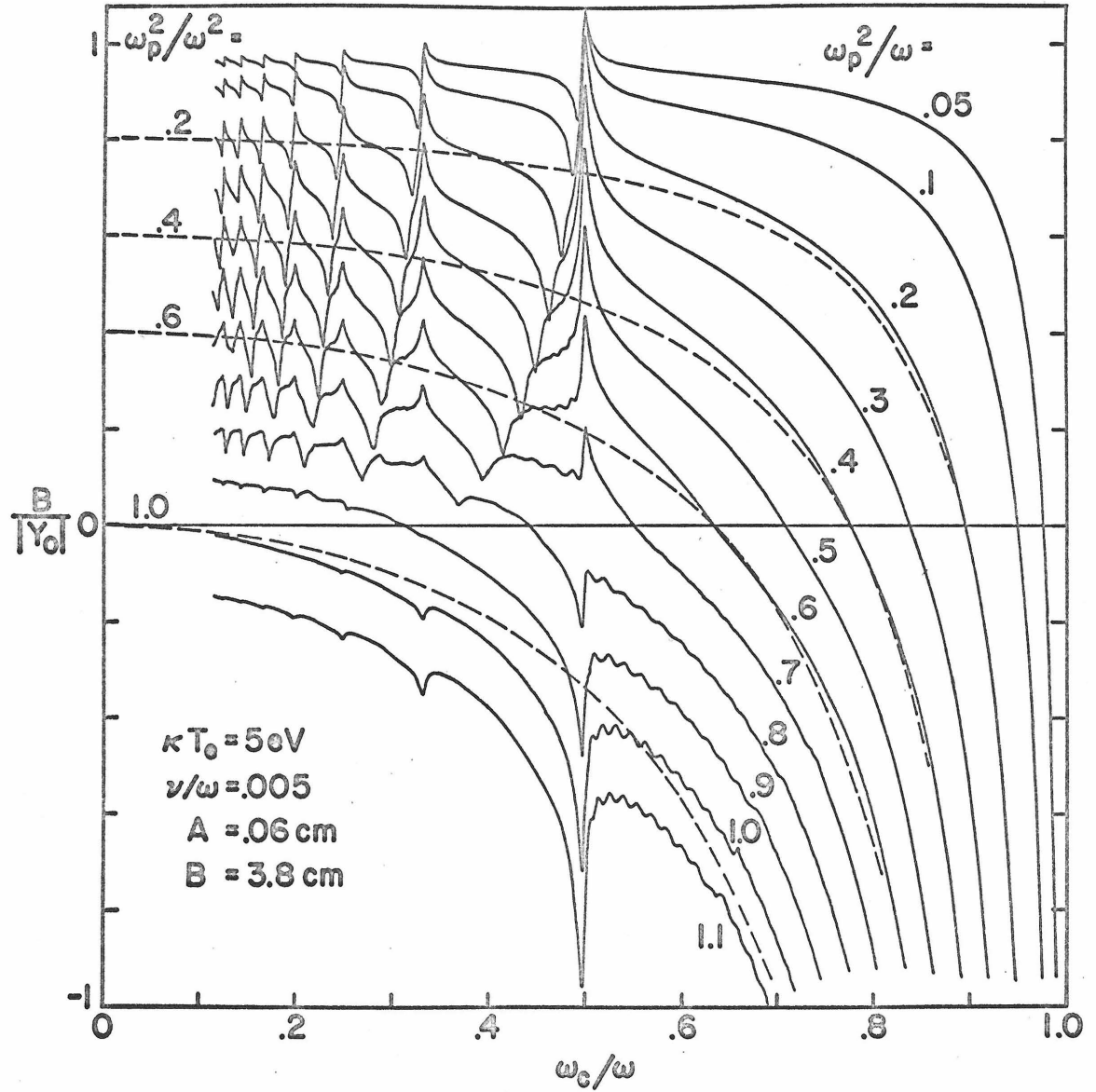


Figure 4.9 Computed normalized susceptance for the cylindrical plasma capacitor with  $kT_e = 5 \text{ eV}$ ,  $\nu/\omega = .005$ ; sheath radius = .06 cm, outside radius = 3.8 cm. The dashed line is the cold plasma normalized susceptance.

larger than the value for the sheath thickness  $A = .06$  cm used for the computed curves. If a larger value for  $A$  were used on the low density theoretical plots, the size of the discontinuities at each harmonic would be much smaller bringing the theoretical curves into closer agreement with experiment.

As  $\omega_p^2/\omega^2$  increases, at first the harmonic resonances become greater in amplitude for both experiment and theory, only to decrease in size above  $\omega_p^2/\omega^2 \approx .3$ . As the density increases, oscillations appear to the right of the harmonics and the resonances become shallow dips.

In general, the experimental curves lie lower than the theoretical curves. This is thought to be caused by stray capacitances, by a nonuniform density, and by radiation losses. The finite capacitor length causes fringing fields which introduce stray capacitances between the probe body, the anode, the cathode, and the center wire. Density nonuniformities are expected to be the more important effect. The average density could be higher than that measured in transmission. Moreover, as previously shown, the presence of a density profile adds a series resistance to the plasma impedance that can lower the susceptance curves. The susceptance curves would be further lowered by radiation losses as discussed in Section 2.5. Evidence in support of this interpretation comes from the behavior of the experimental curves at  $\omega_c/\omega \sim .1$  where  $B/|Y_0|$  is seen to drop abruptly. As the magnetic field decreases, it reaches a value at which the arc is no longer constrained by the field. The arc then expands to fill the entire volume of the vacuum vessel, causing the arc voltage to

increase sharply. A radial gradient develops which causes the susceptibility to drop initially, only to rise at a still lower magnetic field when the average density becomes significantly less than the peak density. At the same time that the susceptibility falls, the conductance rises and the harmonic peaks are seen superimposed on a background conductance. Making allowances for these effects, the experimental results for the susceptibility curves are consistent with the theory.

#### B. Conductance

Strong similarities are also evident between the experimental conductance records (admittance measurement) in Figure 4.10 and the theoretical plots in Figure 4.11, both in the general shape of the peaks and the peak amplitude, as the density is varied. Conductance curves obtained from the absorption measurement are essentially identical to the admittance measurement curves. At low density the peaks are Lorentzian and peak height increases with increasing density, but as the density increases the peaks widen on the low magnetic field side and begin to show structure. The experimental curves show less structure at the top of the peaks than the theoretical curves. This is attributed to a radial density profile and possible a slight misalignment of the center wire. Both would wipe out all but the strongest cyclotron harmonic wave interference effects. In addition, in Chapter 6 it will be seen that passband structure could be decreased by fluctuations in the probe sheath radius. As density increases the harmonic peaks first increase in amplitude and then decrease to a minimum as the upper hybrid frequency passes under the harmonic. The

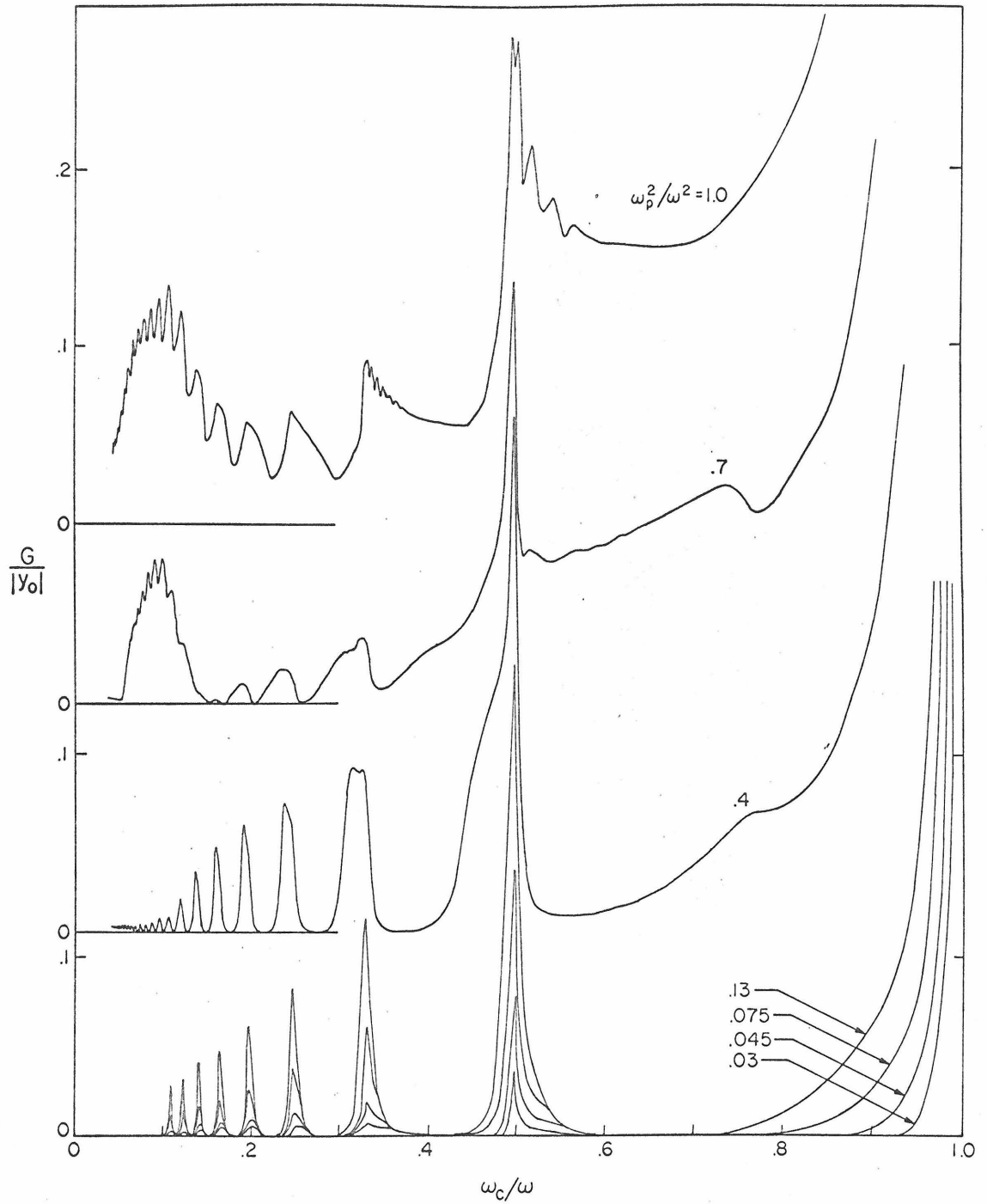


Figure 4.10. Experimental conductance records for the plasma capacitor measured with the phase sensitive admittance measuring system

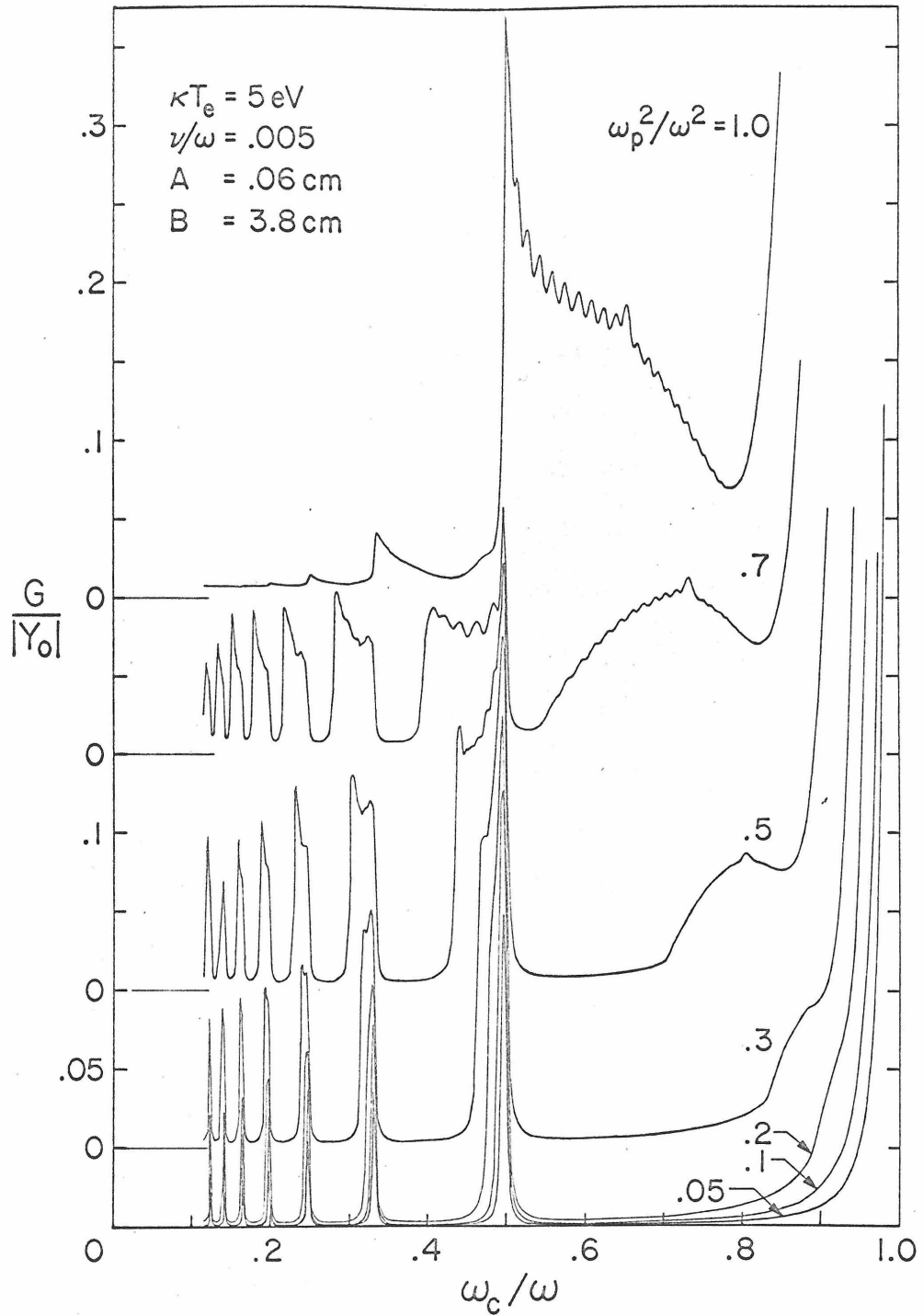


Figure 4.11. Computed conductance for the cylindrical plasma capacitor with  $kT_e = 5 \text{ eV}$ ,  $\nu/\omega = .005$ , sheath radius = .06 cm, outside radius = 3.8 cm.

peaks now become sharp on the low  $\omega_c/\omega$  side and wide on the high side.

Although peak shape changes with density, one may obtain a reasonable value for the effective collision frequency from the peak half width. The low density expansion predicts that as density goes to zero the peaks' half widths approach  $2(\nu/\omega)/N$ ,  $N$  being the harmonic number. Using this relation, and extrapolating the peak half widths to zero density, the normalized collision frequency was calculated. For the admittance measurement this method gave  $\nu/\omega \sim .005$  while for the absorption coefficient measurement it gave  $\nu/\omega \sim .008$ . Both values are in agreement with the estimate based on the pressure and collision data in Brown [34].

One test of the theory developed in Chapter 3 is to see if one choice of parameters  $kT_e$ ,  $A$ , and  $\nu/\omega$  matches the experimental peak height variation with density for both the second and third harmonic. Using the experimental values for  $kT_e$  and  $\nu/\omega$ , the sheath thickness  $A$  was adjusted until the maximum peak height at the second harmonic agreed reasonably with experiment. As is shown in Figure 4.12, this choice for  $A$  also matches the peak height variation with density at the third harmonic for the admittance measurement. Allowing the sheath radius to vary with the Debye length in the integral for the conductance would bring the theoretical curves for  $\omega_p^2/\omega^2 < .3$  closer to the experimental results. As predicted by equation 3.9, peak height varies linearly with density up to  $\omega_p^2/\omega^2 \sim .1$  for the second harmonic, and  $\sim .2$  for the third harmonic.

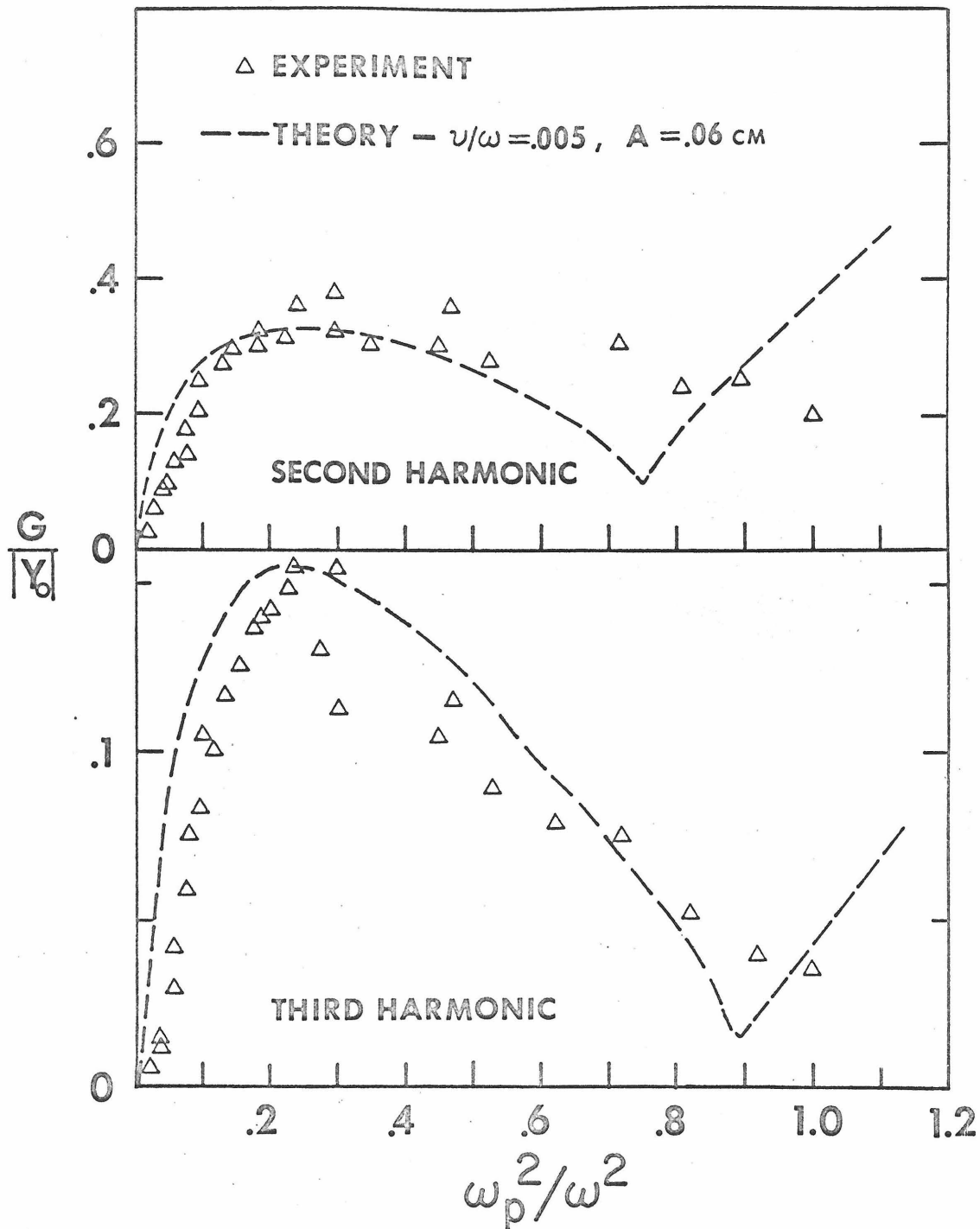


Figure 4.12. Comparison of the experimental values from the admittance measurement with theoretical values for harmonic conductance peak height as density is varied.  $kT_e = 5$  eV,  $\nu/\omega = .005$ ,  $B = 3.8$  cm.

In Figure 4.2 the theoretical peak height increases linearly with density above the minimum point at the upper hybrid frequency. The direct admittance measurement did not show this effect, possibly because of plasma nonuniformity. This effect was observed in the absorption coefficient measurement (Figure 4.13) of peak height. However, the peak height increases more gradually with density than theory predicts. For  $\omega_p^2/\omega^2$  above the upper hybrid frequency, the peak height is influenced by the amplitude and spacing of the CHW oscillations which strongly depend on the density being uniform until the density becomes high enough that the dispersion relation becomes insensitive to the density. Thus, the more gradual increase with density found in the reflection coefficient measurement is not unexpected.

In Figure 4-13 the overall fit of the theoretical curve to the experimental points is much better for the second harmonic than for the third harmonic peak. This may be caused by the peak plasma density increasing as  $\omega_c/\omega$  decreases from the second to third harmonic.

The theory also predicts the variation with density of the location of the low  $\omega_c/\omega$  harmonic peak's base edge. To a first approximation, the edge of base of the harmonic peak is determined by the maximum width of the CHW passband at that density. Both computed and experimental peak base widths (measured from the harmonic) are slightly greater than that given by the passband width for a collisionless plasma with a Maxwellian electron velocity distribution (see Figure 3.2). Adding collisions widens the effective passband width [3,23]. This is shown in Figure 4.14 where the agreement between

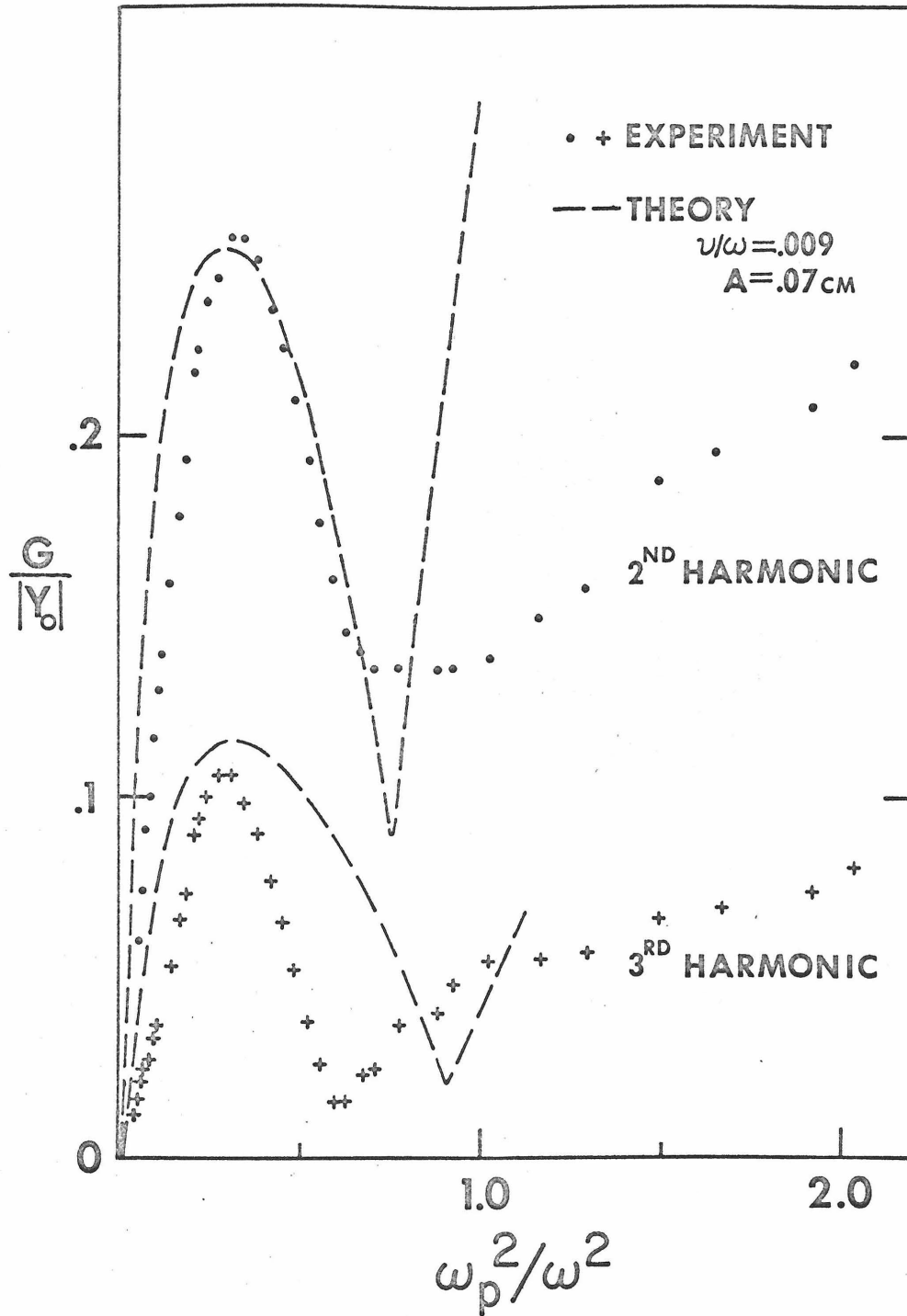


Figure 4.13. Comparison of experimental and theoretical conductance peak height variation found in the absorption coefficient measurement.  $kT_e = 5 \text{ eV}$ ,  $\nu/\omega = .009$ ,  $B = 3.8 \text{ cm}$ .

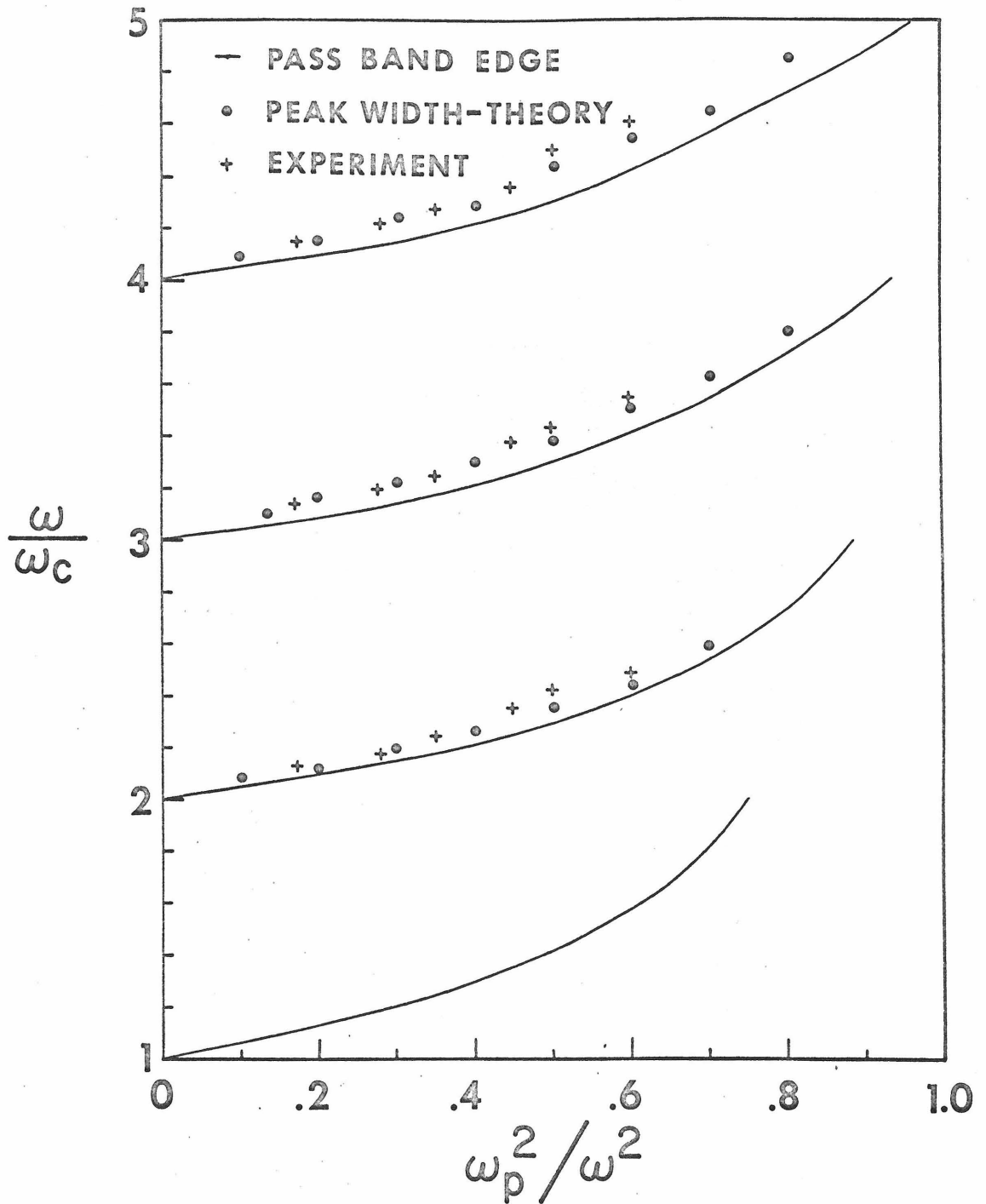


Figure 4.14. Conductance peak base width measured from the harmonic. Experimental and computed results compared with the cyclotron harmonic wave passband edge. Theoretical points for  $kT_e = 5$  eV,  $v/\omega = .005$ ,  $A = .06$  cm.

theory and experiment is seen to be good. The results presented are for the absorption coefficient measurement. Peak base widths for  $\omega_p^2/\omega^2 > .1$  are not very sensitive to collision frequency, so the experimental results could be compared with theoretical results for a slightly lower value of  $\nu/\omega$ .

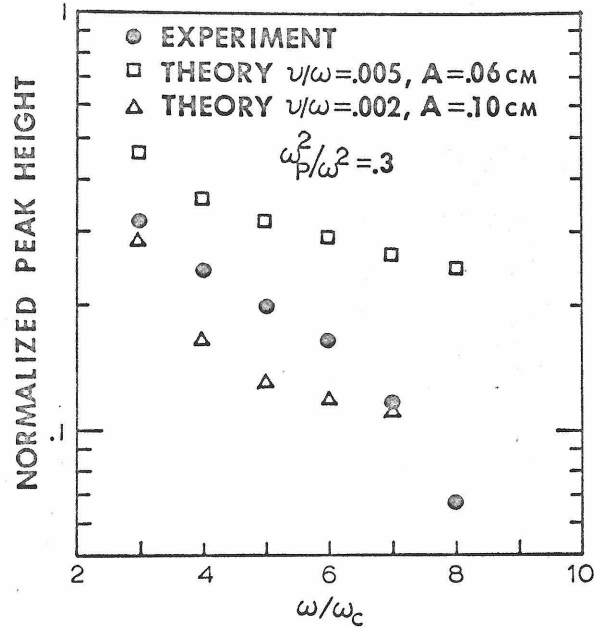


Figure 4.15. Harmonic peak height variation with harmonic number

The theory can account for peak height variation with harmonic number. In Figure 4.15 the experimental harmonic peak height normalized to the height of the second harmonic for the admittance measurement is compared with the height variation for two choices of parameters  $\nu/\omega$  and sheath thickness  $A$ . Both pairs of parameters match the theoretical second harmonic peak height at  $\omega_p^2/\omega^2 = .3$  to the experimental conduction peak height. By choosing  $\nu/\omega$  a bit less than .005, and the sheath radius  $A$  slightly greater than .06 cm, a

closer fit to peak height variation could be obtained.

CHW structure (the oscillating maxima and minima) appears below each harmonic in both conductance and susceptance records when the density becomes large enough. At very high densities where the dispersion relation is insensitive to density, the spacing of the oscillations could be used to determine the electron temperature of the plasma. In this experiment, however, the spacing of the oscillations was not a useful diagnostic and did not agree well with theory, since we were concerned primarily with  $\omega_p^2/\omega^2 \ll 1$  where the column density profile is expected to affect the spacing of these oscillations strongly.

#### 4.8 Discussion and Summary

In this chapter we have presented both an experimental measurement of the admittance of an antenna in a hot magnetoplasma filled capacitor and a theoretical model for the measurement. The qualitative agreement between theory and experiment is, in general, reasonable, and at the harmonics the quantitative agreement is good. The theoretical model can account for changes in the shape of the conductance peaks as density is varied and can predict peak height variation with density and harmonic number. The model predicts more pronounced cyclotron harmonic wave interference effects than are observed experimentally. The observed differences are attributed in part to plasma non-uniformity.

These results indicate that the conductance peaks have potential as a diagnostic tool. From an extrapolation of the half-width of the conduction peaks to zero density, a value for the collision frequency is simply obtained which is in close agreement with that calculated by

other means. At both low and high density the height of the conductance peaks varies linearly with density. It is possible then to use peak height to measure relative density, or if the peak height for a given density is known, to measure the absolute density. At higher harmonics, higher densities can be measured. This method might be useful in studying density fluctuations caused by plasma instabilities or in measuring the density changes in a transient hot magnetoplasma, since the method is able to respond to rapid density changes. Another possible use would be in a space probe experiment used to measure low density interstellar plasmas.

The base width of the conduction peaks gives an absolute method of measuring the peak plasma density in a region near the probe. If only a rough estimate of the density is needed, the density may easily be found from a plot of maximum CHW passband edge location vs. density for a collisionless plasma. This will give densities 20-30% higher than the true density. If greater accuracy is desired, equation 3.6 can be integrated and a plot of peak width vs. density constructed. When this is done, the density may be accurately obtained. This method possesses the advantage that only one probe need be inserted in the plasma. As was demonstrated with the reflection coefficient experiment, conductance records are simple to obtain and contain considerable information on the plasma parameters.

Chapter 5

NOISE OSCILLATIONS ON THE CENTER CONDUCTOR OF  
A CYLINDRIC PLASMA CAPACITOR AT THE CYCLOTRON HARMONICS

5.1 Introduction

Phenomena at the cyclotron harmonics were first observed by Wharton while studying the noise emission from fusion oriented plasma devices [1,4]. He found noise emission peaks at the cyclotron frequency and the second and third harmonics. About a year later Landauer [5] reported observing noise radiation in a PIG discharge occurring up to the 45th cyclotron harmonic. In order to account for the intensity of the observed radiation, Tanaka et al [8] and Canobbio and Croci [9,24] proposed that fast electrons moving through a thermal plasma excite longitudinal waves (cyclotron harmonic waves) which in turn couple to the transverse EM waves observed outside the plasma.

In the past decade numerous additional workers have studied noise emission at the cyclotron harmonics and have demonstrated qualitative agreement between experimental observations and predictions made by assuming the radiation to be caused by cyclotron harmonic waves excited by suprathermal electrons. Dreicer [36,37] repeated and extended the work of Landauer with PIG discharges and demonstrated that the existence of an upper hybrid layer was necessary for harmonic noise emission to occur in his discharge. Lustig [38], Tanaka et al [8], and Ikegami and Crawford [39,40] were among those who observed CHW noise radiation from hot cathode discharges, thereby showing that having substantial numbers of high energy electrons (several hundred eV) is not

necessary for producing harmonic noise radiation. Stone and Auer [41] calculated the internal electrostatic fields associated with the energy loss of monoenergetic fast electrons moving through an essentially Maxwellian plasma. Their results assume only one value of the wave number  $k$  contributes to the observed radiation. Lustig [38] used Stone and Auer's theory to interpret his results, but the agreement between theory and experiment for harmonic peak width vs. density and harmonic peak shape was not good.

Experiments to date do not lend themselves to simple interpretation and comparison to theory. Because the experiments are performed in geometries for which theoretical calculations are very difficult, it is generally assumed that longitudinal oscillations exist and couple to transverse EM waves [28]. Usually no attempt is made to describe analytically the noise output as a summation (or integral) over the wave numbers  $k$  of the internal longitudinal oscillations. Consequently, past experiments on harmonic noise radiation outside a plasma have not predicted successfully noise peak shape and height as the density or harmonic number is varied. As a case in point, Lustig [38], Ikegami and Crawford [39,40] and Tetenbaum [42] observed that the noise power emitted at a harmonic first increased and then decreased as the plasma density was increased. This effect is not predicted by simple considerations of the CHW dispersion relation  $K_{\perp}(\omega, k) = 0$ , or by Stone and Auer's theory.

Experiments on noise emission from a plasma are further hampered because they measure external noise produced by internal noise oscillations which have not been studied and compared with theoretical

predictions. In this chapter we consider the problem of longitudinal noise oscillations inside the plasma. The cylindric plasma capacitor is a good system for this because we already have a theoretical model for the admittance (Chapter 3) which was shown (Chapter 4) to be valid within experimental limitations. As will be seen in Section 5.2, the noise output measured on the center wire of the capacitor is related to the conductance of the capacitor for a plasma in thermal equilibrium. By comparing the noise output that our theoretical model predicts with experiment, we can estimate the regions in which noise radiation can be considered as coming from an essentially thermal plasma.

## 5.2 Longitudinal Noise Oscillations in a Thermal Plasma Capacitor

For a device in thermal equilibrium at absolute temperature  $T$ , Nyquist's theorem [43] gives the mean square short circuit current fluctuation as

$$\langle i_n^2 \rangle = 4kT \Delta f G \quad (5.1)$$

where  $\Delta f$  is the bandwidth of the noise receiver and  $G$  is the conductance of the device. If we consider the plasma as the noise source in our device, then  $\langle i_n^2 \rangle$  is a current source in parallel with the plasma admittance. The equivalent circuit for measuring the noise on the center wire of the cylindric capacitor is shown in Figure 5.1 where  $G_L$ , the receiver's conductance (20 mmhos), and  $Y$ , the capacitor's admittance, are both in parallel with the noise current source  $i_n$ . The voltage at the receiver is

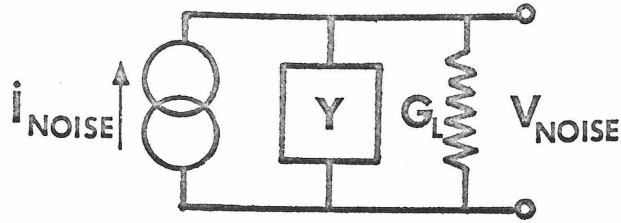


Figure 5.1 Equivalent circuit for measuring the noise of the plasma capacitor

$$V_n = i_n / (G_L + Y) \quad (5.2)$$

The noise power dissipated in the receiver is thus

$$P_n = G_L V^2 = \frac{G_L \langle i_n^2 \rangle}{|G_L + Y|^2} = \frac{4GG_L kT_e \Delta f}{|G_L + Y|^2} \quad (5.3)$$

In equation 5.3 we have replaced the device temperature with the plasma electron temperature. Although for a DC arc discharge  $T_{\text{electron}} \neq T_{\text{ion}}$ , because the electrons are much lighter than the ions, they dominate the noise output sufficiently so that corrections for ion temperature are insignificant at 800 MHz.

Equation 5.3 can be simplified further by comparing the size of  $Y$  to  $G_L = 20$  mmhos. At its largest the capacitor vacuum admittance  $Y = Y_{\text{vacuum}}$  is

$$Y_{\text{vacuum}} = i\omega 2\pi\epsilon_0 / \ln(B/A) \quad (5.4)$$

For a 5 cm long capacitor with  $A = .0025$  cm,  $B = 3.0$  cm, and  $\omega/2\pi = 800$  MHz,  $|Y_{\text{vacuum}}| \approx 1.3$  mmhos, which is much less than  $G_L = 20$  mmhos. Using this, equation 5.2 reduces to

$$P_n = 4G(kT_e \Delta f)/G_L \quad (5.5)$$

If  $T_e$  is constant we expect to observe changes in the plasma noise output from two sources: noise from the hybrid layer's finite conductance as discussed in Section 2.2, and noise associated with cyclotron harmonic waves propagating in the capacitor. Because the plasma has a radial density profile, a hybrid layer will exist between the inner conductor and the outer capacitor wall whenever the magnetic field is such that

$$1 > \omega_c/\omega > (1 - \omega_{p\text{max}}^2/\omega^2)^{1/2}$$

This hybrid layer gives rise to a finite conductance which contributes to the total conductance of the plasma capacitor in equation 5.5. Noise from the hybrid layer is essentially a cold plasma effect [44]. Superimposed on the hybrid layer noise will be cyclotron harmonic noise. This noise should vary at the harmonics as the conductance which we can calculate using equation 3.6. If the electron temperature  $T_e$  changes as  $\omega_c/\omega$  is varied, the noise background will be seen to rise and fall with the temperature. From this we can infer qualitatively how the electron temperature in the arc discharge varies with magnetic field.

### 5.3 Experimental Measurement of Noise Oscillations at the Cyclotron Harmonics

#### A. The Apparatus

Noise measurements at 800 MHz were carried out in a 6 cm diameter, 5 cm long capacitor. A .005 cm diameter tungsten inner wire, supported by glass fibers at each end was used to minimize disturbances to the plasma. The inner wire was connected to the radiometer with glass sheathed .008-inch semirigid coaxial cable. The discharge pressure was  $1.3 \times 10^{-3}$  torr argon. Plasma noise was measured with the radiometer shown in Figure 5.2. The input attenuation of the General Radio 1236 IF amplifier was carefully adjusted so that the output of

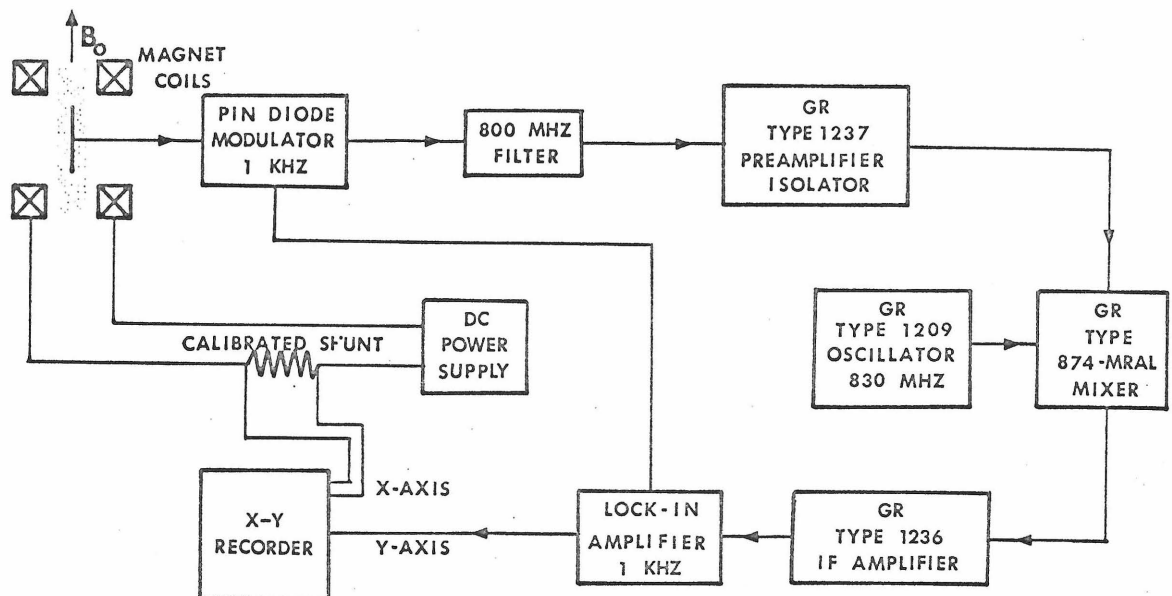


Figure 5.2. Experimental arrangement for measuring the noise of the plasma capacitor

the lock-in amplifier was proportional to noise power. A reference 800 MHz oscillator was used to standardize the amplifier gain over the long periods of time needed to make a complete set of measurements and to calibrate the recorder axis in terms of the power received.

B. Experimental Results

i) Plasma collision frequency. In the course of the noise measurements a way was found both to calibrate the magnetic field axis of the XY recorder and to estimate the effective collision frequency. At very low density (discharge currents less than  $\sim 20$  m amps or  $\omega_p^2/\omega^2$  less than  $\sim .1$ ) with the receiver set at 800 MHz, an 800 MHz oscillator was adjusted to leak a small amount of 800 MHz radiation into the room. The capacitor shields the plasma which is contained directly within it from direct radiation (almost no signal is received with the plasma turned off) but the rest of the plasma interacts with the very weak microwave field. At  $\omega_c/\omega = 1$  the electrons can gain energy from a right circularly polarized wave propagating along the column. The energy may be lost by conversion to longitudinal waves at the cyclotron frequency. This results in a very strong and narrow emission peak which for a cold plasma should occur at the maximum of  $K_I$  (equation 2.8). This occurs at  $\omega_c/\omega \approx 1 - 1/2(\nu/\omega)^2$  which for values of  $\nu/\omega$  typically encountered in these experiments ( $\nu/\omega \sim .002$  to  $.01$ ) occurs at the cyclotron frequency to better than .01% (twenty times the accuracy of the XY recorder). The half width of this peak also gives  $\nu/\omega$ . From the half width of the low density stimulated cyclotron emission line  $\nu/\omega$  was estimated to be  $\nu/\omega \sim .003 - .004$

for  $p \sim 1.3 \times 10^{-3}$  torr argon.

ii) Harmonic noise. Figures 5.3 a-g and 5.4 show noise curves obtained in this experiment for a receiver frequency  $f = 800$  MHz and discharge currents  $I_d$  up to .5 amp at a pressure  $p = 1.3 \times 10^{-3}$  torr argon. The data presented are for a relatively quiet plasma. When low frequency (94-200 MHz) instabilities became large as measured by fluctuations in probe open circuit voltage, the noise curves developed extra peaks (Figure 5.3a) whose shape and position are not predicted by the known conductance of the capacitor.

Strong similarities exist between these curves and the conductance curves previously discussed in Chapter 4. As the density increases the harmonic peaks widen and show increased structure. These peaks are seen to lie upon a background noise level that increases with increasing  $\omega_p^2/\omega^2$  and  $\omega_c/\omega$ . This background noise is essentially a cold plasma effect caused by the upper hybrid layer's contribution to the capacitor conductance as discussed in Section 2.4. The background noise dominates the noise records at high discharge currents as seen in Figure 5.4a. As predicted in Section 2.4, the hybrid layer noise has a maximum value whose position shifts toward lower  $\omega_c/\omega$  as the plasma density increases. In Figure 5.4b the noise emission at the harmonics at higher discharge currents is shown. As predicted by theory, after the background noise level is graphically subtracted out, the noise peak height at the second harmonic is seen to decrease to a minimum as the upper hybrid frequency's location passes under the second harmonic (i.e.,  $\omega_p^2/\omega^2 = .75$ ) only to rise again as the electron plasma density increases further.

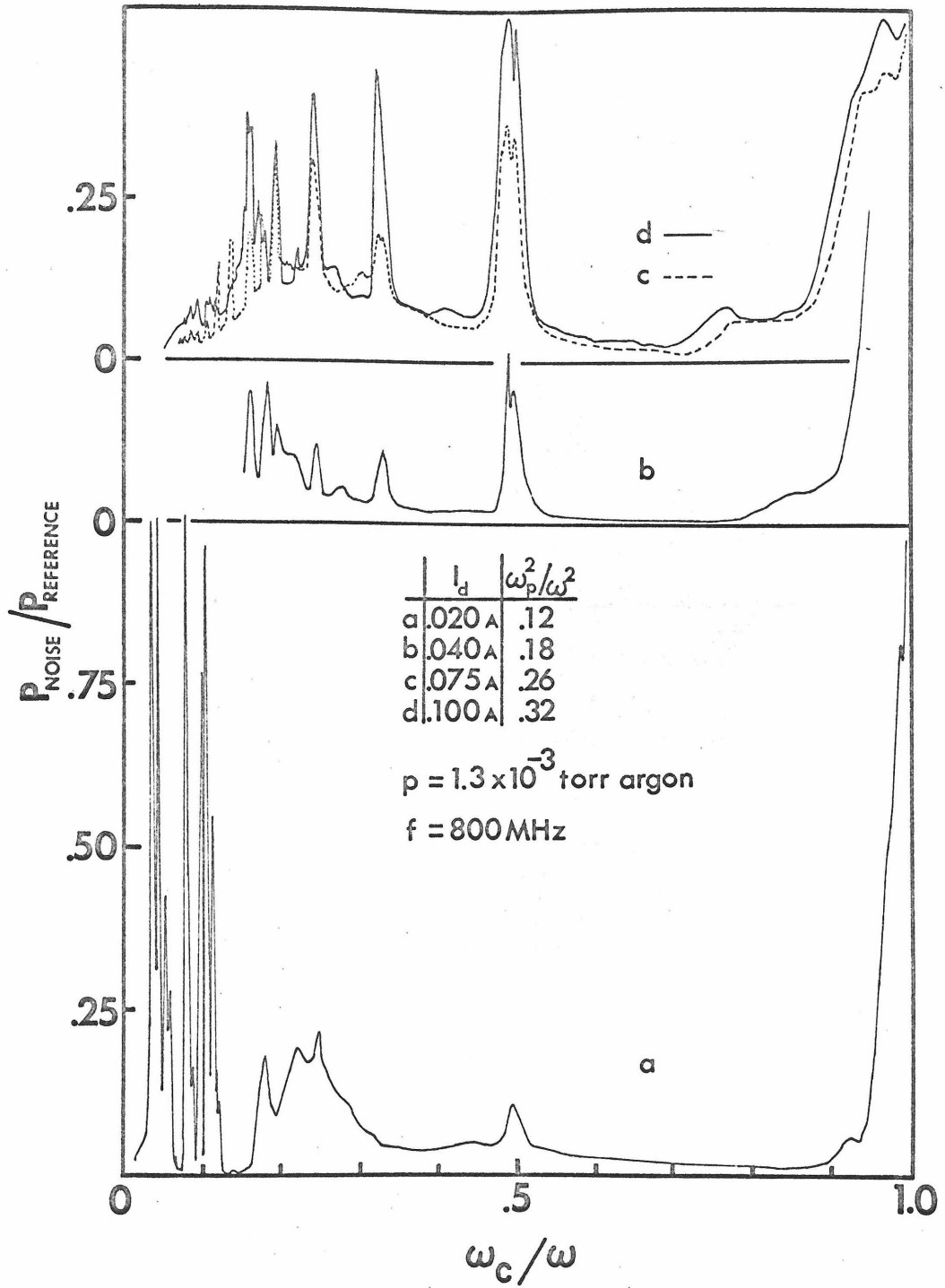


Figure 5.3a-d. Experimental noise power output from a cylindrical plasma capacitor

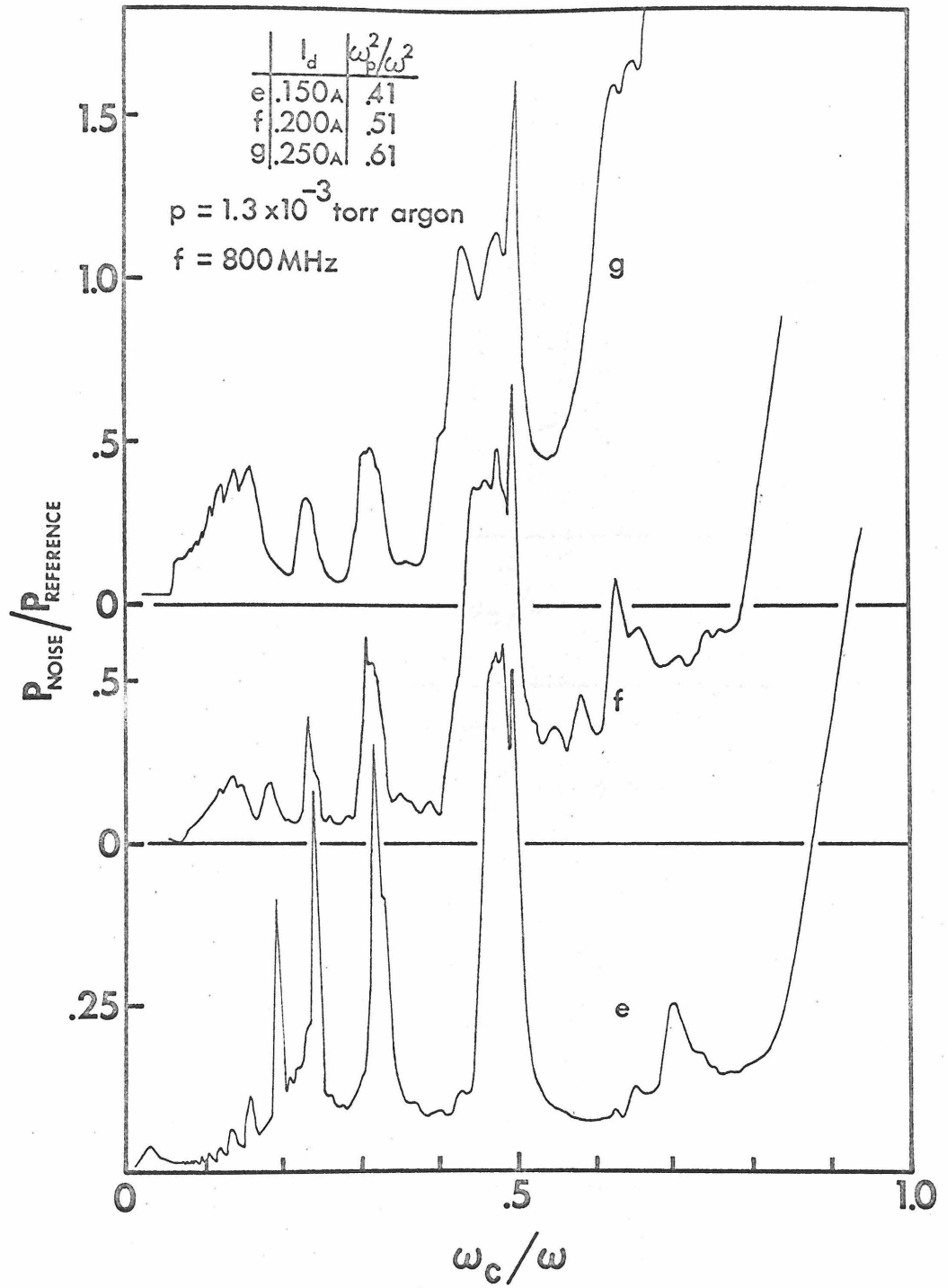


Figure 5.3e-g. Experimental noise power output from a cylindrical plasma capacitor

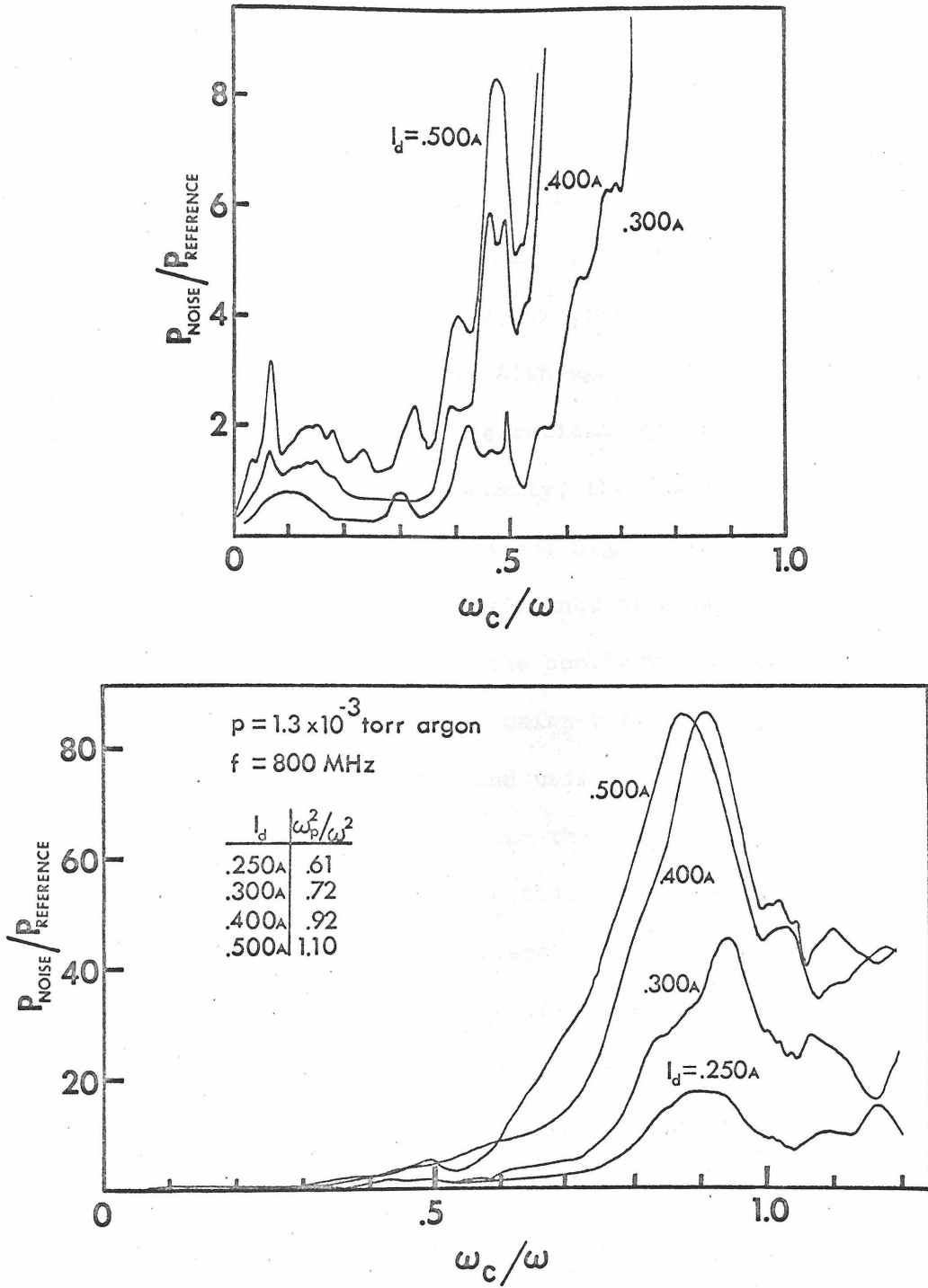


Figure 5.4. Noise output of the plasma capacitor. (Bottom) Effect of the upper hybrid layer on noise output. (Top) Enlarged portion of bottom curves showing the noise emission at the harmonics.

In Figure 5.5 the experimental noise peak height above the background for the second and third harmonic is compared to the theoretical variation with density for the second harmonic. Because the received noise power was considerably greater than what could be expected from a purely thermal noise source, the theoretical curve's maximum height was scaled to match the experimental curve's maximum height at  $\omega/\omega_c = 2$  for comparison. Although the experimental second and third harmonic noise peaks and theoretical conductance peaks show similar peak height variation with density, the density corresponding to maximum peak height in Figure 5.5 seems high by about  $\omega_p^2/\omega^2 \sim .3$ . This is attributed primarily to the existence of a low density region near the center wire and secondly to the nonthermal nature of the noise.

The density was measured both using the location of the UHF in two probe transmission experiments, and using the base widths of the noise peaks. This method of determining the density was discussed in Section 4.7. The densities determined this way agreed to within  $\omega_p^2/\omega^2 = .1$ . However, both methods respond to the peak plasma density rather than the local density at the center wire. As previously mentioned, since the electric field falls off as  $1/r$ , the local density near the wire in a nonuniform plasma should be a major determinant of the conductance peak height. Because the center wire of the capacitor was supported by glass fibers  $\sim 5$  times the diameter of the .005 cm center wire, a low density shadow region will exist around the center wire. At low densities the shadow region will be thicker because the Debye shielding length is larger at low density. This effect is seen in Figure 5.5. The deviation between experiment and theory is largest

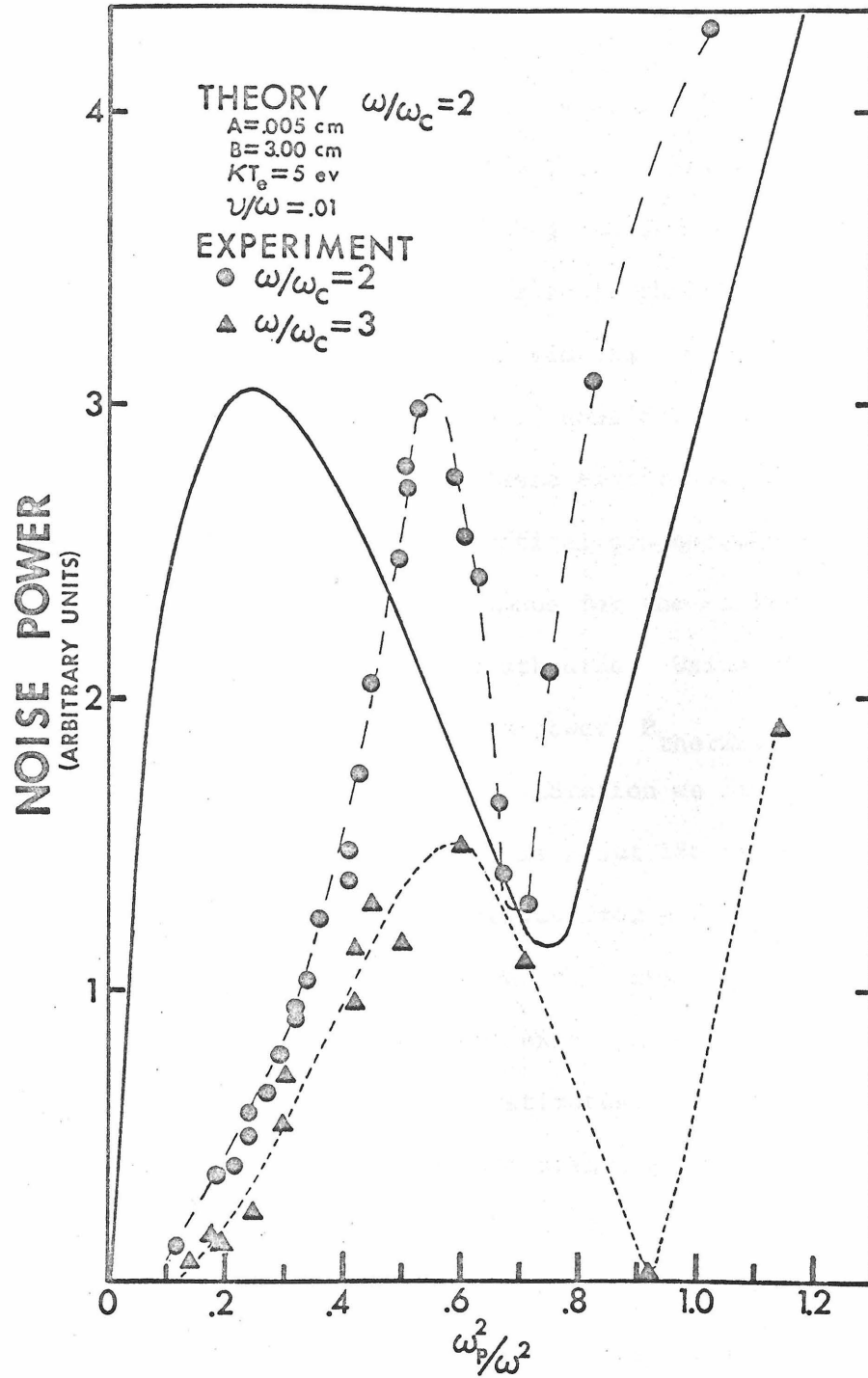


Figure 5.5. Noise power measured at the second and third cyclotron harmonic. The reference oscillator was set at 2 units on the power scale.

when the plasma density is lowest. In addition, because the linear relationship between the conductance and the noise power is only completely valid when the plasma is in thermal equilibrium, part of the discrepancies between experiment and theory can be accounted for because the noise emission is too intense to be thermal.

For a specific comparison of experimental noise power with noise power calculated using equation 5.5, consider the case of  $\omega_p^2/\omega^2 \sim .3$  and  $\omega_c/\omega \cong .5$  for 5 eV plasma electrons. The radiometer has a bandwidth  $\Delta f = 4$  MHz. The theoretical conductance of the capacitor was estimated to be  $G \sim .5 - .7$  mmhos for the collision frequency found earlier and for the estimated sheath size. Using these values in equation 5.5, we estimate the maximum power  $P_{\text{thermal}} \sim 4.7 \times 10^{-10}$  milliwatts. From the reference level calibration we find  $P_{\text{received}} \sim 8.7 \times 10^{-8}$  milliwatts which is about 180 times the second harmonic noise power that would be received from a thermal plasma. Even allowing for the fact that the power estimate is based on a model with several adjustable parameters, the experimental noise is still considerably greater than theoretical estimates. This is not surprising, since the positive column of an arc discharge is not in thermal equilibrium, and since previous noise radiation measurements find one to two orders of magnitude excess radiation over that expected from a thermal plasma [28,30,32]. Because the noise is not completely thermal in origin, noise peak height will depend both on density and on the mechanism producing the noise which in turn may depend on various plasma parameters.

Figures 5.3a-d show various aspects of the nonthermal nature of the noise. In Figure 5.3a intense noise peaks develop below  $\omega_c/\omega = .15$ . These peaks are caused by low frequency instabilities generating noise at their harmonics and will be discussed in the next section. In each of Figures 5.3a,b,c,d regions exist below  $\omega_c/\omega = 1/2$  where the background noise level rises. In these regions the discharge arc voltage increases from around 16 volts to over 20 volts which causes the average electron temperature to rise. At close to zero magnetic field the plasma column expands to fill the entire volume of the discharge tube, the electron temperature decreases, and harmonic noise vanishes.

Although the noise radiation is nonthermal, the theory correctly predicts trends in shape and size of the noise peaks. The shape and behavior of the noise peaks suggest that "fast" electrons are exciting noise oscillations in a plasma with essentially a Maxwellian electron velocity distribution perpendicular to the magnetic field.

iii) Instability stimulated harmonic noise. As mentioned previously for an unstable plasma, noise curves had peaks not predicted by equation 5.5 and the capacitor's theoretical conductance. Low frequency instabilities were found primarily at low discharge currents and magnetic fields which excited large amounts of 800 MHz noise. For a thermal plasma, the noise power should successively decrease at each harmonic in a manner similar to Figure 4.15. However, under certain conditions instability stimulated noise peaks (see Figure 5.3a) could be over 10 times the height at the second harmonic

noise peak and four times the cyclotron frequency noise peak. This is in contrast to the direct conductance and absorption measurements of harmonic peak height discussed in Chapter 4. For  $\omega/\omega_c > 10$  the conductance peaks were measured to be over 50 times smaller than the second harmonic peak. Even if the second harmonic peak in Figure 5.3a represented the correct noise power for a thermal plasma, the peaks below  $\omega_c/\omega = .15$  would represent noise power over 500 times that expected from the thermal plasma.

These noise peaks were found to exist at  $\omega_c/\omega = 2/n$ ,  $n = 10, 11, 12, \dots$  to within 1% and appear to be the type found by Landauer and Muller [45] in the X-band radiation spectra emitted from a beam plasma when a metal probe was inserted into the electron beam. Landauer and Muller found that probes aligned perpendicular to the magnetic field produced noise radiation out of the plasma at half harmonics  $\omega = n\omega_c/2$ , whereas probes aligned parallel to the field produced radiation only at the cyclotron harmonics. Radiation was also emitted if the probes were enclosed in an insulating ceramic tube. They attributed the noise emission at the half harmonics to the presence of a two-beam instability of the type discussed by Etievant et al [46,47] who showed that counterstreaming electron beams can give rise to radiation at  $\omega = n\omega_c/2$ . The metal probes in Landauer's experiment reflected beam electrons, thus creating counterstreaming electron beams.

In our experiment, because the capacitor's center wire and the piece of semirigid coaxial cable connecting the center wire to the radiometer satisfy the conditions of being respectively parallel and

perpendicular to the magnetic field, noise peaks can occur by means of this two-beam instability. Initially, the center wire of the capacitor was connected to the radiometer with .085 inch diameter semirigid coaxial cable. With this size cable the shape of harmonic noise peaks did not agree well with the theoretical model based on a thermal plasma and half-harmonic peaks occurred at most densities. Construction of the center wire assembly out of .005 cm diameter tungsten wire and .008 inch diameter semirigid coaxial cable virtually eliminated this problem except at low density where the sheath surrounding the wire and the cable was comparatively large. Since the strength of the instability should decrease as the area of the reflected beam decreases, our results upon changing to a smaller size center wire and coaxial cable are consistent with the assumption that the instability responsible for the enhanced harmonic emission is the same as observed by Etievant et al.

The origin of the 800 MHz noise was found to be a low frequency beam plasma instability with a fundamental frequency between 94 and 200 MHz. The instability was observed directly on a Tektronix 1L20 spectrum analyzer. Typical conditions for an instability were: pressure =  $1.3 \times 10^{-3}$  torr argon, arc voltage = 25 volts (the arc voltage with no instabilities present is around 15-17 volts), discharge current = 18 m amps ( $\omega_p \sim 250$  MHz), and  $\omega_c = 120$  MHz. Under these conditions a fundamental instability frequency of 196 MHz with a bandwidth of  $\sim .5$  MHz was observed (slightly greater than  $3/2 \omega_c$ ). Strong harmonics of this frequency were observed at  $\sim 400, 600,$  and 800 MHz. Weak noise was found at 300, 500, 700 MHz.

The instability stimulated radiation was present in the experiment using the .008 inch diameter semirigid coaxial cable only when emission from the cathode was nonuniform. After the cathode had been emitting for some time and its emission (as judged by the light intensity of the column) became uniform, the instabilities disappeared and the voltage stayed below 20 volts. Because it was not possible to produce the instability consistently, no additional attempts were made to study it.

#### 5.4 Discussion and Summary

In this chapter we have considered longitudinal noise oscillations at the cyclotron harmonics in a cylindric capacitor. Although harmonic noise peaks were found to be over two orders of magnitude greater than would be expected for a thermal plasma with a Maxwellian electron velocity distribution, the noise peak shape, width and height variations with density qualitatively agreed with theoretical predictions made for a thermal 5 eV plasma. Instabilities were found to play a significant role in the intensity of the noise peaks at low magnetic field and low discharge currents. These peaks occurred at  $\omega_c/\omega = 2/n$  where  $n$  is an integer, and they are thought to be produced by a beam plasma instability.

This experiment helps explain some unresolved questions relating to cyclotron harmonic noise emission. First, Ikegami and Crawford [29,30], Lustig [38], and Tetenbaum [42] all reported that noise radiation first increased and then decreased (saturated for Lustig) as the plasma density increased. A confusing aspect of these results was that Ikegami reported his plasma frequency to be below the

upper hybrid frequency at a given harmonic, whereas both Lustig and Tetenbaum found the peak plasma frequency to be above the average upper hybrid frequency.

Although the existence of an upper hybrid layer (at the receiving frequency) is the most often proposed mechanism for converting longitudinal plasma waves into transverse electromagnetic waves, it is not the only mechanism. This was illustrated by Landauer and Muller [45] who demonstrated that radiation is emitted at the cyclotron harmonics when a metal probe is inserted into an electron beam parallel to the beam and to the magnetic field. They proposed that longitudinal waves propagating perpendicular to the magnetic field collide with the sharp density gradient at the probe surface, exciting it to radiate transverse waves. Landauer and Muller's data suggest that there was no hybrid layer in their plasma at their receiver frequency: Simon and Rosenbluth [48] proposed a mechanism in which the electrons in a longitudinal wave would themselves radiate if the longitudinal wave collided with a density gradient or a wall.

Ikegami also used a beam produced discharge. The beam was  $\sim .5$  cm in diameter and was surrounded by a less luminous mercury plasma region 2.5 cm in diameter. The central beam's suprathermal electrons excite cyclotron harmonic noise oscillations throughout the plasma. The noise oscillations in turn propagate into the central core and modulate the electron beam which can radiate in essentially the same way that Landauer's metal probe radiated. Now the amplitude of the noise oscillations at the center of the plasma should vary with density in a manner similar to that measured in our plasma capacitor.

Consequently the harmonic radiation should first increase with density and then decrease as the density increases further. This is what Ikegami observed.

The results of Lustig and Tetenbaum, while apparently in contradiction to Ikegami's results, can also be explained. Neither a central core nor a metal probe existed in the center of Lustig's or Tetenbaum's plasma. Consequently the hybrid layer played the dominant role in mode conversion. As the peak density of the radial density profile in these experiments increases, the upper hybrid frequency at  $\omega_c/\omega = 1/2$  initially occurs at the center of the column. Longitudinal waves originating in the less dense regions of the plasma propagate inward to the hybrid layer where mode conversion occurs. Since longitudinal noise amplitude is a minimum near the upper hybrid frequency, the primary contribution to the radiation would come initially from noise oscillations propagating inward from less dense regions. Thus it is reasonable to expect the noise radiation first to increase and then to decrease as the average density increases, in the same manner as the internal noise oscillations we have studied. However, as the density increases, the upper hybrid frequency region moves away from the center toward the walls. The radiation contribution can now come both from within and without the hybrid layer and it is difficult to predict how harmonic noise radiation will vary with density.

A second unresolved question is the width of harmonic peaks. Although the noise peak base width was used as an independent check of the plasma density measurement in this experiment, it is also possible to compare the internal noise peak half widths vs. density to the

noise radiation peaks' half width variation as observed by Ikegami [39,40] and Lustig [42]. The conductance model predicts the noise peaks widening on the low  $\omega_c/\omega$  side as density increases, until the upper hybrid frequency passes under the harmonic at which point the half width decreases. As previously mentioned, the conductance peak width is influenced by the peak plasma density. Ikegami reported half widths increasing with discharge current for densities  $\omega_p^2/\omega^2 \leq 1$ . Lustig, however, had a plasma with an average density  $\langle \omega_p^2/\omega^2 \rangle \leq 1$ , with a peak density  $\omega_p^2/\omega^2|_{\max} > 1$ , and he reported the noise peak half widths decreasing with increasing discharge current. In the light of our present experiment these results are consistent. Both Ikegami and Lustig found that harmonic radiation peaks shifted toward higher harmonics as density increased. This shift was observed in this experiment and is predicted by the theoretical model (Figure 4.11) because the wave number spectrum excited is shifting toward higher values as density increases.

A final point to consider is the mechanism for producing intense, suprathermal radiation at the harmonics in various discharge devices as reported in the literature. The present experiment indicates that a low frequency beam plasma instability can be the dominant mechanism in producing intense radiation peaks at the harmonics. The use of an internal probe allowed instability-stimulated noise to be separated from the internal noise from other thermal and nonthermal mechanisms. Instabilities may also play a significant role in the harmonic emission spectra of PIG discharges. S. Bliman [49] used internal probes in a PIG discharge and found low frequency instabilities

between  $\sim 50$  and 300 MHz. However, in experiments in which noise radiation is measured at one or two frequencies outside the plasma, it is difficult to tell whether or not a low frequency instability is playing a role in producing noise radiation at some harmonic frequency. Furthermore, a low frequency instability may couple so poorly to electromagnetic radiation that it is difficult to observe outside the plasma. An internal probe for detecting longitudinal noise oscillations is thus an important tool for understanding cyclotron harmonic radiation.

Chapter 6

SHEATH MODULATION OF CYCLOTRON HARMONIC WAVES

6.1 Introduction

The transparent cylinder admittance model developed in Chapter 3 was used successfully to analyze the experiments in Chapters 4 and 5. Because these experiments are relatively insensitive to sheath thickness, successful comparison of experiment with theory says little about the validity of treating the rf sheath as a vacuum region several Debye lengths thick. Previous workers concluded that sheath size was not usually a major influence on their results [2,3]. That this should be the case is not at all obvious, since the sheath plays a major role in launching and detecting cyclotron harmonic waves.

The easiest way of launching and detecting CHW is with a thin rf probe aligned parallel to the magnetic field. Nonlinear coupling between the rf voltage and the plasma electrons occurs in the probe sheath [50]. Because the vacuum wavelength of the rf voltage ( $\sim 38$  cm at 800 MHz) is much larger than the sheath dimensions, the electrons within the sheath and for several Debye lengths into the plasma see an essentially static electric field. The ions are too heavy to respond to this field, but they act as a restoring force for charge density perturbations propagating in the plasma. Electrons approaching the probe are reflected in the sheath. If the electron sheath-transit time is close to the period of the applied field, the electrons gain or lose, on the average, an energy increment proportional to the average amplitude of the sheath electric field which they experience

between the reflection point in the sheath and the plasma-sheath boundary [21,51]. The sheath electric field acts to bunch together a fraction of the reflected electrons which entered the sheath region at different phases of the electric field. These bunched electrons form a cylindrical charge density perturbation which propagates radially outward from the probe as a longitudinal wave.

Because launching CHW is essentially a nonlinear effect, it would be useful to know whether the linear model used in Chapters 3, 4, and 5 treats the sheath in an essentially correct manner. If the model is valid, it should be possible to predict how the strength and spectra of wave numbers is affected by probe sheath diameter.

In this chapter we examine the effect on transmission and noise records as the sheath radius is varied and compare the experimental results with computer calculations.

## 6.2 The Effect of Sheath Size on Harmonic Conduction Peaks

In Chapters 4 and 5, harmonic conductance peaks were studied directly and indirectly by absorption and noise measurements respectively. The experimental results were in good overall agreement with the calculated results. However, the computed results showed more sharply defined passband structure than the experimental results. In this section we wish to show some of the effects of sheath size on these results.

In the following experiments the effective probe sheath radius is reduced by applying a positive bias to the center wire of the capacitor. In Figure 6.1a, the noise on the center wire is measured with

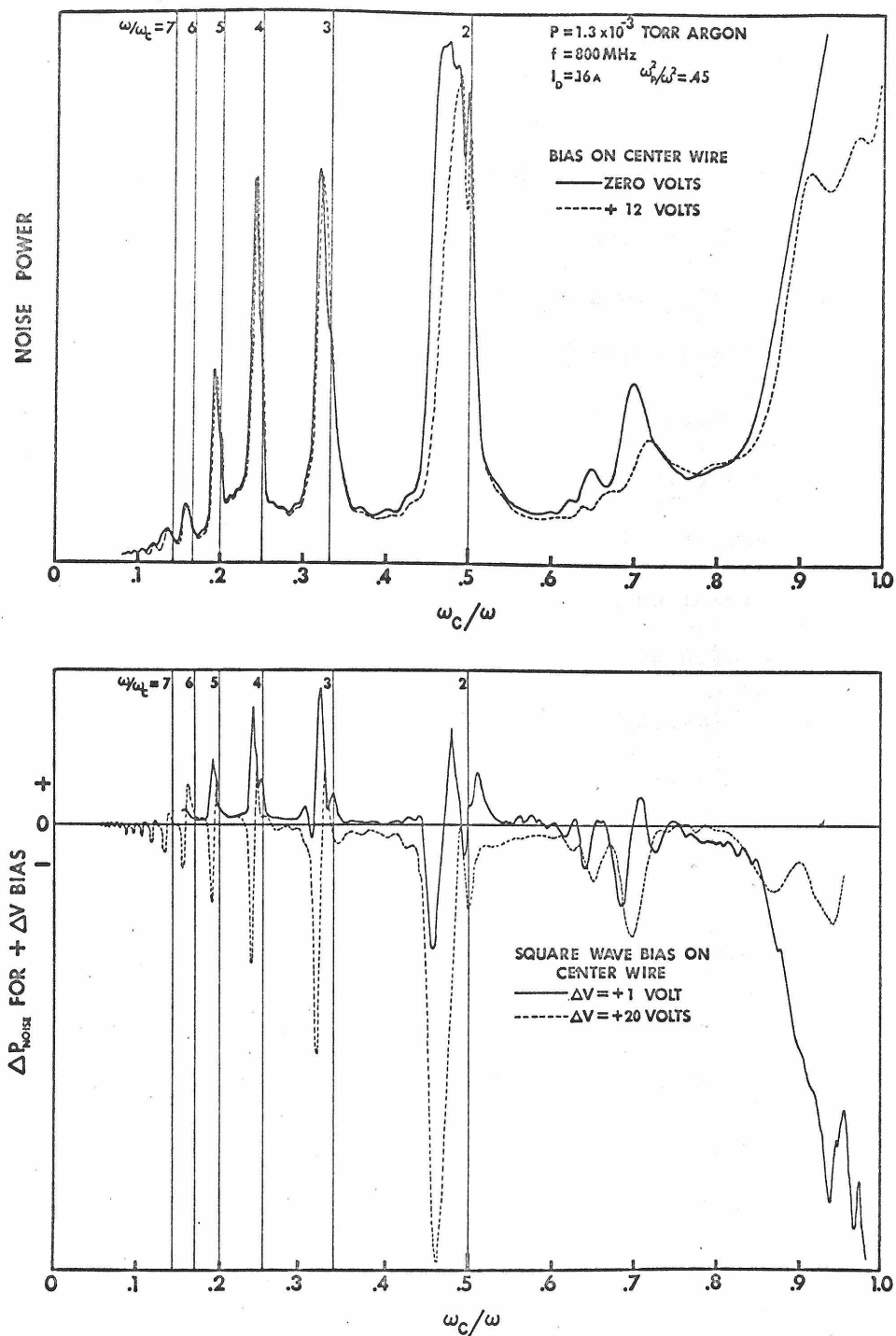


Figure 6.1a (Top) Effect of probe bias on center wire noise  
6.1b (Bottom) Effect of modulating the probe sheath with a square wave bias

and without positive bias. As is seen in the figure, the thickness of the center wire sheath affects both the location and the strength of structure within a harmonic passband. For no bias applied to the probe, the harmonic noise peaks behave the same as discussed in Chapter 5. For a positive 12-volt bias, the effective sheath size is reduced, and the shape, width, and height of the harmonic peaks is altered. The effect of varying probe biases on harmonic noise peaks was found to be greater with the .005 cm diameter wire probe than for previously reported probe sizes [52] because the strength of the electric field at the plasma sheath boundary goes up inversely with the sheath radius. The positive bias used in Figure 6.1a might be increasing the local electron plasma density. However, this is not thought to be a major effect in changing shape of the noise peaks, because the peak width decreased. If the local maximum plasma density increased, one would expect the peak width to widen (see Figure 4.14) as a positive probe bias was applied. The major effect is thought to be a shift of the spectrum of wave numbers launched by the probe toward higher values. The measurement presented in Figure 6.1a has the disadvantage that to get the size of the effect vs.  $\omega_c/\omega$  one must subtract one graph from another and that relatively large bias voltages must be applied to produce an easily observable effect.

The effect of sheath thickness on harmonic conductance peak structure can be isolated by measuring the change in conductance peak height vs.  $\omega_c/\omega$  as the sheath radius is varied between two radii. To do this, the radiometer described in Chapter 5 with the pin diode modulator removed is used to measure the noise power as the sheath

thickness is modulated at 1 KHz. The noise power is proportional to the conductance for a thermal plasma. A General Radio bias insertion unit supplies to the capacitor's center wire, the 1 KHz square wave voltage  $V_{\text{floating}} + \Delta V$ . As the center wire becomes positive relative to its floating potential, electrons are collected, thereby decreasing the effective sheath radius. A PAR Model 120 lock-in amplifier measures the difference in the output of the receiver for the two sheath thicknesses. For a thermal plasma this difference in power is proportional to the difference in conductance  $\Delta G$  for the two sheath thicknesses. The capacitor and experimental conditions were described in Section 5.3. Typical results are shown in Figures 6.1b and 6.4.

To compute  $\Delta G$  accurately for small changes in sheath size, a series sheath capacitance must be included in the total capacitor admittance (see Section 2.4), thus making the center wire ( $r = R_0$ ) the source of rf current in the admittance integral. With this change, equation 3.6 for the plasma admittance between the sheath of radius  $A_1$  and the outside capacitor radius  $B$  becomes

$$Y_p(A_1) = 2\pi i \omega \epsilon_0 \left\{ \int_0^{\infty} \frac{dk J_0(kR_0)[J_0(kA_1) - J_0(kB)]}{k K_1(\omega, k)} \right\}^{-1} \quad (6.1)$$

Including a series sheath capacitance, the total admittance is

$$\frac{Y(A_1)}{Y_0} = \frac{Y_p(A_1)}{Y_0} \left\{ 1 + \frac{Y_p(A_1)}{Y_0} \frac{\ln(A_1/R_0)}{\ln(B/R_0)} \right\}^{-1} \quad (6.2)$$

where  $Y_0 = 2\pi i \omega \epsilon_0 / \ln(B/R_0)$  is the vacuum admittance of the capacitor.

Using equations 6.1 and 6.2,

$$\Delta(G/|Y_o|) = (G(A_1) - G(A_2))/|Y_o| \quad (6.3)$$

At low density ( $\omega_p^2/\omega^2 \lesssim .1$ ) the calculated amplitude of  $\Delta G/|Y_o|$  at the second harmonic increases almost linearly for small decreases  $\Delta A$  in sheath size. This is shown in Figure 6.2a for an initial sheath thickness of .06 cm and up to a 30% decrease in sheath thickness. From Figure 6.2a we can infer that the sheath modulation of the second harmonic conductance peak height will be linear if the sheath is modulated by only several percent.

To estimate what the modulation voltage  $\Delta V$  should be so that the change in sheath size will be linear with voltage, consider a vacuum sheath (containing ions but no electrons) separating the plasma from a planar surface at potential  $V$  with respect to the plasma. For this case the sheath thickness  $A$  is given by

$$A = (2\epsilon_o/ne)^{1/2} V^{1/2} \quad (6.4)$$

where  $n$  = the electron density in the plasma, and  $e$  = the electronic charge. If the planar surface is modulated between  $V$  and  $V + \Delta V$ , to first order

$$\Delta A = (\epsilon_o/ne)(\Delta V/A) = \frac{(6.9 \times 10^{-5}) \Delta V}{A(\omega_p^2/\omega^2)} \quad (6.5)$$

where  $A$  is in cm and  $V$  is in volts. For a 4-5 eV plasma with a sheath  $\approx 3$  Debye lengths thick,  $\Delta A/A \sim (1.5 \Delta V)\%$ , so for  $\Delta V < 2$  volts  $\Delta A$  varies approximately linearly with the modulation voltage. This is demonstrated in Figure 6.2b in which the experimental change in

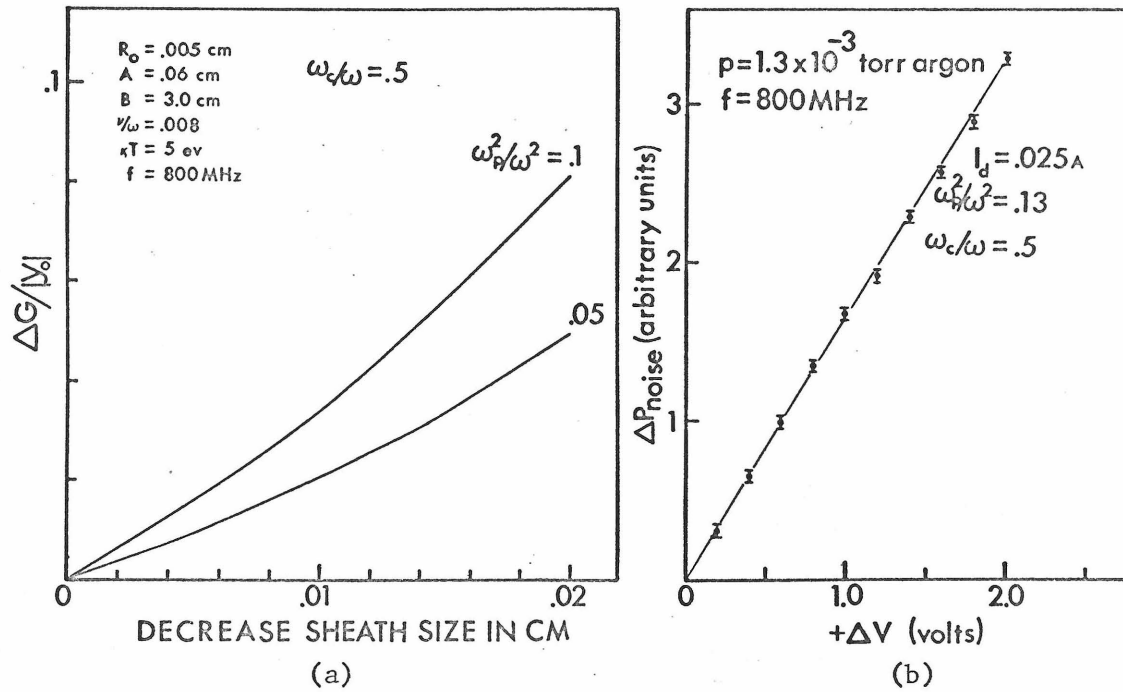


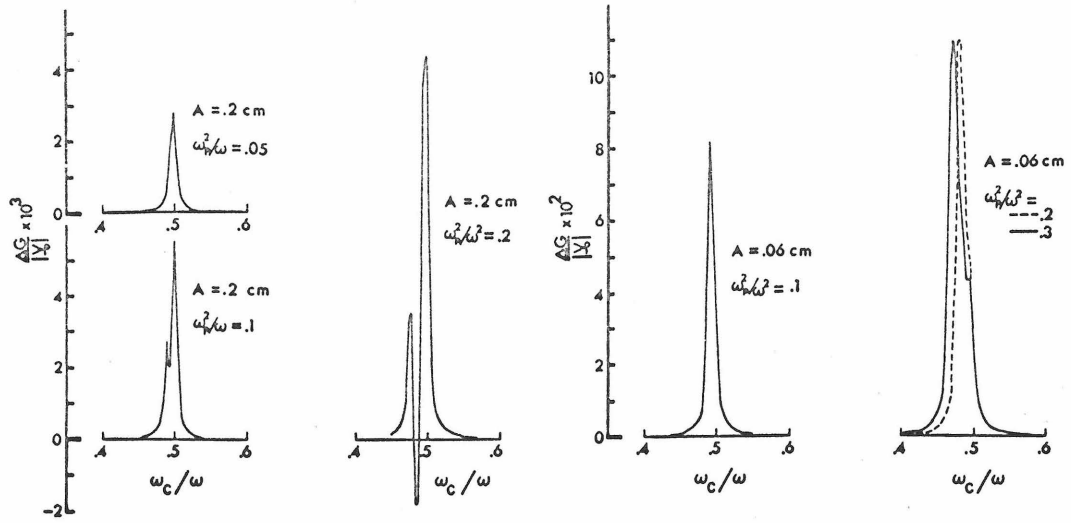
Figure 6.2a Computed increase in conductance as the sheath thickness decreases at the second harmonic

6.2b Increase in the second harmonic noise peak amplitude as  $\Delta V$  increases

noise peak amplitude ( $\omega_p^2/\omega^2 \sim .13$ ,  $\omega_c/\omega = .5$ ) as the probe bias is varied by  $\Delta V$  is plotted against  $\Delta V$ . In Figure 6.1b it is seen that modulating the center wire with a 20 volt square wave produces a curve which differs greatly from that made using a 1 volt square wave. For voltages less than  $\sim 3$  volts, sheath modulation conductance curves were essentially identical except for amplitude. Based on these results, a modulation voltage of  $\Delta V = 1$  volt was chosen to use in experiments on sheath modulation.

In Figure 6.3 theoretical curves are shown of  $\Delta G/|Y_o|$  vs.  $\omega_c/\omega$  calculated using equations 6.1 and 6.2. The size of  $\Delta A$  in the theoretical calculations was larger than in the experimental case so that  $\Delta G$  would be large enough to calculate on the computer using single precision. Figures 6.1b and 6.4 show experimental measurements of the change in noise power  $P_{\text{noise}} = P_{\text{noise}}]_{\text{bias}} - P_{\text{noise}}]_{\text{no bias}}$   $\sim \Delta G$  as the center wire voltage is modulated with a 1 volt square wave.

At low density ( $\omega_p^2/\omega^2 \leq .2$ ) the theoretical curves for  $A = .2$  cm,  $\Delta A = .02$  cm most closely approximate the experimentally observed double peaks at the harmonics, while at higher densities, curves for  $A = .06$  cm,  $A = -.02$  cm are more appropriate. Modulation peaks exist both at the harmonics  $\omega_c/\omega = 1/N$  and within the cyclotron harmonic wave passband  $\omega_c/\omega \leq 1/N$ . The passband modulation peak increases in size and moves toward lower  $\omega_c/\omega$  as the density increases. As it grows larger it obscures the harmonic modulation peak.



$f = 800 \text{ MHz}$

$R_0 = .005 \text{ cm}$   $\psi\omega = .008$

$B = 3.0 \text{ cm}$   $\kappa T = 5 \text{ ev}$

$\Delta A = -.02 \text{ cm}$

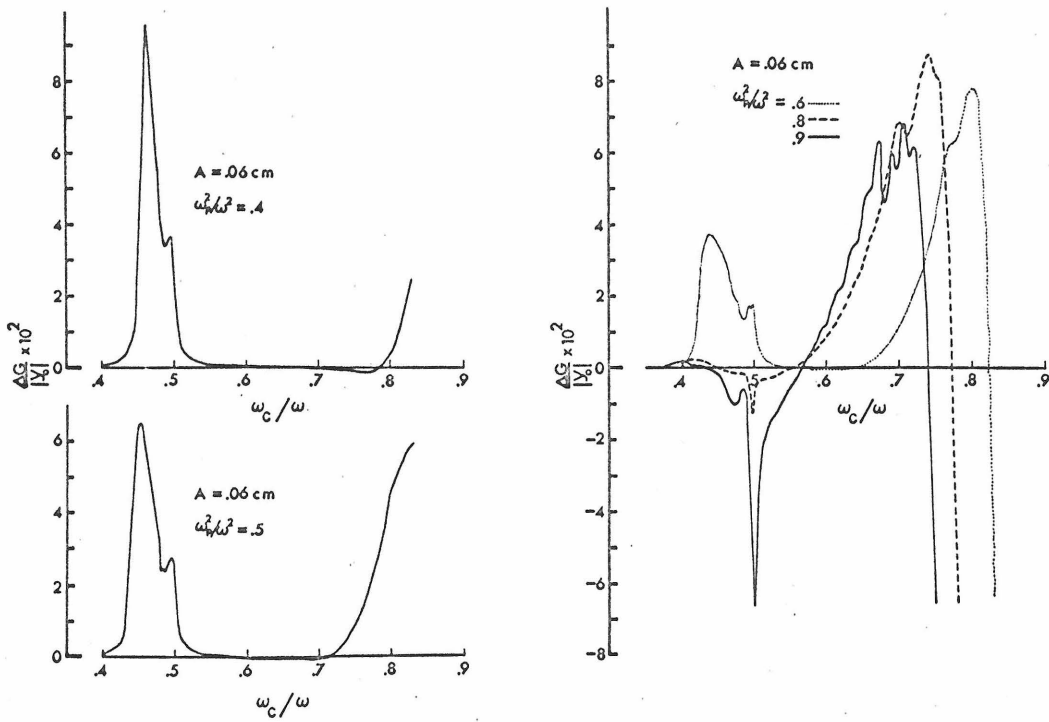


Figure 6.3 Computed change in conductance as the probe sheath thickness is varied



Figure 6.4 Experimental effect of varying the center wire bias

The movement of the passband modulation peak can qualitatively be understood by reference to the dispersion diagram for cyclotron harmonic waves (Figure 3.2). As the plasma density increases, two effects tend to shift the passband modulation peaks toward lower  $\omega_c/\omega$ . First, if the sheath size were to change negligibly as the density increased, the peak would shift toward lower magnetic field because for a fixed  $k$  spectrum (with positive group velocity  $d\omega/dk$ ), increases in density find  $\text{Re } K_{\perp}(\omega, k) = 0$  at progressively lower values of  $\omega_c/\omega$ . This is the case for the computer results because the value of  $A$  was held constant as the density was varied. Second, in a real plasma increasing the density decreases the sheath size. This shifts the spectrum of wave numbers  $k$  excited in the capacitor toward larger  $k$  values. Referring to the dispersion diagram, Figure 3.2, if the group velocity  $d\omega/dk$  of the excited cyclotron harmonic waves is positive, the shift in excited wave numbers will move the location of the peak toward lower  $\omega_c/\omega$ . The dimensions of the plasma capacitor used primarily excite CHW with positive group velocity.

The height variation and structure of the modulation peaks is complicated. At low density, increasing the average value of  $k$  excited in the capacitor results in larger contributions to the conductance coming from regions where  $\text{Im}(K_{\perp}(\omega, k))$  is increasing (see Figure 3.3). As density increases, the contribution to the change in conductance from propagating cyclotron harmonic waves also increases, and shifting the  $k$  spectrum results in structure appearing within the modulation peaks. Finally, as the density at a harmonic increases

past the upper hybrid condition  $\omega_p^2/\omega^2 \geq 1 - \omega_c^2/\omega^2$ , cyclotron harmonic wave propagation is cut off and their contribution to the conductance decreases as the sheath size decreases.

The significance of these results is that they help explain why cyclotron harmonic structure within the conductance peaks is usually far less sharp in experiments than in theoretical computations. The results in Figures 6.1 to 6.4 show that both in experiment and in theory, the amplitude of a conductance peak is very sensitive to the sheath radius or equivalently, to the separation between the sheath and the outer conductor. Specifically, regions within the CHW pass-band are more sensitive to a changing sheath size than values of  $\omega_c/\omega$  close to the exact harmonic. In Figures 6.1a and b, a change in probe bias of +1 volt produces a 16% decrease in amplitude of the second harmonic conductance peak.

Now while the rf properties of a sheath region may be adequately described by a vacuum region for a quiet plasma, if the plasma is noisy so that the plasma potential at the sheath is oscillating with a spectrum of frequency components, then the sheath region which launches and detects cyclotron harmonic waves becomes actually far more diffuse than assumed in the theory. As a consequence the sharply defined CHW effects predicted by our model for the conductance peak structure should be averaged out.

Likewise because the sheath acts as a vacuum region whose radius is constantly changing with the plasma noise, specular reflection of cyclotron harmonic waves with wavelengths less than  $\sim 10$  times the sheath fluctuation distance, will not occur. Different parts of

the center wire sheath and the outside capacitor wall's sheath will have different thicknesses at different times. Because of the random nature of noise oscillations and because of the time averaging involved in the basic detection system, the phase coherence required for short wavelength standing wave resonances to occur will be destroyed. In addition, any misalignment of the center wire will also tend to average out peak structure.

Because the conductance peaks within the passbands are very sensitive to sheath modulation, sheath modulated transmission was also investigated to see how CHW transmission through an essentially uniform plasma region is affected by changing the sheath size. This experiment is discussed in the next section.

### 6.3 Sheath Modulated Transmission of Cyclotron Harmonic Waves

As discussed in Section 3.5, CHW transmission between two parallel wires in an infinite uniform plasma can be theoretically described by an expression for the admittance between the probes similar to equations 6.1 and 6.2. Now, however,  $B$  in equation 6.1 becomes the separation between the probes. For a square law receiver the transmitted signal is proportional to  $|Y/Y_0|^2$  (equation 6.2 includes sheath effects).

A transmission experiment was set up as in Figure 4.4 except that the pin diode modulator was removed and a 1 KHz square wave with  $\Delta V = 1$  volt above floating potential was applied to the receiver probe, using a General Radio bias insertion unit. The fixed sending and receiving probes whose general construction is described in

Section 4.4, were .005 cm diameter, tungsten wire, 1 cm apart.

Equation 6.1 for transmission implies that the admittance change is independent of whether the receiving probe sheath or the transmitting probe sheath is varied. This was experimentally verified by interchanging rf transmitter and receiver connections while leaving the 1 KHz bias on the center probe.

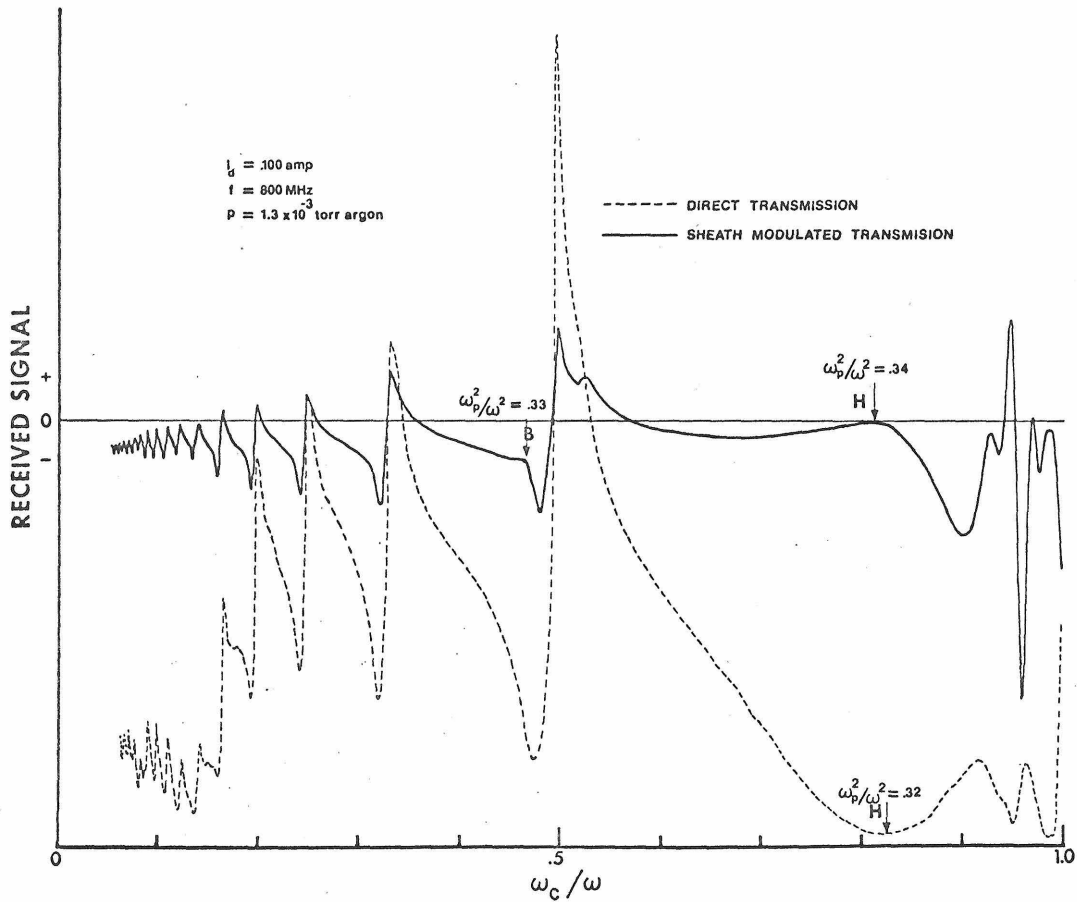


Figure 6.5. Sheath modulated transmission compared with standard two-probe transmission record for probes 1 cm apart

Experimental sheath modulated transmission curves are shown in Figure 6.5 and in Figure 6.6 for various densities. Both figures compare a sheath modulated transmission curve to a standard transmission curve taken under otherwise identical conditions. In each figure the location of the upper hybrid frequency found in transmission measurements is marked with an "H".

On the experimental curves  $\Delta\{|Y/Y_0|\}$  is negative at low density from the upper hybrid frequency  $\omega_c/\omega = \sqrt{1 - \omega_p^2/\omega^2}$  to the cyclotron frequency  $\omega_c/\omega = 1$ . This is consistent with the assumption that smaller sheaths shift the wave number spectrum excited by a probe toward higher  $k$  values. As was shown in Chapter 4, the low density plasma admittance is dominated by the susceptance between the probes. The susceptance is negative between the upper hybrid frequency and the cyclotron frequency. Also, Figure 3.1 implies that for an increase in average wave number  $k$  the plasma susceptance becomes less negative at a given  $\omega_c/\omega$  in the hybrid range. Hence  $|Y|_{k>k_1} - |Y|_{k_1}$  is mostly negative in the upper hybrid range.

Because the UHF is a minimum of transmission ( $\partial|Y|/\partial\omega_c = 0$ ), modulating the sheath by a small amount  $\Delta A$  should produce curves for which  $\Delta[|Y|^2]$  both equals zero and has zero slope at this point. The experimental curves have their zero slope point toward lower values of  $\omega_c/\omega$  when compared with the location of the UHF found in the two-probe transmission measurement. This suggests the plasma density is slightly higher for the experimental sheath modulated transmission curves. This difference between experiment and theory can be explained by realizing that when the probe is biased positive, the local electron density

increases slightly. For the curves presented in Figure 6.5, the normalized plasma frequency found from a transmission measurement is  $\omega_p^2/\omega^2 = .32$ . The upper hybrid frequency's location found from sheath modulated transmission yields a plasma density of  $\omega_p^2/\omega^2 = .34$  which is an increase in apparent density of  $\sim 6\%$ . If greater accuracy in density measurements is desired, a smaller modulation voltage may be used.

An alternate way of determining the density is to use the location of the second harmonic bandpass edge. In sheath modulated transmission records at low density ( $\omega_p^2/\omega^2 \lesssim .5$ ) as in Figure 6.5, as  $\omega_c/\omega$  goes below a harmonic, the curves dip sharply negative, rise, and then abruptly "break" to a flat curve. This experimentally observed break point occurs almost exactly at the bandpass edge for CHW propagation using the density found from the minimum of transmission as a standard. The second harmonic bandpass edge (using Figure 4.14) is marked with a "B" in Figures 6.5 and 6.6. In Figure 6.5 the location of the "break" point implies a plasma density of  $\omega_p^2/\omega^2 = .33$ . At higher densities as in Figure 6.6 the bandpass edge is not as well defined by a sharp break in the curve. The transition region between the passband and the region outside the passband is more gradual, possibly because density gradients within the capacitor increase as the peak plasma density increases. However, with care the passband edge may still be found and used to find the plasma density.

One distinct advantage of sheath modulated transmission of cyclotron harmonic waves as a diagnostic tool is that it can enhance CHW interference effects over direct transmission effects. For example

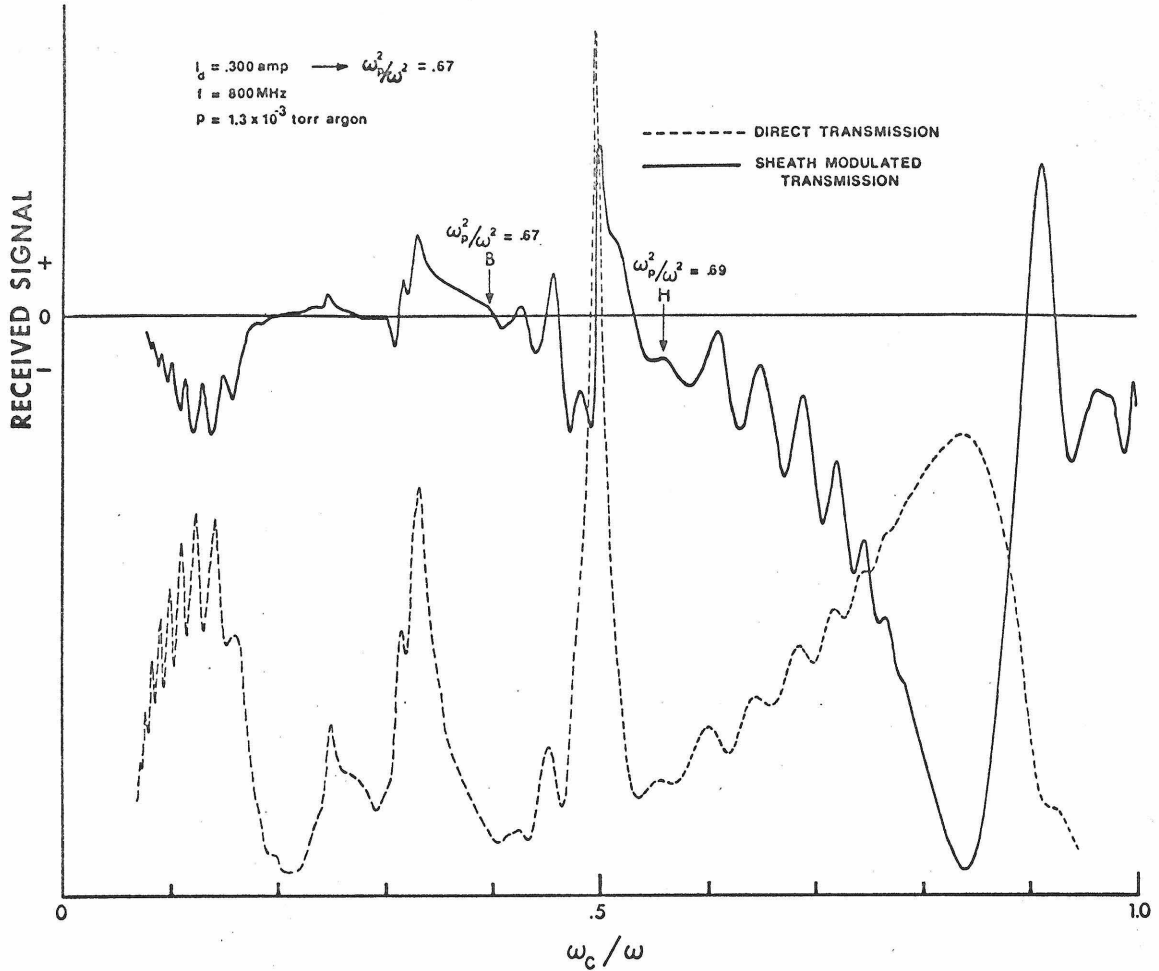


Figure 6.6 Sheath modulated transmission compared with standard two-probe transmission record for probes 1 cm apart

when the second harmonic transmission peak is very large compared to the amplitude of the CHW interference oscillations, it is difficult to obtain the spacing and location of these oscillations accurately without switching the amplifier gain. Because sheath modulation affects the launching of cyclotron harmonic waves more than the direct coupled transmitted signal, it can be used to take complete transmission records without switching the amplifier gain for various parts of the transmission record. An example of this enhancement is shown in Figure

6.6. The location of the oscillations from sheath modulated transmission gives essentially the same information on the dispersion characteristics of cyclotron harmonic waves (hence  $kT_e$ ) as does a direct transmission experiment, although the maximum of the oscillations now corresponds to the longitudinal wave being  $\pi/2$  out of phase with the direct coupled signal. In addition, the plasma density can be obtained either from the location of the second harmonic band-pass edge or from the location of the upper hybrid frequency as given by the position of zero slope.

#### 6.4 Summary

In this chapter we have studied the effect of sheath size on the launching and detecting of cyclotron harmonic waves. In general the results obtained are in qualitative agreement with the theoretical model which assumes a vacuum sheath several (3-5) Debye lengths thick.

Sheath modulation of the noise on the capacitor's center wire showed the same effects with density and magnetic field as predicted by the theory for the change in conductance. At low density the noise received at a harmonic peak increased as the sheath became smaller. As the plasma density increased and the location of the upper hybrid frequency passed under a harmonic peak, the noise received decreased with decreasing sheath size.

In both experimental and theoretical results, the height of the conductance peak within a passband proved to be very sensitive to the sheath size. Because the thickness of the sheath region changes along different parts of the center wire and capacitor wall in response to the

local noise oscillations with plasma potential, strong phase coherence of cyclotron harmonic waves will be hard to obtain except in extremely quiet plasmas. Noise oscillations on the sheath at the probe and outer capacitor wall will have an effect similar to collisions in that they are a randomizing process which attenuates a reflected cyclotron harmonic wave. More significantly, their presence creates diffuse boundary conditions which inhibit specular reflection.

Sheath modulated transmission is proposed as a useful diagnostic in detecting and interpreting cyclotron harmonic wave phenomena. Besides yielding essentially the same information found in direct transmission experiments, it enhances cyclotron harmonic effects, shows the location of the second harmonic passband edge, and aids in the intuitive understanding of the wave number spectrum of cyclotron harmonic waves launched by an antenna.

Chapter 7

SUMMARY AND SUGGESTIONS FOR FURTHER WORK

In the preceding chapters various aspects of the complex admittance of a cylindric plasma capacitor have been experimentally studied and compared with theoretical models. Particular attention has been paid to the behavior of the conductance peaks at the cyclotron harmonics. In this chapter we wish to summarize the results and successes of this study, point out its limitations, mention applications to plasma diagnostics, and outline areas where further investigations would be useful.

Summary

In Chapter 4 we measured the capacitor susceptance directly and its conductance both directly and indirectly by absorption measurements. In general the experimental results could be explained qualitatively by using a superposition of the admittance for a cold nonuniform plasma (Chapter 2) and for a hot uniform plasma (Chapter 3). The primary area where the experimental measurements and theoretical predictions disagreed was in the spacing as a function of  $\omega_c/\omega$  of the CHW interference oscillations between harmonics. The difference between the experimental and theoretical spacing of the oscillations was caused by the radial density profile in the capacitor. Better agreement between experiment and theory would be possible in an experiment with a more uniform plasma, or if  $\omega_p^2/\omega^2 \gg 1$ . As  $\omega_p^2/\omega^2$  goes to infinity the CHW dispersion relation becomes increasingly insensitive to density variations.

In spite of plasma nonuniformities, the experiment showed good agreement with theory. Areas where experiment and theory agreed were:

- i) For  $\omega_p^2/\omega^2 < .3$  the plasma density agreed with that found from the location of the UHF using two-probe transmission measurements. The general shape of the experimental curves agreed with the theoretical curves (Figures 4.8, 4.9).
- ii) The height of the second and third harmonic conductance peaks varied with density as predicted by theory (Figures 4.12, 4.13). Only one choice of the value of the collision frequency and the sheath thickness was needed to produce good quantitative agreement between experiment and theory at both the second and third harmonics.
- iii) The experimental location of the low  $\omega_c/\omega$  base of the conductance peaks agreed closely with theoretical predictions (Figure 4.14).
- iv) The height variation of harmonic peaks with harmonic number can be approximated by an appropriate choice of sheath thickness and collision frequency (Figure 4.15).
- v) The general shape and passband structure of the experimental conductance peaks resembles that of the theoretical curves.

The close agreement between the experimental measurements and the theoretical calculations of conductance peaks suggested that if the arc plasma under study was near thermal equilibrium the internal harmonic noise peaks could be theoretically predicted from Nyquist's

theorem

$$\text{Noise Power} = P_{\text{noise}} = 4G(kT_e \Delta f) / G_L$$

where  $G$  is the conductance of the plasma capacitor.

The noise oscillations on the center wire of the plasma capacitor were measured with a noise radiometer described in Chapter 5. The shape and height of the noise peaks were found to vary with density in the same way that the theoretical conductance peaks varied. However, the capacitor's noise power output was over two orders of magnitude greater than that predicted by using the known conductance of the capacitor and Nyquist's theorem. One source of this excess, suprathermal noise, was traced to the presence of a two-stream instability in the plasma caused by reflection of electrons from the coaxial feed to the center wire of the capacitor. This observation of internal, suprathermal harmonic noise oscillations in the capacitor is in general agreement with noise radiation measurements (made external to a plasma) which invariably show that harmonic noise radiation is suprathermal. The significant part of this measurement is that as the density is varied the harmonic noise peak shape and height variation can be predicted by the theory even if the absolute magnitude of the noise power cannot. This fact was used to help interpret some previous experiments on harmonic noise radiation in which certain results were poorly explained.

Finally, the role of the sheath around the center wire of the capacitor was investigated. Throughout this study it was assumed that the sheath region could be treated as a vacuum region several Debye lengths thick. While the role of the sheath in launching and detecting

cyclotron harmonic waves is not exactly understood because of the nonlinear nature of the process, it was thought useful to investigate how well the theoretical model could account for changes in the conductance and admittance as the probe sheath size is varied. Our model predicted that the primary effect of decreasing the sheath size will be to shift toward higher  $k$  values the wave number spectrum of the cyclotron harmonic waves launched by the probe. To test this prediction, sheath modulation experiments were performed and compared with theory. While detailed agreement between experimental and theoretical curves was not good, the same trends were shown. As the sheath size decreases, the harmonic conductance peak heights increased with density until the upper hybrid frequency passed under that harmonic, at which point the height of the conductance peak decreases. In addition both theory and experiment showed that the passband modulation peak moves toward lower  $\omega_c/\omega$  as the density increases. This implies that CHW propagation near the passband edge is very sensitive to the size of the sheath.

The sensitivity of the conductance peaks to sheath size variation helped to explain why the structure within the conductance peaks was usually far less sharp in experiments than in theoretical computations. The noise oscillations studied in Chapter 5 modulate the sheath. This modulation of the effective sheath size creates a more diffuse region for launching and detecting cyclotron harmonic waves than assumed in the theory. In addition, although the rf properties of the sheath seem well approximated by a vacuum region several Debye lengths thick, in

reality the sheath is a diffuse region and cyclotron harmonic waves will tend to originate from a more poorly defined region. As a consequence the sharply defined cyclotron harmonic wave interference effects and structure at the harmonics which is predicted by theory would be more averaged out if a more diffuse sheath region is considered.

In the course of the experiments presented in Chapters 4 through 6, several potentially useful plasma diagnostic techniques have been developed which are useful when studying warm magnetoplasmas via cyclotron harmonic wave effects.

- i) The effective collision frequency of the system can be obtained either by extrapolating the half widths of the harmonic conductance peaks to zero density, or by leaking a small amount of radiation into the plasma at low density at the cyclotron frequency and measuring the half width of the stimulated longitudinal noise peak on the center wire of the capacitor.
- ii) The cyclotron frequency for a given magnetic field can be obtained by leaking a small amount of radiation at a known frequency into the plasma ( $\omega_p^2/\omega^2 < .1$ ). When the known frequency equals the cyclotron frequency an intense, narrow peak occurs in the noise oscillations received on the capacitor's center wire. This peak marks the location of the cyclotron frequency to better than .01% which is usually more than adequate for most plasma experiments.

- iii) At both low density ( $\omega_p^2/\omega^2 < .1 - .2$ ) and high density ( $\omega_p^2/\omega^2 < 1$ ) the height of the harmonic conductance peaks varies linearly with the plasma density. If the density is known for two values of a conductance peak at either low or high density, the electron plasma density in that region can be determined by measuring the conductance at that harmonic. This method of measuring the plasma density possesses the advantage that it is capable of following rapid changes in density. A possible application of this technique would be to measure the density changes associated with low frequency instabilities.
- iv) The plasma density can be found by measuring the location of the low  $\omega_c/\omega$  base of the conductance peaks and comparing it to calculations similar to those presented in Figure 4.14. As a rough estimate the location is determined by the bandpass edge for CHW propagation in a collisionless plasma. Using this approximation will give plasma densities 20-30% too high.
- v) Sheath modulated transmission of cyclotron harmonic waves can be used to supplement standard two-probe transmission measurements. Sheath modulation has been shown to delineate clearly the second harmonic bandpass edge for  $\omega_p^2/\omega^2 < .5$ . The location of the bandpass edge can be used to determine the plasma density. In addition, at high density, sheath modulation emphasizes CHW interference effects.

### Suggestions for Further Work

The primary disagreement between experiment and theory encountered in this work is the magnitude of the longitudinal noise oscillations in the capacitor; over two orders of magnitude greater than that predicted by theory. The cause of this discrepancy is thought to be in the nonthermal plasma used (an arc discharge) and in the possible presence of "fast" electrons in excess of those present in a purely Maxwellian electron velocity distribution.

These difficulties could possibly be overcome by using a pulsed plasma and looking at the noise oscillations in the early afterglow. By looking at the noise early in the afterglow, the plasma temperature would still be high enough to see hot plasma effects and the plasma electron velocity distribution would be more closely Maxwellian. Under these conditions better agreement between experiment and theory might be obtained.

It would also be useful to relate externally observed harmonic noise radiation directly to the internal longitudinal noise oscillations. To do this, internal plasma noise on the probe is measured using a radiometer as described in Chapter 5. The probe (antenna for longitudinal waves) can be positioned radially in the plasma column to measure the noise variation with radius. At the hybrid layer where conversion to EM waves supposedly occurs, CHW are cut off and the characteristics of the noise curves should drastically change.

External electromagnetic radiation can be measured by putting the plasma column axially through a right circular cavity so that extraordinary waves will excite the  $TE_{011}$  cavity mode. Comparison of

the cavity noise radiation vs. magnetic field at various densities with the longitudinal noise oscillations should provide insight into the mechanism by which longitudinal waves couple to electromagnetic waves. Such a study would also help in understanding the intensity of the observed radiation.

For complete understanding of harmonic noise radiation, the role of plasma instabilities should also be investigated. In Chapter 5 it was seen that instabilities can play the major role in producing longitudinal noise oscillations at the harmonics. Plasma noise can be divided into two categories: coherent noise and incoherent noise. The incoherent noise is produced by random electron thermal motion and results in radiation having no phase coherence. Because of the large index of refraction of the plasma at the harmonics, this radiation (if produced internally) may directly escape from the plasma. Coherent radiation would result if a plasma instability is acting as a driving term for longitudinal oscillations which in turn couple to electromagnetic waves.

A useful experiment would be to measure the autocorrelation of both the noise on the probe and the cavity radiation. The degree of autocorrelation is a measure of what fraction of the noise emitted at the harmonics is related to coherent processes producing the noise (i.e., instabilities). By performing a cross correlation of the noise on the probe with the cavity radiation the region of the plasma responsible for producing the noise may be determined.

Conclusion

The complex admittance of a cylindrical plasma capacitor with particular emphasis on the conductance has been investigated, both experimentally and theoretically. The agreement obtained was generally good. The results of this study have been applied to a study of the longitudinal noise oscillations in the capacitor and the effects of sheath size on cyclotron harmonic wave transmission. Several potentially useful plasma diagnostics have been developed and their applications discussed.

Appendix I

THE ADMITTANCE OF A COLD, NONUNIFORM CYLINDRICAL PLASMA CAPACITOR

In the main text certain results were quoted for the effects of density inhomogeneities on the measured admittance. In this appendix the problem of computing the admittance of a coaxial capacitor with a radial density profile is mathematically formulated.

In the cold plasma limit, measuring the normalized admittance  $Y/Y_0$  between any two transparent cylinders within the plasma yields the same value, i.e.,  $K_{\perp}$ . This is not the case, of course, if a density profile is present in the plasma. However, for simplicity we do not attempt to formulate the problem with physically correct density profiles as the integration must then be done numerically. But rather, we assume an approximate density profile and measure  $Y/Y_0$  between  $r = A$  and  $r = B$ .

The admittance per unit length of the capacitor is defined by

$$Y = \frac{1}{Z} = \frac{I}{\Delta V} \quad (\text{I-1})$$

where  $Y$  is the admittance per unit length,  $Z$  is the impedance per unit length,  $I$  is the total rf current per unit length injected by the external circuit, and  $\Delta V = V(A) - V(B)$  is the voltage drop from the center wire to the outside wall.

As discussed in Section 2.1, assuming an infinitely long capacitor requires  $\partial/\partial z = \partial/\partial \phi = 0$ . This means the rf current moves only in the radial direction. Under this condition and using the quasistatic approximation (assume an  $e^{-i\omega t}$  time dependence for all variables)

$$\nabla \times \bar{E} = 0 \quad ; \quad \nabla \times \bar{H} = 0 = \bar{J}_r + \frac{d\bar{D}}{dt} = \bar{J}_r - i\omega\bar{D} \quad (\text{I-2})$$

Charge conservation requires that

$$\bar{I} = 2\pi r \bar{J}_r = \text{constant} = - \frac{\partial \lambda}{\partial t} \quad (\text{I-3})$$

where  $\lambda$  = the charge per unit length on the center wire, and  $\bar{J}_r$  = the particle current flux per unit length in the capacitor.

In the plasma the displacement vector  $\bar{D}(r)$  and the electric field  $\bar{E}(r)$  are related by the local dielectric constant  $\epsilon(r)$ . Since both  $\bar{D}(r)$  and  $\bar{E}(r)$  are perpendicular to the magnetic field  $B_o$

$$D(r) = \epsilon_o K_{\perp}(r) E(r) \quad (\text{I-4})$$

where  $K(r) = \epsilon_{\perp}(r)/\epsilon_o$ .

Combining equations I-2, I-3, and I-4

$$\bar{J}_r = \frac{I}{2\pi r} = i\omega\epsilon_o K_{\perp}(r) E(r) \quad (\text{I-5})$$

or

$$E(r) = \frac{I}{2\pi i\omega\epsilon_o K_{\perp}(r)r} \quad (\text{I-6})$$

Using

$$V(B) - V(A) = - \int_A^B E(r) dr \quad (\text{I-7})$$

to calculate the voltage drop across the capacitor

$$\Delta V = V(A) - V(B) = \frac{I}{2\pi i\omega\epsilon_o} \int_A^B \frac{dr}{r K_{\perp}(r)} \quad (\text{I-8})$$

Using equation I-1,

$$Y = 2\pi i \omega \epsilon_0 \left\{ \int_A^B \frac{dr}{r K_{\perp}(r)} \right\}^{-1} \quad (I-9)$$

For a uniform plasma  $K_{\perp}(r) = \text{constant} = K_{\perp}$  so

$$Y = 2\pi i \omega \epsilon_0 \ln(B/A) K_{\perp} = Y_0 K_{\perp} \quad (I-10)$$

The primary effect we wish to show is that a density profile gives rise to an upper hybrid layer which results in a finite conductance for even a collisionless plasma. As a particularly simple example, consider the plasma to be composed of two concentric shells with plasma densities proportional to  $\omega_{p1}^2$  and  $\omega_{p2}^2$ . This is illustrated in Figure I-1. As was previously shown, the normalized admittance of a uniform coaxial capacitor is

$$Y/Y_0 = K_{\perp} = K_{\perp}(\omega_p^2) \quad (I-11)$$

In Figure I-2 is sketched the normalized admittance for the two

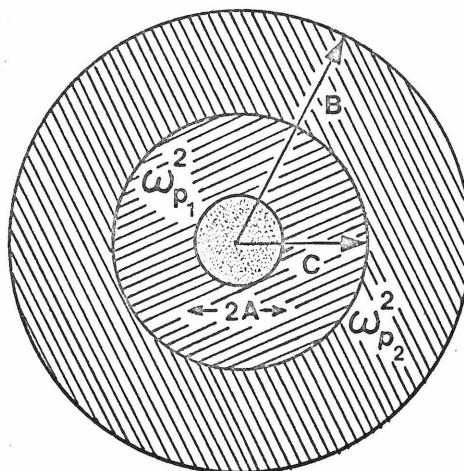


Figure I-1 Coaxial capacitor with two uniform plasma shells

densities for a collisionless plasma.

The total admittance of the capacitor in Figure I-1 is found by considering the admittance of one shell to be in series with the other. It is easily shown that

$$Y = 2\pi i \omega \epsilon_0 \left\{ \frac{\frac{K_{\perp}(\omega^2_{p1})}{\ln(C/A)} \frac{K_{\perp}(\omega^2_{p2})}{\ln(B/C)}}{\frac{K_{\perp}(\omega^2_{p1})}{\ln(C/A)} + \frac{K_{\perp}(\omega^2_{p2})}{\ln(B/C)}} \right\} \quad (I-12)$$

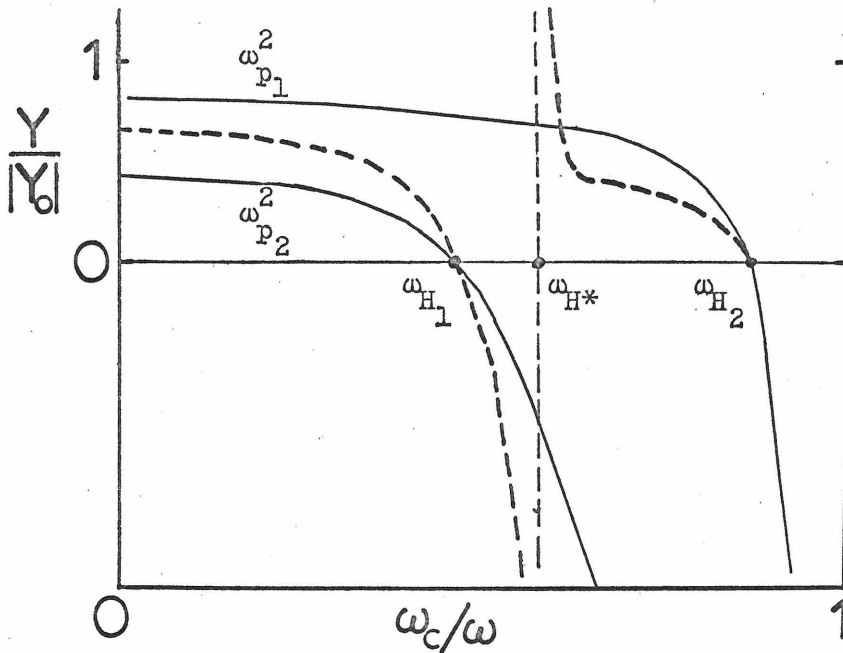


Figure I-2. Normalized admittance for two plasma shells taken separately (solid lines) and for the total normalized admittance of the capacitor (dashed line)

In equation I-12 zeros occur at  $\omega_{H_1}$  and  $\omega_{H_2}$  (see Figure I-2). Infinities occur at  $\omega_c/\omega = 1$  and at  $\omega_{H^*}$ , some point between  $\omega_{H_1}$  and  $\omega_{H_2}$ . This behavior is sketched in Figure I-2 with the dotted line. The Kramers-Kronig relations now require that  $\text{Re}(Y/|Y_0|) = G/|Y_0|$  have a delta function at both  $\omega_c = \omega$  and  $\omega_c = \omega_{H^*}$ . Physically, as  $Y/Y_0 \rightarrow \infty$ ,  $Z/Z_0 \rightarrow 0$  and the particle oscillations become large.

This two-shell model exhibits an elementary type of hybrid resonance. In a plasma with a density profile  $\omega_p^2(r)$  at some radius  $r'$  two infinitesimal shells exist, one above  $r'$  and one below  $r'$  such that the inner shell is inductive, the outer shell is capacitive, and the two are in resonance. A series resonance occurs in this infinitesimal layer at a radius  $r'$  where  $\omega_p^2(r')/\omega^2 + \omega_c^2/\omega^2 = 1$  (the hybrid resonance) and the Kramers-Kronig relations [17] require a delta function in  $G/|Y_0|$ . Since the density profile is continuous, the delta function maps out a finite conductance from the maximum to the minimum upper hybrid frequency in the density profile.

To find the impedance for a continuous density profile we must use equation I-9 where  $K_{\perp}(r) = 1 - [(\omega_p^2(r))/(\omega^2 - \omega_c^2)] = (\omega^2 - \omega_H^2(r)) / (\omega^2 - \omega_c^2)$  and equation I-1. The impedance is

$$Z = \frac{(\omega^2 - \omega_c^2)}{2\pi i \epsilon_0 \omega} \int_A^B \frac{dr}{r[\omega^2 - \omega_c^2 - \omega_p^2(r)]} \quad (\text{I-13})$$

For a parabolic density profile

$$\omega_p^2(r) = \omega_{p_0}^2 \left[ 1 - \frac{(r^2 - A^2)}{(B^2 - A^2)} \right] \quad (\text{I-14})$$

The integration of equation I-13 is straightforward, but some care must be exercised because of the simple pole in the denominator.

Integrating equation I-13 yields,

$$Z = (2\pi i \omega \epsilon_0)^{-1} \left( K_{\perp 0} - \frac{\Delta^2}{\omega^2 - \omega_c^2} \right)^{-1} \left\{ \ln \left| \frac{B}{A} K_{\perp 0}^{1/2} \right| - i R/2 \right\} \quad (\text{I-15})$$

where

$$R = \pi \quad \text{for} \quad 1 - \omega_p^2 / \omega^2 \leq \omega_c^2 / \omega^2 \leq 1$$

$$= 0 \quad \text{otherwise}$$

and where

$$K_{\perp 0} = 1 - \omega_p^2 / (\omega^2 - \omega_c^2) \quad \text{and} \quad \Delta^2 = A^2 \omega_p^2 / (B^2 - A^2)$$

From equation I-15 we see that the hybrid layer adds a series resistance to the plasma impedance.

Appendix II

THE DISPERSION RELATION FOR PERPENDICULARLY PROPAGATING  
CYCLOTRON HARMONIC WAVES

For completeness in this appendix we outline the mathematical formalism leading to the expression for  $K_{\perp}(\omega, k)$  given in equation 3.1. Special emphasis is placed on the approximations made along the way.

II.1 General Dispersion Relation

For waves to propagate in a warm magnetoplasma, their electric  $\underline{E}$  and magnetic  $\underline{H}$  fields must represent solutions to Maxwell's equations in an anisotropic medium. The dispersion relation represents the set of solution pairs  $(\omega, k)$  that satisfy Maxwell's equations and the relevant plasma properties.

Since in the linear limit, superposition of fields within the plasma is valid, one need only look for plane wave solutions of Maxwell's equations of the form  $\exp[-i\omega t + i\mathbf{k} \cdot \mathbf{r}]$ . The plasma properties are contained in the tensor dielectric constant  $\underline{K}(\omega, k)$  relating the electric field  $\underline{E}(\omega, k)$  to the displacement vector  $\underline{D}(\omega, k)$ . Fourier transforming Maxwell's equations in space and time in a source free plasma (circumflex ^ implies that the variable is Fourier transformed)

$$\underline{k} \times \hat{\underline{E}} = -\omega \mu_0 \hat{\underline{H}} \quad (\text{II-1})$$

$$\underline{k} \times \hat{\underline{H}} = \omega \epsilon_0 \underline{K} \cdot \hat{\underline{E}} \quad (\text{II-2})$$

$$\underline{k} \cdot \underline{K} \cdot \hat{\underline{E}} = 0 \quad (\text{II-3})$$

$$\underline{k} \cdot \hat{\underline{B}} = 0 \quad (\text{II-4})$$

Eliminating  $\underline{H}$  between II-1 and II-2 we get the general dispersion relation

$$\underline{k} \times (\underline{k} \times \hat{\underline{E}}) + \frac{\omega^2}{c^2} \underline{K} \cdot \hat{\underline{E}} = 0 \quad (\text{II-5})$$

Since we are interested only in the cases where both  $\underline{k}$  and  $\underline{E}$  are perpendicular to the applied static magnetic field  $\underline{B}_0$  (taken parallel to the z-axis), assume  $\underline{k} = k_x$  and  $E_z = 0$ . Equation II-5 then becomes

$$k_x^2 K_{xx} - \frac{\omega^2}{c^2} (K_{xx} K_{yy} - K_{xy} K_{yx}) = 0 \quad (\text{II-6})$$

Equation II-6 contains both solutions representing longitudinal wave propagation and solutions for extraordinary ( $\underline{E} \perp \underline{B}_0$ ) transverse EM waves [53,54].

The quasistatic approximation discussed in Section 2.1 sets  $\underline{k} \times \hat{\underline{E}} = 0$  and reduces equation II-5 to

$$K_{xx}(\omega, k) = K_{\perp}(\omega, k) = 0 \quad (\text{II-7})$$

Comparing equation II-7 and II-6, this approximation is justified if

$$(\omega^2/k_x^2 c^2)(K_{yy} - K_{xy} K_{yx}/K_{xx}) = (v_{ph}^2/c^2)(K_{yy} - K_{xy} K_{yx}/K_{xx}) \ll 1$$

where  $v_{ph} = \omega/k$  is the wave phase velocity. Hence essentially pure longitudinal waves can propagate if the wave phase velocity is very much less than the speed of light.

## II.2 Evaluation of the Longitudinal Dielectric Constant $K_{xx}$

Numerous authors have given complete derivations of the form of  $K_{xx} = K_{\perp}$  [10,11,12]. The aim here is not to repeat the derivations in

great detail but rather to sketch the method generally employed.

The motion of the plasma electrons is assumed to be described by the Vlasov equation

$$\frac{df}{dt} = \frac{\partial f}{\partial t} + \underline{v} \cdot \nabla f + \frac{e}{m} (\underline{E} + \underline{v} \times \underline{B}_0) \cdot \frac{\partial f}{\partial \underline{v}} \quad (\text{II-9})$$

where  $f$  is the electron distribution function,  $\underline{v}$  is the electron velocity and  $\underline{B}_0$  is the magnetic field. Collisions may be added by setting

$$\frac{df}{dt} = \left( \frac{df}{dt} \right)_{\text{coll}} = -\nu f_1 \quad (\text{II-10})$$

where  $\nu$  is the collision frequency and subscripts "o" and "1" refer to the unperturbed and perturbed parts of the variables. Expressing the variables in terms of their unperturbed and perturbed parts

$$\begin{aligned} n &= n_o + n_1 \\ f &= f_o + f_1 \\ \underline{E} &= \underline{E}_1 \quad (\text{The rf electric field is the perturbed electric field}) \\ \underline{B} &= \underline{B}_0 + \underline{B}_1 \quad (\text{The static DC field is } B_o \hat{z}) \end{aligned} \quad (\text{II-11})$$

After Fourier transforming in space and time by assuming that the perturbed variables have an  $\exp[i\underline{k} \cdot \underline{r} - i\omega t]$  dependence, one gets the perturbed Vlasov equation

$$\{(\nu - i\omega) + i\underline{k} \cdot \underline{v}\} f_1 - \omega_o (\underline{v} \times \hat{z}) \cdot \frac{\partial f_1}{\partial \underline{v}} = -\frac{e}{m} \underline{E}_1 \cdot \frac{\partial f_o}{\partial \underline{v}} \quad (\text{II-12})$$

After expressing the velocity  $\underline{v}$  in cylindrical coordinates

$\underline{v} = (u_{\perp} \cos \phi, u_{\perp} \sin \phi, u_{\parallel})$  one finds, ( $f_o$  is assumed isotropic and

symmetric in velocity space  $\Rightarrow f_0$  independent of  $\phi$ .)

$$\frac{\partial f_1}{\partial \phi} + h(\phi) f_1 = S(\phi) \quad (\text{II-13})$$

where

$$h(\phi) = -\{v - i(\omega - \underline{k} \cdot \underline{v})\} / \omega_c$$

and

$$S(\phi) = -\frac{e}{m\omega_c} \underline{E}_1 \cdot \bar{\nabla}_v f_0$$

An explicit expression for  $f_1$  in terms of an integral over  $\phi$  can now be obtained

$$f_1(\phi') = \int_{-\infty}^{\phi'} G(\phi', \phi) S(\phi) \quad (\text{II-14})$$

where

$$G(\phi', \phi) = \exp \int_{\phi}^{\phi'} h(\phi'') d\phi''$$

is the integrating factor for equation II-13.

For a Maxwellian electron velocity distribution we can solve for  $f_1(v)$  explicitly. We can then solve for the particle current

$$\underline{J}_1 = -e \int (\underline{v} \cdot \frac{\underline{J}_1}{|\underline{J}_1|}) f_1 \underline{u}_1 du_1 d\phi \quad (\text{II-15})$$

and using  $\underline{J}_{1x}(\omega, k) = \sigma_{xx}(\omega, k) \underline{E}_{1x}(\omega, k)$  we can obtain after several lengthy integrations, an expression for  $\sigma_{xx}(\omega, k)$  which we relate to the perpendicular dielectric constant  $K_{\perp}(\omega, k)$  with

$$K_{\perp}(\omega, k) = K_{xx}(\omega, k) = 1 - \frac{\sigma_{xx}(\omega, k)}{i\omega\epsilon_0} \quad (\text{II-16})$$

Finally we get

$$K_{\perp}(\omega, k) = 1 - \left(1 - \frac{i\nu}{\omega}\right) \frac{\omega_p^2}{\omega_c^2} \frac{e^{-\lambda}}{(\lambda/2)} \sum_{n=1}^{\infty} \frac{I_n(\lambda)}{\left\{\frac{\omega - i\nu}{n\omega_c}\right\}^2 - 1} \quad (\text{II-17})$$

where  $\lambda = (k v_{th}/\omega_c)^2$ .

References

- [1] F. W. Crawford, "A Review of Cyclotron Harmonic Phenomena in Plasmas", J. Nuclear Fusion 5, 73 (1965).
- [2] R. S. Harp, "The Dispersion Characteristics of Longitudinal Plasma Oscillations near Cyclotron Harmonics", Proc. 7th Intern. Conf. on Ionization Phenomena in Gases, Belgrade, Yugoslavia, Gradevinska Knjiga Publ. House, Belgrade, 1966, 2, 294 (1965).
- [3] T. D. Mantei, "Cyclotron Harmonic Wave Phenomena", Stanford University, Institute for Plasma Research, Report No. 194, August (1967).
- [4] C. B. Wharton, "Microwave Radiation Measurements of Very Hot Plasmas", Proc. 4th Intern. Conf. on Ionization Phenomena in Gases, North Holland Publishing Co., Amsterdam, 1960, 2, 737 (1959).
- [5] G. Landauer, "Generation of Harmonics of the Electron Gyro-frequency in a Penning Discharge", J. Nucl. Fusion Part C 4, 395 (1962).
- [6] J. D. Jackson, Classical Electrodynamics, John Wiley & Sons, Inc., New York, 1963.
- [7] G. Bekefi, J. D. Coccoli, E. B. Hooper, S. J. Buchsbaum, "Microwave Emission and Absorption at Cyclotron Harmonics of a Warm Plasma", Phys. Rev. Let. 9, 6 (1962).
- [8] S. Tanaka, K. Mitani, and H. Kubo, "Microwave Radiation from a Plasma in a Magnetic Field", Institute of Plasma Physics Report No. 13, Nagoya University, Nagoya, Japan (1963).
- [9] E. Canobbio and R. Croci, "Harmonics of the Electron Frequency in a PIG Discharge", Proc. 6th Intern. Conf. on Ionization Phenomena in Gases, Paris, S.E.R.M.A., Paris, 1964, 3, 269 (1963).
- [10] I. B. Bernstein, "Waves in a Plasma in a Magnetic Field", Phys. Rev. 109, 10 (1958).
- [11] T. H. Stix, Theory of Plasma Waves, McGraw-Hill Book Co., New York, 1962.
- [12] J. A. Tataronis, "Cyclotron Harmonic Wave Propagation and Instabilities", Stanford University, Institute for Plasma Research Report No. 205, December (1967).

- [13] F. W. Crawford, T. D. Mantei, and J. A. Tataronis, "The Plasma Capacitor in a Magnetic Field", Int. J. Electronics 21, 341 (1966).
- [14] P. E. Vandenplas, Electron Waves and Resonances in Bounded Plasmas, John Wiley & Sons, New York, 1968, p. 8 ff.
- [15] V. Bevc, "Dynamic Potentials in Gyrotropic Plasma", J. Appl. Phys. 41, 2408 (1970).
- [16] M. A. Heald and C. B. Wharton, Plasma Diagnostics with Microwaves, John Wiley & Sons, New York, 1965, p. 29 ff.
- [17] W. K. H. Panofsky and M. Phillips, Classical Electricity and Magnetism, Addison-Wesley Publ. Co., Reading, Massachusetts, 1962, p. 416.
- [18] F. A. Blum, "Echoes and Scattering from a Plasma in a Magnetic Field", California Institute of Technology, Technical Report No. 39, Nonr 220(50), May 1968.
- [19] R. S. Harp and F. W. Crawford, "Characteristics of the Plasma Resonance Probe", J. Appl. Phys. 35, 3436 (1964)
- [20] R. S. Harp, G. S. Kino, and J. Pavkovich, "RF Properties of the Plasma Sheath", Phys. Rev. Let. 11, 310 (1963).
- [21] R. W. Gould, "Radio Frequency Characteristics of the Plasma Sheath", Phys. Let. 11, 236 (1964).
- [22] F. W. Crawford and G. S. Kino, "Cyclotron Harmonic Amplification in Beams and Plasmas", Stanford Microwave Laboratory Report No. 1204 (1964).
- [23] J. A. Tataronis and F. W. Crawford, "Cyclotron and Collision Damping of Propagating Waves in a Magnetoplasma", Proc. 7th Intern. Conf. on Phenomena in Ionized Gases, Belgrade, Gradevinska Knjiga Publ. House, Belgrade, 1966, 2, 244 (1965).
- [24] J. G. Downward and R. S. Harp, "Admittance of a Thin Antenna in a Plasma at Cyclotron Harmonics", Proc. 9th Intern. Conf. on Phenomena in Ionized Gases, Bucharest, Editura Akademie Republicii Socialistic Roumania, 1969, 521 (1969).
- [25] F. W. Crawford, R. S. Harp, T. D. Mantei, "On the Interpretation of Ionospheric Resonances Stimulated by Alouette I", J. Geophys. Res. 72, 57 (1967).
- [26] S. G. Gruber and G. Bekefi, "Excitation of Longitudinal Waves near Electron-Cyclotron Harmonics", Phys. Fluids 11, 122 (1968).

- [27] T. Stix, "Absorption of Plasma Waves", *Phys. Fluids* 3, 19 (1960).
- [28] H. H. Kuehl, "Coupling of Transverse and Longitudinal Waves below the Second Cyclotron Harmonic", *Phys. Rev.* 154, 124 (1967).
- [29] S. J. Buchsbaum and A. Hasegawa, "Longitudinal Plasma Oscillations near Cyclotron Harmonics", *Phys. Rev.* 143, 303 (1966).
- [30] F. Leuterer, "Bernstein Waves in Inhomogeneous Plasma Columns", Proc. 9th Intern. Conf. on Phenomena in Ionized Gases, Bucharest, Editura Akademie Republicii Socialistic Roumania, 1969, 449 (1969).
- [31] Fred Rosebury, Handbook of Electron Tube and Vacuum Techniques Addison-Wesley Publ. Co., Reading, Massachusetts, 1965.
- [32] R. H. Huddlestone and S. L. Leonard (Editors) Plasma Diagnostic Techniques, Ch. 4, "Electric Probes", F. F. Chen, Academic Press, New York, 1965.
- [33] C. A. Ventrice and C. G. Massey, "Radial Density Distribution in a Wide Unstable Plasma Column", *Phys. Fluids* 11, 1990 (1968).
- [34] S. C. Brown, Basic Data of Plasma Physics, 1966, MIT Press, Cambridge, Mass., Second Edition Revised (1967).
- [35] E. Canobbio and R. Croci, "Harmonics of the Electron Gyrofrequencies in Plasmas", *Phys. Fluids* 9, 549 (1966).
- [36] H. Dreicer, "Transmission and Emission of Radiation by a Magnetized Laboratory Plasma", from Plasma Waves in Space and in the Laboratory, J. C. Thomas and B. Landmark, Ed., American Elsevier Publ. Co. 1969, 1 (1969).
- [37] H. Dreicer, "Enhanced Radiation from Gases", Proc. 6th Intern. Conf. on Ionization Phenomena in Gases, Paris, S.E.R.M.A., Paris, 1964 3, 261 (1963).
- [38] C. D. Lustig, "Electron Density Dependence of Cyclotron Harmonic Radiation from a Plasma", *Phys. Rev.* 139, A63 (1965).
- [39] H. Ikegami and F. W. Crawford, "Noise Radiation from a Warm Magnetoplasma", Proc. 7th Intern. Conf. on Ionization Phenomena in Gases, Belgrade, Gradevinski Snjiga Publ. House, Belgrade, 1966, 2 503 (1965).
- [40] H. Ikegami, "Microwave Emission at Electron Cyclotron Harmonics" Stanford University Institute for Plasma Research, Report No. 29, Stanford University, 1965.

- [41] P. M. Stone and P. L. Auer, "Excitation of Electrostatic Waves near Electron Cyclotron Harmonic Frequencies", *Phys. Rev.* 138, A695 (1965).
- [42] S. J. Tetenbaum, "Cyclotron Harmonic Resonances in an Electrodeless Discharge", *Phys. Fluids* 10, 1577 (1967).
- [43] G. Bekefi, Radiation Processes in Plasmas, Ch. 4, John Wiley & Sons, New York 1966.
- [44] R. L. Stenzel, "Microwave Absorption and Emission from Magnetized Afterglow Plasmas", Ph.D. Thesis, California Institute of Technology (1969).
- [45] G. Landauer and G. Muller, "Radiation of Harmonics  $n\omega_c$  and  $n\omega_c/2$  from a Beam Generated Plasma", *Phys. Let.* 23, 555 (1966).
- [46] E. Etievant and M. Perulli, "Excitation of Cyclotron Oscillations by the Collision of Two Electron Beams", Proc. 6th Intern. Conf. on Ionization Phenomena in Gases, S.E.R.M.A., Paris 1964, 3, 209 (1963).
- [47] J. Olivain, C. Etievant, M. Perulli, "Génération D'Harmoniques Dans Un Système Double Faisceau en La Présence D'un Champ Magnetique", *Journal de Physique* 26, 505 (1965).
- [48] A. Simon and M. N. Rosenbluth, "Single-Particle Cyclotron Radiation near Walls and Sheaths", *Phys. Fluids* 6, 1566 (1963).
- [49] Samuel Bliman, "Double Beam Type Instabilities in a Cold Cathode PIG Discharge" (in French), Proc. 6th Intern. Conf. on Ionization Phenomena in Gases, S.E.R.M.A., Paris, 1964, 3, 233 (1963).
- [50] A. Clinckemallie, "Propagation of Longitudinal Electron Cyclotron Waves in a Finite Plasma Column", Contributed at Meeting of the NATO Advanced Studies Institute on Plasma Waves in Space and in the Laboratory, RØROS, Norway, 17-26 April 1968.
- [51] J. M. Pavkovich, "Numerical Calculations Related to the RF Properties of the Plasma Sheath", Stanford University Microwave Laboratory Report No. 1093, October (1963).
- [52] J. G. Downward and R. S. Harp, "Conductance Peaks in a Cylindrical Plasma Capacitor at the Cyclotron Harmonics", *J. Appl. Phys.* 41, 4652 (1970).
- [53] Yu. N. Dnestrovski and D. P. Kostomarov, "The Dispersion Equation for an Extraordinary Wave Moving in a Plasma across an External Magnetic Field", *Sov. Phys. JETP* 14, 1089 (1962).

- [54] H. Oya, "Conversion of Electrostatic Plasma Wave into Electromagnetic Wave--A Numerical Calculation of the Dispersion Relation for all Wavelengths", NASA, Goddard Space Flight Center, X-621-70-352, Sept. 1970.